Study of Extracellular Electron Transfer in Bio-corrosive Bacteria for Electrochemical Sensor Application

（電気化学センサー応用に向けた腐食性細菌の
細胞外電子移動に関する研究）

Luo Dan

Graduate School of Chemical Sciences and Engineering

Hokkaido University

Title Study of Extracellular Electron Transfer in Bio-corrosive Bacteria for Electrochemical Sensor Application

Author Luo Dan

Degree Doctor of Philosophy (Physics)

Supervisor Professor Okamoto Akihiro

CONTENTS

Chapter 1. General Introduction

Microorganisms hold a prominent ecological position on Earth, performing vital functions in both the human body and the surrounding environment [1]. In a state of homeostasis, microorganisms within the human body facilitate the normal functioning of diverse tissues and the overall physiological equilibrium. Nevertheless, alterations in the microbial community composition or the emergence of pathogenic microorganisms can instigate attacks on human tissues, jeopardizing human health and precipitating the onset of various diseases [2]. Similarly, marine microorganisms exert profound influence on the planet, given that the majority of Earth's surface comprises oceans harboring diverse microorganism species [3]. In the marine ecosystem, these microorganisms serve indispensable roles in the cycling of environmental elements and contribute to the removal and sequestration of environmental pollutants. Consequently, there exists an ongoing body of research focusing on microorganisms, encompassing their intrinsic characteristics, such as gene expression, metabolic pathways, and population dynamics, as well as their integration with other processes [4-6]. This integration involves leveraging the distinctive capabilities of microorganisms for tasks such as pollutant remediation, extraction of elements, fabrication of biocompatible materials, and advancement of microbial sensors [7].

Microorganisms exhibit a diverse range of metabolic strategies, including aerobic, anaerobic, and facultative anaerobic modes, which primarily depend on their surrounding environmental conditions [8]. Aerobic microorganisms typically utilize oxygen as the ultimate electron acceptor and derive energy through the respiration of various inorganic electron donors. In contrast, anaerobic microorganisms lack the ability to employ oxygen as an electron acceptor, thus obtaining energy through fermentation or transferring electrons to alternative inorganic terminal electron acceptors. Among these microorganisms, those capable of transferring electrons from intracellular to extracellular spaces are referred to as electrochemically active microorganisms (EAMs), and this electron transfer process is termed as extracellular electron transfer [9]. Many microorganisms can electrically interact with solid extracellular substances such as minerals, electrodes, and other microbes. The transport of metabolically generated electrons to extracellular solids and the uptake of electrons from solids to the inside of cells are referred to as extracellular electron transfer (EET) and extracellular electron uptake (EEU), respectively [10]. EET and EEU have several biotechnological applications, including microbial fuel cells (MFC) [11],

bioremediation [12], microbial electrosynthesis (MES) [13] and biosensors [14]. EET and EEU also couple microbial metabolism via intercellular electron transport and enable dual-species syntrophic reactions, thus significantly contributing to biogeochemical elemental cycling [15, 16]. In addition, biocorrosion, well-known as microbially induced iron corrosion (MIC), is accelerated by EEU, which can directly oxidize Fe^0 to Fe^{2+} or Fe^{3+} [17-20]. Biocorrosion also occurs on our tooth surface. Microbial biofilms on teeth, also known as dental plaque, may contain acid-producing bacteria (APB), causing localized acidity leading to dental caries and bioerosion of certain dental alloys [21]. While numerous electroactive microorganisms have been identified, a significant proportion remains understudied, necessitating further research in this field.

The utilization of EAMs as the sensing or recognition component enables the detection of biocorrosion and the assessment of environmental pollutant toxicity [22, 23]. Consequently, microbial biosensors have predominantly emerged as valuable tools for environmental monitoring purposes [24]. Owing to the intricate nature of environmental samples, the application of this method for specific microorganism detection in such samples has remained limited. Nevertheless, through ongoing research into the mechanisms underlying extracellular electron transport and advancements in sample purification technologies, biosensors based on EET or EEU hold promise for enabling direct, uncomplicated, and cost-effective microbial detection [25]. This breakthrough can facilitate the identification of specific microbial markers in the environment, including the detection of pathogens for disease prediction and prevention purposes. Therefore, study on the improvement of EET- and EEU-based detection of bacteria cells based on diverse directions is necessary. In this research, the author mainly focused on the extracellular electron transfer process of two bio-corrosive species for biocorrosion in different environment for the development of electrochemical biosensors. One is iron corrosive bacteria *Desulfovibrio ferrophilus* IS5 (IS5), a model EEU bacteria for microbiologically influenced corrosion (MIC), and the other is an EET-capable bacteria with undefined EET mechanism, *Porphyromonas gingivalis* (*P. gingivalis*), a typical periodontal pathogen causing dental corrosion. The author studied the electron transfer mechanism by using electrodes with different wettability. These results not only demonstrate extracellular electron transfer process of these two species, but the impact of electrode surface wettability on the sensitivity of EET- or EEU-based biosensors. This shed light on

the interplay between these microorganisms and the physical properties of the electron acceptor or donor within the environmental context, which hold practical significance for various applications, such as the surface modification of dental implants and the corrosion mitigation of ferrous materials. These implications provide valuable guidance for implementing effective strategies in these domains.

1.1 Electrochemically active microorganisms (EAMs) for biocorrosion

Microbes appear everywhere we live and affect every aspect of human life. Researchers predicted that one trillion (10^{12}) microbial species inhabit Earth [26]. The successful growth and habitat of microorganisms on Earth is largely due to their propensity to form biofilms [27], e.g. on organs and tissues (e.g. the human oral microbiome [28, 29]), or in industrial settings (e.g. biocorrosion [21, 30] and biofouling [31]). These biofilms engage in electrical interactions among their constituent microorganisms and with the surrounding extracellular environment, collectively referred to as "electrochemically active microorganisms". These microorganisms have a wide distribution across diverse natural ecosystems, including soil, water, sediments, intestinal systems, corroded metal surfaces, and digesters [32]. Biocorrosion arises from microbial biofilms through two distinct mechanisms: direct corrosion, wherein microorganisms secrete corrosive metabolites or extract electrons from a metal, and indirect corrosion, whereby the biofilm compromises the integrity of the preformed passive film, typically a metal oxide film, leading to accelerated corrosion [21].

EET is a specific mechanism that allows microorganisms to electrically interact with extracellular insoluble substates by electron transfer. EET was first discovered in the iron-reducing *Shewanella* and *Geobacter* genera, which reduce metal oxide minerals as the electron acceptor [33, 34]. Since then, an increasing spectrum of Gram-negative and Gram-positive microbes have been discovered to be capable of transporting metabolic electrons to anodes or extracellular metal cations, which processes have been widely applied in microbial fuel cells and bioremediation [35-38]. Meanwhile, some microbes utilize extracellular solid electron donors by importing electrons. For example, sulfate-reducing bacteria (SRB) cells extract electrons from cathodes coupled with sulfate reduction[39-41]. The electron extraction likely also occurs on the surface of iron, which has been proposed as a crucial cause for SRB-mediated anaerobic iron corrosion [18, 40, 42, 43]. Acetogens have been shown to extract electrons from

electrodes and reduce CO_2 to organics, which pave ways for microbial electrosynthesis systems [44-47]. To distinguish the exportation of cellular electrons to solids and importation of electrons from solids, EET and EEU are used, respectively [10]. EET and EEU can occur simultaneously in dual-species consortia for carrying out syntrophic metabolic reactions. For example, in the anaerobic-methane oxidizing consortia, the archaea excreted electrons obtained by methane oxidation, and the electrons are then readily received by SRB for sulfate reduction [16, 48, 49]. Therefore, EET and EEU processes play important roles in biogeochemical cycling of elements, biotechnologies, microbial energy conservation, biocorrosion, [35, 50-58].

The presence of electrogenic bacteria can be detected by measuring the current production on an electrode. This method offers a suitable approach for diagnosing biocorrosion in different environments by leveraging the electrogenic signals generated by electrochemical active materials that serve as biomarkers. This study focuses on the EAMs that perform EET in oral biofilms for biocorrosion of tooth and that perform EEU in iron corrosion biofilm for biocorrosion of mental pipes, respectively.

1.1.1 Sulfate-reducing bacteria (SRB) for iron biocorrosion

Anoxic iron corrosion in oil and gas pipelines has close connection with iron reducing bacteria, well known as sulfate-reducing bacteria (SRB) [18]. Corrosion associated with the action of microorganisms is known as microbiologically influenced corrosion (MIC), which is one of the most important corrosion pathway [59]. *D. ferrophilus* IS5 (IS5) is one of the most important bacteria for iron the only electron donor. The electron transfer capability IS5 is essential for anoxic sulfate-rich environments (e.g., anoxic seawater), because corrosion rate of IS5 is quicker than most of other SRB bacteria. Many researches have focused on mechanism of electron transfer of IS5, less of them mentioned how physics characters of electrode effect on EEU of IS5. In this study, the author focused on the wettability of electrode surface effect on electron transfer capability, activity and distribution of IS5.

MIC has been studied using various microbes including SRB, nitrate-reducing bacteria, methanogens, and iron-reducing bacteria [20]. Among these, SRB have been recognized as the major cause of MIC, especially in anaerobic marine and soil environments where they thrive. SRB have long been considered to corrode iron by producing corrosive hydrogen sulfide (chemical MIC), or consuming

cathodic hydrogen accumulated on iron to promote anodic iron dissolution. However, neither of these mechanisms can explain the persistent corrosion observed even after the iron surface is fully covered by corrosion products. In contrast, following the isolation of highly corrosive sedimentary SRB strains (IS5 and *Desulfobacterium corrodens* IS4) which can utilize metal iron as the sole electron donor, a new electrical MIC model in which SRB directly extract electrons from iron was proposed [17]. The electrical MIC model best explains the observed corrosion behavior at the real corrosion sites. Thus, the SRB-mediated EEU process is considered to be the major cause of MIC, and identifying EEU pathways in SRB has therefore attracted significant attention with the aim of developing new anti-MIC methods.

Although EEU in SRB was first proposed in an iron corrosion system, the iron electrode, which is easily chemically transformed by SRB metabolites and medium components and produces hydrogen as a potential electron mediator for SRB, remains unsuitable for studying EEU by SRB at the solid interface. Recent development of inert electrodes with large overpotentials for hydrogen evolution, such as indium-tin doped oxide (ITO) and graphite electrodes [60], has enabled the discovery of EEU capabilities in IS5 [61], *D. corrodens* IS4 [62], and *D. vulgaris* Hildenborough [55]. Cytochrome proteins were found not only on the cell surface but also on OM extensions as nanowires structure as visualized through 3,3-diaminobenzidine-H_2O_2 staining [10]. EEU capability was also found in the methanogens *Metahnococcus maripaludis* and *Metahnosarcina* [63, 64]. *Metahnococcus maripaludis* uses [Ni-Fe] hydrogenase for direct EEU from the iron surface [65]. Other methanogens such as *Metahnobacteirum* IM1, and *Metahnosarcina barkeri*, are capable of hydrogenase-independent EEU, while the redox-active component in them has not yet been identified [66, 67].

Although *D. vulgaris* Hildenborough lacks an intact biological EEU pathway, it can conduct EEU via self-synthesized FeS NPs as explained above [55]. And although the detailed mechanism of FeS NPs biosynthesis remains unclear in SRB, it is achieved by the chemical reaction between H_2S and Fe^{2+} [68]; thus, FeS NP biosynthesis is likely ubiquitous in SRB [69]. During MIC, Fe^{2+} is released from corroded iron, which facilitates the formation of FeS NPs on the cell surface. Therefore, FeS NPs-mediated EEU may be a ubiquitous mechanism for accelerating electric MIC. In accordance with this notion, electrical MIC-like behaviors have also been reported in SRB strains other than IS5 and IS4 [70-72]. *D. vulgaris* Hildenborough cells survived on iron surface and caused corrosion for 55 days, long after the exhaustion

of organic content [71]. It has also been reported that carbon starvation promotes iron corrosion by *D. vulgaris* [73]. These results suggest that EEU via FeS NPs ubiquitously drives MIC kinetics.

Investigating different SRBs and their involvement in the microbiologically influenced corrosion process can provide a deeper understanding of the mechanistic aspects of biocorrosion. Furthermore, such studies hold significant implications for the development of effective strategies for preventing and mitigating iron biocorrosion. For instance, exploring the electron uptake mechanisms employed by SRBs and identifying the factors influencing electron transfer rates can offer valuable insights in this regard.

1.1.2 Electrogenic pathogens as biomarkers of dental biocorrosion

There are hundreds of species of microorganisms in the human oral cavity, which colonize and interact in different habitats of the oral cavity to maintain oral health against invasion of external undesirable stimulation [74]. However, dysbiosis of the oral microbiome can lead to oral diseases [75]. The Human Oral Microbiome Database (HOMD) is the first to describe the curated inventory of microbiome that is associated with human mouth and aerodigestive tract, offering various resources to aid in comprehending the microbiome's influence on both health and illness. The HOMD includes an enumeration of 774 oral bacterial species, of which 58 percent have been formally named, 16 percent have been cultivated but not named, and 26 percent are known only as uncultivated phylotypes (Homepage, 2023). In human saliva, the distribution of Gram positive is much higher than Gram negative bacteria [76]. More than 400 species have been recognized to exist within the periodontal pocket, among which Gram-negative anaerobic bacteria are predominantly the type of bacteria associated with periodontal diseases [77].

Periodontitis is a common disease that destroys periodontal attachments and support structures, which contributed to dental biocorrosion [40]. This particular illness is caused by the microorganisms that create the biofilm on the surface of the tooth, known as plaque, which contains both Gram-positive and Gram-negative bacteria, aerobic and anaerobic organisms. **Figure 1.1** shows the predicted spatial structure and distribution of the plaque microbiome based on the analysis of real human samples using fluorophore probes, which clearly shows the location of each species [78]. The presence and composition of microorganisms in a host's body are affected by multiple factors, including both

environmental and host-related factors [41]. Many of the indigenous microbiota are anaerobes and lead to oral infections and serve as the source of infections in other parts of the body [42, 43]. Furthermore, the host's immune response to these bacteria can trigger inflammation, leading to additional damage [32]. The bacteria that can cause periodontitis is called periopathogens that though to occupy a smaller number of all strains in subgingival plaque. Different periodontal diseases can be caused by different periodontal pathogens. Such as *Streptococcus mutans* is the main cause of tooth decay [44, 45], dental plaque is close contact with *Capnocytophaga ochracea*. Besides, the disorder of non-pathogenic microbes in the biofilm also can induce periodontal diseases. The presence of *Porphyromonas gingivalis* (*P. gingivalis*), *Bacteroides forsythus* (*B. forsythus*), and *Treponema denticola*, collectively known as the "red" complex, is closely associated with the clinical diagnosis of periodontal disease, including symptoms such as bleeding on probing and a progressive increase in pocket depth. *B. forsythus* and *P. gingivalis* are the strongest bacterial markers for this disease and are infrequently cultured from subjects without periodontal bone loss [79].The inclusion of these putative periopathogens should be taken into consideration in the treatment approach for adult patients with periodontitis.

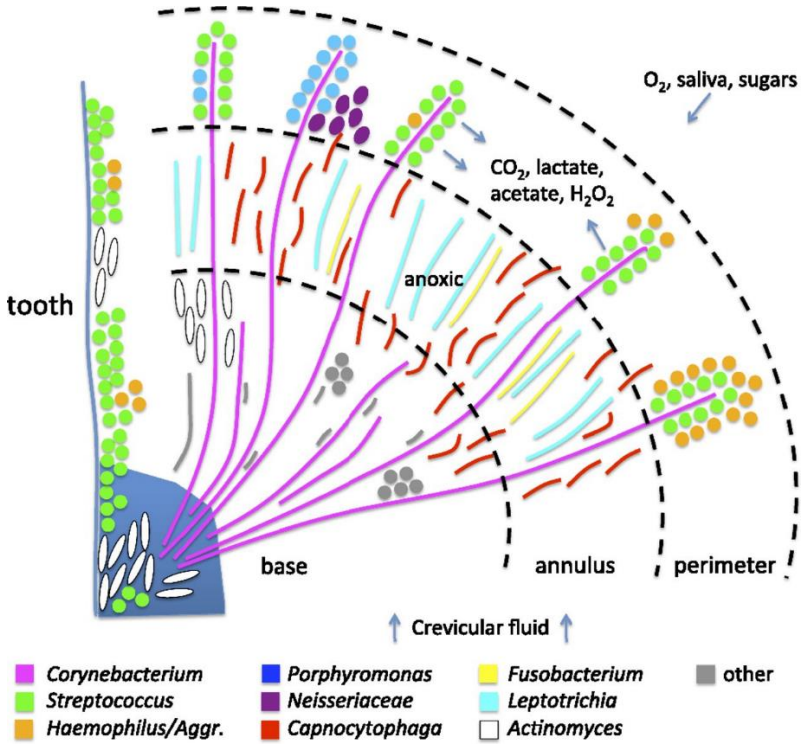

Figure 1.1 Summary hypothesis for interpretation of hedgehog structures [78].

The oral pathogens not only cause oral disease (eg. inflammation, tooth loss and periodontitis) but systemic diseases (gastrointestinal cancer risk [80], diabetes [81], cardiovascular diseases [82], respiratory tract infection [83, 84], Alzheimer's disease [85], preterm birth [86], liver disease [87]), such as the exit of *Selenomonas noxia* is link with obesity, *Streptococcus mitis* is associated with oral cancer, pancreatic cancer and chronic pancreatitis [88], *P. gingivalis* plays a key role in periodontitis and Alzheimer's disease [89]. **Figure 1.2** shows some complications induced by periodontitis. Therefore, the diagnosis of periodontitis is essential not only for dental health but human body.

Figure 1.2 The complications of periodontitis caused by pathogenic bacteria

The human mouth has been identified as a favorable environment for electrogenic bacteria, as demonstrated by Divya et al., who identified five species of oral bacteria capable of extracellular electron transfer associated with sugars oxidation, including *P. gingivalis* and several other oral pathogens (eg. *Streptococcus mutans*, *Capnocytophaga ochracea*, *Aggregatibacter actinomycetemcomitans*, and *Corynebacterium matruchotii*) [90-93]. Most of them are pathogenic not only for dental healthy but human body, because of the pathogen transfer by gut. Therefore, these pathogens can act as biomarkers of diseases, and the electrochemical detection of these pathogen based on the electrogenic capability provides a novel way for oral disease diagnosis. There still numerous oral microbes haven't been studied or isolated. The EAMs in the dental biofilm still need to be further investigated to clarify the electrogenic phenomenon and its effect on dental diseases as well as systemic

diseases.

1.2 The knowns and unknowns of extracellular electron transport mechanisms

1.2.1 Electron transport mechanism between bacterial cell and electrode

EET was first recognized following the isolation of bacteria GS-15 and *Alteromonas putrefaciens* (later renamed *Shewanella oneidensis* MR-1) [51, 52, 94, 95], which are capable of anaerobic reduction of ferric oxide and manganese oxides, respectively, as the terminal electron acceptors coupled with the oxidation of organic electron donors. In comparison, EEU was first proposed 17 years after EET in context of biocorrosion [17]. That same year, EEU from cathode was also reported in EET-capable *G. sulfurreducens* [96]. These mechanisms include a "direct" type mediated by redox components located on the cell surface, after direct attachment of cells to solid surfaces **(Figure 1.3A)** [19, 97-99], and an "indirect" type that is mediated by soluble redox mediators that cyclically shuttle electrons between cells and electrodes passing the cellular membranes [100-102] **(Figure 1.3B)**. These direct and indirect mechanisms can function either independently or in concert [95]. The best-studied cell surface redox components are outer-membrane cytochromes (OMCs), which are transmembrane protein complexes often containing multiple heme (Fe^{3+}/Fe^{2+}) centers to transport electrons from the inside to outside of outer-membrane (**Figure 1.3A**). The crystal structures of OMCs have been estimated for the entire complex of MtrCAB in *S. oneidensis* MR-1, which contains 20 heme redox centers aligned through the protein complex [103]. The energy levels of hemes and the kinetics and dynamics of sequential inter-heme electron transfer have been extensively studied based on the crystal structure of MtrC and its homolog MtrF [104]. Potential OMCs have been detected in iron-reducing and -oxidizing bacteria [105-107], sulfate-reducing bacteria (SRB) [10], and methanotrophic archaea [105]. In addition to heme cofactors, riboflavin and flavin mononucleotide enhance the rate of electron transfer in some OMCs, as redox cofactors in *S. oneidensis* MR-1 and *G. sulfurreducens* [99, 108-110].

In addition to OMCs, some bacterial strains such as *G. sulfurreducens* PCA, *S. oneidensis* MR-1, and *Desulfovibrio ferrophilus* IS5 produce nanofilaments [111-113] which potentially mediate long-distance direct EET and EEU **(Figure 1.3C-D)**. However, the identities of nanofilaments and the underlying electron conduction mechanism have not been fully understood [114]. For example, the

conductive *G. sulfurreducens* nanowires have been previously considered as type IV pili composed of PilA protein which potentially transport electrons via aromatic amino acid side chains, because the deletion of the PilA gene prevented conductive filament production and decreased electricity production by the biofilm [115]. However, given that OmcS and OmcZ were recently found to assemble into filaments through electron microscopy [116, 117], the function of PilA could be the translocation of OMCs such as OmcS and OmcZ to form filaments that are the primary conduits for long-range electron transport [115, 117-121] **(Figure 1.3D)**. On the other hand, based on membrane-specific fluorescence staining and transmission electron microscopy observation, the *S. oneidensis* MR-1 and *D. ferrophilus* IS5 nanowires were identified as outer membrane (OM) extensions covered by OMCs [10, 122] **(Figure 1.3C)**. Nonetheless, a recent study reported that *D. ferrophilus* IS5 also produces electrically conductive pili, possibly by a gene encoding an aromatic amino acid-rich protein [123]. There are still many unknowns about the mechanisms underlying the function of nanowires, and further research is needed.

Soluble redox mediators such as flavins [124], quinones [125], and phenazines [126] mediate an indirect mechanism. These redox mediators diffuse across the lipid membranes of gram-negative bacteria or the thick cell wall matrices of gram-positive bacteria to shuttle electrons from/to redox proteins located in the cell interior [127, 128] or the cell wall [124], respectively. Various microbes secrete electron mediators [129, 130], and natural substrates such as humic substances [131] and industrial dyes in the environment [132] may also serve as electron mediators in MFCs for wastewater treatment.

1.2.2 Proton transfer during extracellular electron transfer process

Because electrons are transferred from the interior to the exterior of microbial cells during EET, ions with positive charge need to simultaneously move in the same direction as the electron flow to maintain charge neutrality **(Figure 1.3A)**. Accordingly, a previous study demonstrated that proton transfer is the rate-limiting factor of EET in *S. oneidensis* MR-1 [133]. The introduction of deuterium oxide to microbes conducting EET significantly decreased the rate of EET. The strong kinetic isotope effect indicates that the slower kinetics of deuterium limit the rate of EET. Furthermore, it was found that the proton uptake capability of the bound flavin cofactor limits the rate of EET by comparing the effect of flavin analogues [134]. A proton-dependent EET process based on pH dependency in anode

biofilms has also been reported for anode-respiring gram-positive *Thermincola ferriacetica* [135]. EET by cyanobacterium *Microcystis aeruginosa* was also found to be solely driven by high pH, suggesting the involvement of proton transfer in EET [136].

The extracellular emission of protons during EET may maintain the charge neutrality of the cells, but this would impair energy conservation by ATP production using proton motive force. This proton motive force is usually needed for ATP production via F-type ATPase, but *S. oneidensis* MR-1 respiring on an anode does not require F-type ATPase. Instead, it synthesize ATP via substrate-level phosphorylation [133]. However, Li et al. observed that proton-associated redox compounds [such as riboflavin and anthraquinone-2,6-disulfonate (AQDS)] decrease current production by *S. decolorationis* NTOU1, possibly because these compounds translocate protons across the OM during EET, leading to reduced ATP production via oxidative phosphorylation [137]. This suggests that different electrochemically active bacteria may utilize different strategies for ATP synthesis during EET. On the other hand, in the EEU process, protons are imported into the cells along with electrons [138]. However, the proton translocation process during EEU has not been investigated and requires further study.

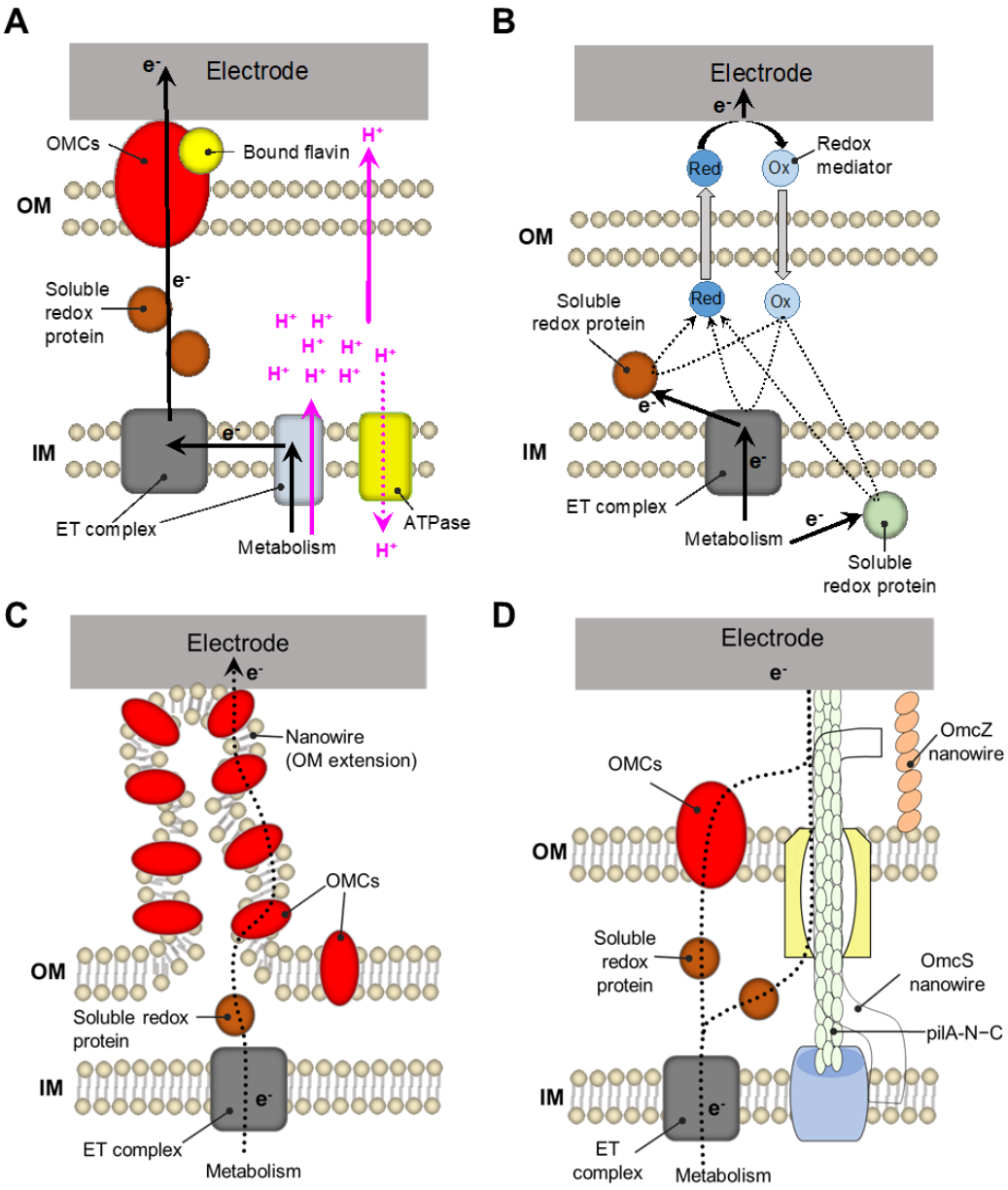

Figure 1.3 Proposed extracellular electron transport (EET) mechanisms in exoelectrogens. (A) Direct mode of EET mediated via outer-membrane-cytochromes (OMCs) complex with bound flavin cofactor. Black and pink arrows indicate the flow of electrons (e^-) and protons (H^+), respectively. To maintain charge neutrality, protons co-translocate with electrons to extracellular space during EET. **(B)** Indirect mode of EET mediated via soluble redox mediators that diffuse across lipid bilayers, and shuttle electrons and protons between the bacterial cell and the electrode. **(C, D)** Less understood direct mode of EET possibly mediated via nanowires, which are made of outer membrane extensions (C), or via cytochromes (OmcS) or pili (PilA-N–C) (D). Dotted black lines indicate unidentified flow of electrons. IM, inner membrane; Red, reduced; Ox, oxidized; ET, electron transfer.

1.3 The applications of electrochemically active microorganisms

Extracellular electron transfer is a specific way that microbes can transfer electrons (intracellular or extracellular) to some insoluble substates, such as electrodes, oxides, bacterial and other substrates [139, 140]. Specifically, two terms, namely extracellular electron transport (EET) and extracellular electron uptake (EEU) have been specifically used to differentiate the direction of electron flow from cell interior to exterior solids, and electron flow from an exterior electron donor to cell interior, respectively [10]. EET has been reported to be important for microbial energy generation (eg. microbial fuel cell), bioremediation of environmental pollutants, biosensors, biosynthesis of nanomaterials and biomining as showed in **Figure 1.4** [35, 50-54]. Meanwhile, the importance of EEU has been reported in matter and energy flow in the biosphere, biocorrosion, enhancement of cell growth, microbial electrosynthesis and biosynthesis of nanomaterials [55-58].

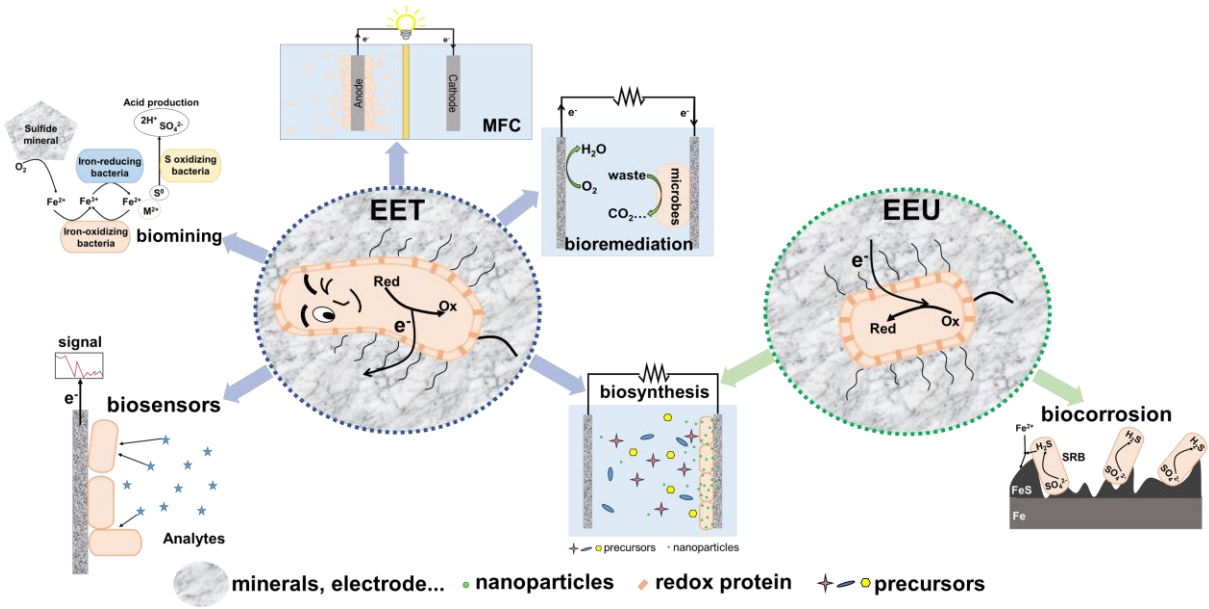

Figure 1.4 The applications of electrochemically active microorganisms

1.3.1 Microbial fuel cells (MFCs)

With the continuous discovery of electrochemically active bacteria (EAB) and studying mechanism of EET process, microbial fuel cell (MFC) has been developed and applied for renewable energy generation and wastewater treatment [141-147]. As showed in **Figure 1.4**, the biofilm formed on anode can decompose organics (eg. wastewater) and transfer electrons to the electrode, meanwhile on the

cathode surface CO_2 would be converted to other chemicals, such as acetate, formic or fatty acids. Microbial fuel cells have been studied for more than fifty years. Bacterial combined with fuel cell first reported in 1964 [148], they examined the interaction between photosynthetic microorganisms and an inert electrode material. The main limitation of MFCs for practical application is the low capability of electric generation [149]. Therefore, the objective of most of MFCs studies is to increase the electron transfer efficiency from bacteria to electrodes by using nanoparticles, modifying electrode surface, regulating the EET pathways and modifying genes [150-153]. More than 600 studies have reported the use of nanoparticles (NPs) to increase the power density of MFCs. Both metallic and semiconductive NPs largely enhanced microbial current generation from EET in MFCs. Metals, iron sulfides, metal oxides, carbon nanomaterials, and mixed NPs have been introduced into MFC anode chambers to enhance the performance of MFCs for their real applications [154-165].

1.3.2 Microbial electrosynthesis (MES)

EEU-capable microbes that produce valuable substrates can serve as electrode catalysts for MES [166]. By supplying cells with sufficiently energetic electrons via cathodes, microbial metabolic pathways can synthesize valuable microbial metabolites such as hydrogen, methane, organic acids, and alcohols from chemicals with almost no economic, such as CO_2. The electric current can ideally be produced by a renewable power source, and microbial electrocatalysts have many advantages over artificial ones, such as low cost, self-repair, and high product selectivity [167]. Furthermore, compared to artificial electrocatalysts, these MES systems require much less input electrical voltage, mild reaction conditions, and are more stable. Therefore, MES is a promising technology that, in combination with renewable energy, has the potential to replace some of the non-sustainable methods of chemical production that depend on fossil fuels [168]. The biggest challenge preventing the widespread practical use of MES is the slow reaction rate. Although it remains to be tested, conductive NPs might help to shorten the initiation time of MES systems, as they did in case of MFCs [169].

On the other hand, EET process have been widely used for biosynthesis of nanoparticles [170-172]. Now many bacterial which can fabricate NPs themselves has been found [173]. Biofabricated NPs have received more and more attention due to good biocompatibility, cost effective and sustainability. Plants, bacterial (eg. *Escherichia coli* (E. coli), *S. oneidensis*), fungi and yeast have been used to synthesize

NPs [174]. Nonetheless, traditional biofabricated NPs have many limits, for example, low productivity and poor controllability on product quality compared to chemical synthetic methods. Many modified methods to improve biosynthesis NPs product efficiency have been developed (such as regulating the EET process) [172]. Moreover, NPs can be flexibly fabricated by abiotically synthesized and added to the microbial system achieving biohybrid systems. Kelsey et al. induced the self-photosensitization of a nonphotosynthetic bacterium (*Moorella thermoacetica*) with cadmium sulfide nanoparticles to enable the photosynthesis of acetic acid from carbon dioxide. Among this, biologically precipitated cadmium sulfide nanoparticles served as the light harvester to sustain cellular metabolism, while self-augmented biological system selectively produced acetic acid continuously, which formed a self-replicating route toward solar-to-chemical carbon dioxide reduction. Katherine et al. demonstrated that cadmium sulfide (CdS) nanocrystals can be used to photosensitize the nitrogenase molybdenum-iron (MoFe) protein, where light harvesting replaces ATP hydrolysis to drive the enzymatic reduction of N_2 into NH_3. This CdS:MoFe protein biohybrids provided a photochemical model for achieving light-driven N_2 reduction to NH_3. Therefore, these advantages are difficult to be obtained based on simply biological methods, such as gene mutation.

1.3.3 Biocorrosion

Microbially induced corrosion (MIC) indicates corrosion induced by the metabolic activities of microbes. Iron corrosion occurs in anaerobic environments such as underground buried oil and gas pipelines and storage tanks is predominantly MIC process. MIC of these underground infrastructures causes oil spill and gas leakage, which severely pollute our environments. The economic losses caused by MIC is enormous. It has been estimated that corrosion costs equivalent to about 3%–4% of each nation's gross domestic product (GDP) [175], and 20–30% of corrosion costs are MIC related [176]. In addition, biocorrosion also occurs on tooth or implants surface which cause tooth decay or even loss. Therefore, studying the MIC mechanisms has attracted much attention in the industry and tooth healthy.

While MIC has been studied using various types of microbes including sulfate-reducing bacteria (SRB), nitrate-reducing bacteria, and iron-reducing bacteria, SRB have been recognized as the major cause of MIC, especially in anaerobic marine and soil environments where SRB thrive [18]. SRB were long considered to corrode iron by producing corrosive hydrogen sulfide, which is known as the

chemical MIC mechanism, or consume cathodic hydrogen accumulated on iron to promote anodic iron dissolution. However, neither mechanism could explain the persistent high-rate corrosion behavior observed even after the iron surface has been fully covered by corrosion products. On the other hand, followed by the isolation of highly corrosive sedimentary SRB strains, IS5 and *Desulfobacterium corrodens* IS4 , which can utilize metal iron as the sole electron donor, a new electrical MIC (EMIC) model in which SRB directly extract electrons from iron was proposed [62]. EMIC model best explains observed corrosion behavior in real corrosion sites, and thus the EEU process by SRB has been considered to be the crucial cause for MIC and identifying EEU pathways in SRB has received much attention to understand the MIC mechanism and develop new anti-EMIC methods.

The formation of dental plaque on the surface of teeth or restorative materials exhibits the ability to alter their surface properties, thereby contributing to the occurrence of MIC [177]. This change can facilitate the accumulation of bacteria, thereby potentially compromising the long-term durability of the human tooth and dental restoration. Several types of sulfate-reducing bacteria can transiently occur in the oral cavity and potentially contribute to biocorrosion processes, including bacteria from the *Desulfovibrio* (*desulfuricans, fairfieldensis*) and *Desulfotomaculum nigrificans* genera [178]. Within the oral environment, a coexistence of microorganisms capable of sulfate reduction, such as *Bacteroides corrodens*, sulfur-oxidizing bacteria like *Thiotrix*, and acid-producing bacteria such as *Lactobacilli* and *Streptococcus*, is observed [179]. It was found that *P. gingivalis*, an important biomarker of periodontitis, can also generate acids during the fermentation of amino acids and EET process with glucose oxidation [90, 180]. The biocorrosion of dental material is mainly caused by the corrosive acids produced by oral microbes, whose metabolites consist of various organic acids such as formic, succinic, or citric [181]. These microorganisms form biofilms, which have been identified as a significant risk factor for the biological corrosion of dental alloys. The disorder of oral microbes can also cause systemic diseases. There are lots of studies focus on the inhibition of acid production in dental plaque bacteria to prevent biocorrosion of dental material [182].

1.4 Extracellular electron transport based biosensor for biocorrosion

EAMs have been commonly applied to microbial fuel cells, biosynthesis and bioremediation [183].

In fact, there are many EAMs can act as biomarkers to reflect or predict the condition in specific environment. For instance, electroactive bacteria for biocorrosion can be detected to diagnosis of MIC in the surrounding environment of dental materials and oil or gas pipelines. EET-based biosensors have garnered significant interest for their potential application in self-powered portable biosensing devices, offering the opportunity for long-term and remote environmental monitoring [22]. In the realm of environmental biosensing, one prominent application of EET-based biosensors lies in the analysis of biological oxygen demand (BOD) for wastewater monitoring, which well-known as MFC-based biosensors [184, 185]. In this context, a stable current output is typically associated with specific levels of organic matter concentration. Beyond BOD analysis, microbial current production has been employed for the detection of various other toxins, including heavy metals such as copper, chromium, or zinc, and organic compounds such as diazinon, PCBs, p-nitrophenol, and levofloxacin [184, 186]. These EET-based biosensors offer the advantage of reducing analysis time (ranging from minutes to hours) and minimizing workload compared to traditional analytical approaches.

However, there is few studies focusing on EET-based biosensors of specific strain till now. This is primarily due to the ongoing fundamental research on the mechanisms underlying extracellular electron transfer in most microorganisms. Furthermore, the ability of bacteria to transfer electrons outside the cell is generally weak and challenging to detect directly. The rate enhancement of electron transfer is important not only for energy and environmental biotechnology but also for microbially induced events in natural environments [187]. Consequently, the majority of research efforts have been directed towards microbial fuel cells and microbial electrosynthesis technologies [142]. The existing biosensors predominantly concentrate on specific antibody recognition and the exploration of suitable electrode materials or electrochemical approaches to enhance sensor sensitivity [188-190]. In contrast, the utilization of microorganisms' extracellular electron transfer function as a distinct microbial electrochemical sensor does not require biological modification of the electrode, ensuring electrode stability. However, when applied to complex sample detection, this approach loses specificity. To address this, it is crucial to investigate the specificity of different microbial electricity production processes and the influence of physical characteristics of the electrode on microbial electricity generation. By studying these factors, it becomes possible to effectively enhance the specificity and

sensitivity of microbial electrochemical sensors.

1.4.1 The effect of electrode surface properties on extracellular electron transfer-based biosensor

The surface properties (such as surface charge, surface wettability, roughness, topography, stiffness) influence the biofilm formation on solid extracellular substances (eg. minerals, electrodes dental materials or pipes) [191, 192], which may also affect the redox state of outer membrane (OMCs) for electron transfer, inducing quicker or lower electron transfer rate on the substances' surface [193]. An increase in surface roughness augments the available surface area for bacterial attachment, thereby serving as a scaffold for adhesion [194]. The initial adhesion of microbes is very essential for the formation of biofilm, which is more difficult to be killed or removed. This plays a key role in persistence of biofoulings in both medical and industrial settings. Electrode surfaces characterized by positive charges, high functionalization, and hydrophilicity exhibited favorable conditions for the growth of uniform biofilms of *Shewanella oneidensis* MR-1 [195]. Moreover, these surfaces facilitated efficient electron transfer processes. These results indicate the EET capability can be regulated by modifying the substance surface.

The effects of material properties on dental bacterial adhesion, biofilm formation and EET process have been well studied [196]. However, few researches focus on the influence of material properties on EEU process of sulfate-reducing bacteria, which is the main cause of microbially influenced corrosion. Based on the surface properties influence of EET process, it is possible that the surface properties of substances have effect on EEU process of SRB. Studying these influences and regular pattern give advice to remove and prevent biocorrosion. Moreover, regardless of multiple studies on the EEU mechanism of IS5, it remains unclear whether this bacterium could use a direct mechanism. While it has been suggested that IS5 use outer-membrane cytochromes (OMCs) for EEU [197, 198], the direct EEU mechanism was suggested only by the observation of immediate current increase following the addition of IS5 cells on electrodes, which shouldn't contain redox mediators [197]. Given the construction of mutant strain lacking OMCs is technically difficult, direct EEU mechanism via OMCs is still not fully confirmed. Recently, a few studies have demonstrated that electrode hydrophilicity altered the interaction between OMCs and electrode, and enhanced current production in the iron-reducing bacterium *Shewanella loihica* PV-4 on anodes [199, 200]. Also, the electrode wettability can impact cell

attachment [201] and protein redox properties on electrode [202]. Given that the cell-electrode interface is inevitable for direct EEU mechanism to occur, it is highly likely that wettability impacts EEU especially in the case of a direct mechanism without using mediator shuttles. In this study, the author investigated how electrode wettability affects cell adhesion and EEU in IS5.

1.4.2 EET-based biosensor for detection of oral pathogen - a novel noninvasive diagnostic methodology for home-care

The microbiome is a crucial constituent of the human organism, influencing diverse physiological processes both within and beyond the body [4]. Notably, bacterial populations comprise a substantial component of the human microbiota, extensively colonizing various bodily compartments, including blood, tissue surfaces, interstitial fluid, and saliva [203]. Bacteria play a crucial role in maintaining the normal metabolic functions of the human body, aiding in digestion, energy production, toxin breakdown, intestinal tract protection, and immune system enhancement [204]. However, an imbalance in the bacterial flora or the presence of pathogenic microorganisms can lead to inflammation and pathological changes in the body [75]. Certain pathogens can serve as biomarkers for specific diseases, such as *Klebsiella pneumoniae* for gut disease and *P. gingivalis* for Alzheimer's disease and periodontitis [205, 206]. Numerous studies have been conducted to investigate the pathogenic mechanisms of various pathogens and identify suitable methods for diagnosing and treating clinical diseases. The current study focuses specifically on periodontal pathogens that are responsible for periodontitis.

Periodontal diseases are highly prevalent globally, particularly among the elderly, which can cause gum inflammation, tooth decay, pain, bleeding, and even tooth loss [207]. Periodontitis, which is a common dysbiotic oral disease, increases the risk of systemic inflammatory diseases in patients. The disruption of the steady state of oral microbial communities due to an imbalance in the relative abundance or emergence of diversely functioning flora leads to the formation of pathogenic microbial communities [2]. As the elderly population continues to grow, the incidence of periodontal diseases caused by oral pathogens is rising worldwide. Clinical detection of periodontitis is typically performed through probing depth or bleeding-on-probing, which is inconvenient, expensive, and requires a certain degree of disease progression before successful test results can be obtained [208]. Thus, the development of a low-cost and reliable home diagnosis of oral pathogens is a promising solution to the drawbacks of

clinical methods. Currently, 16s rRNA gene sequencing is the only commercial method available for home diagnosis; however, it is expensive, time-consuming, and requires sending samples to an analysis agency. Therefore, there is a significant need for a new diagnosis for home care. It has been proved that the appearance of "red" complex, consisting of *P. gingivalis*, *Treponema denticola*, and *Bacteroides forsythus*, is closely corelated to periodontitis progress[209-211] in many areas, such as Japan [212], China [213] and Indian [214]. Among these three pathogens, *P. gingivalis* is considered a significant biomarker and predictor of periodontitis. Therefore, the development of an easy-to-use and inexpensive biosensor that targets *P. gingivalis* is a viable approach to detect and predict periodontitis.

Conventional methods for detecting *P. gingivalis* include culturing, polymerase chain reaction (PCR), DNA probing, and the enzyme-linked immunosorbent assay (ELISA) [215]. However, these methods are laborious, time-consuming, expensive, or require unstable reagents, making them unsuitable for practical chair-side applications. Although much research has been conducted to develop *P. gingivalis* biosensors in conjunction with traditional methods, no practical applications have emerged due to their complexity, time-consuming nature, or cost [216, 217]. Electrochemical salivary biosensors offer promise for home care as they can be made into sensitive, handheld devices [218]. Nevertheless, few studies have focused on this approach. Thus, the development of a non-invasive and easy-to-use electrochemical sensor for the detection of *P. gingivalis* is highly desirable for point-of-care diagnosis and hygiene.

In the recent discoveries of Prof. Okamoto's group, the extracellular electron transfer (EET) capability was found in *P. gingivalis* and several other oral pathogens (eg. *Streptococcus mutans* (Sm), *Corynebacterium matruchotii* (Co), *Aggregatibacter actinomycetemcomitans* (Aa), and *Corynebacterium matruchotii* (Cm)) [90-93]. The electricity-generating ability of these pathogenic bacteria can enable the in-situ metabolic activity monitoring and the evaluation of drug resistance. The utilization of electrochemical measurement as a means of detecting these oral pathogens in saliva is a potential diagnostic tool for periodontitis. The development and implementation of an EET-based biosensor for the detection of periodontal pathogens represent a viable and impactful approach towards enabling at-home diagnosis of periodontal diseases. The identification and comprehensive understanding of the underlying reasons and mechanisms behind EET in pathogenic bacteria play a

pivotal role in unraveling the intricate dynamics of infection and disease progression. The oral biofilm primarily harbors anaerobic bacteria, which relies on EET as an alternative energy synthesis mechanism rather than oxygen respiration. These bacteria adeptly utilize the cell debris present within the oral biofilm, which contains amino acids, as both a carbon source and an electron donor. Notably, *P. gingivalis*, a prominent periodontal pathogen, demonstrates asaccharolytic behavior and cannot sustain its survival solely on glucose or carbohydrates [219]. It derives its energy from the metabolism of amino acids [180, 220]. Hence, it is conceivable that the utilization of amino acid metabolism-linked EET holds promise for the development of a targeted EET-based biosensor specifically designed for the detection of *P. gingivalis* in saliva. Although significant research has been conducted on the classification and mechanisms of pathogenic microorganisms in the oral cavity, there remains a lack of investigation regarding the utilization of their electrochemical properties for the development of novel biosensors. In this study, our investigation focused on elucidating the distinctive EET capabilities associated with various substrates including amino acids, peptides and sugars, with the objective of identifying specific substrates that promote current production specifically in the context of the periodontal pathogen *P. gingivalis*. Additionally, the application of redox mediators was explored as a means to enhance the current production while minimizing the required induction period, which are crucial parameters for optimizing the sensitivity of the biosensor.

1.5 Outline of thesis

As described above, the biosensor of electrogenic bio-corrosive bacteria serves a straightforward and readily implementable design, rendering it accessible for practical application to diagnose environmental biocorrosion compared with other biosensors. Furthermore, this biosensor possesses the unique capability to assess cell activity and evaluate drug efficacy, surpassing the functionalities offered by alternative biosensor systems. The author mainly researched the extracellular electron transport process between two typical bio-corrosive species in different environments and electrodes to develop electrochemical biosensors. One is iron-corrosive bacteria *Desulfovibrio ferrophilus* IS5 (IS5), a model EEU bacteria for microbiologically influenced iron corrosion (MIC), and the other one is an EET-capable bacteria with undefined EET mechanism, *Porphyromonas gingivalis* (*P. gingivalis*), an

important periodontal pathogen causing dental corrosion.

In this thesis, the electrical interaction between electrodes and electrogenic bio-corrosive bacteria (IS5 and *P. gingivalis*) was examined the to enhance biosensor sensitivity and selectivity. In detail, the effect of electrode surface property, metabolic pathway, and shuttles on electron transfer rate was studied. In Chapter 2, the author examined the impact of electrode wettability on the electron transport mechanism at the interfaces between cells and electrodes as well as the sensitivity of the EEU-based electrochemical biosensor of IS5. In Chapter 3 and Chapter 4, the author further studied the effect of substrate metabolism and redox mediators on the electron transfer process of bio-corrosive bacteria and designed a highly sensitive and specific EET-based electrochemical biosensor of *P. gingivalis* for the diagnosis of biocorrosion on the dental surface as well as periodontitis. Finally, in Chapter 5, conclusions, implications of this study, and future perspectives are discussed.

References

1. Gupta, A., R. Gupta, and R.L. Singh, *Microbes and Environment.* 2017: p. 43-84.
2. Hajishengallis, G., *Periodontitis: from microbial immune subversion to systemic inflammation.* Nat Rev Immunol, 2015. **15**(1): p. 30-44.
3. Hunter-Cevera, J., D. Karl, and M. Buckley, *American Academy of Microbiology Colloquia Reports*, in *Marine Microbial Diversity: The Key to Earth's Habitability: This report is based on a colloquium, sponsored by the American Academy of Microbiology, held April 8–10, 2005, in San Francisco, California*. 2005, American Society for Microbiology

Copyright 2005 American Academy of Microbiology.: Washington (DC).

4. Maurice, C.F. and P.J. Turnbaugh, *Quantifying the metabolic activities of human-associated microbial communities across multiple ecological scales.* FEMS Microbiol Rev, 2013. **37**(5): p. 830-48.
5. Allaband, C., et al., *Microbiome 101: Studying, Analyzing, and Interpreting Gut Microbiome Data for*

Clinicians. Clin Gastroenterol Hepatol, 2019. **17**(2): p. 218-230.

6. Marcos-Zambrano, L.J., et al., *Applications of Machine Learning in Human Microbiome Studies: A Review on Feature Selection, Biomarker Identification, Disease Prediction and Treatment.* Front Microbiol, 2021. **12**: p. 634511.

7. Sorbara, M.T. and E.G. Pamer, *Microbiome-based therapeutics.* Nat Rev Microbiol, 2022. **20**(6): p. 365-380.

8. Joubert, W.A. and T.J. Britz, *Characterization of aerobic, facultative anaerobic, and anaerobic bacteria in an acidogenic phase reactor and their metabolite formation.* Microb Ecol, 1987. **13**(2): p. 159-68.

9. Kumar, R., L. Singh, and A.W. Zularisam, *Exoelectrogens: Recent advances in molecular drivers involved in extracellular electron transfer and strategies used to improve it for microbial fuel cell applications.* Renewable and Sustainable Energy Reviews, 2016. **56**: p. 1322-1336.

10. Deng, X. and A. Okamoto, *Electrode Potential Dependency of Single-Cell Activity Identifies the Energetics of Slow Microbial Electron Uptake Process.* Front Microbiol, 2018. **9**: p. 2744.

11. Lovley, D.R., *Bug juice: harvesting electricity with microorganisms.* Nat. Rev. Microbiol., 2006. **4**(7): p. 497-508.

12. Shi, L., et al., *Extracellular electron transfer mechanisms between microorganisms and minerals.* Nature Reviews Microbiology, 2016. **14**(10): p. 651-662.

13. Rabaey, K. and R.A. Rozendal, *Microbial electrosynthesis - revisiting the electrical route for microbial production.* Nat. Rev. Microbiol., 2010. **8**(10): p. 706-16.

14. Belkin, S., *Microbial whole-cell sensing systems of environmental pollutants.* Curr Opin Microbiol, 2003. **6**(3): p. 206-12.

15. Kato, S., K. Hashimoto, and K. Watanabe, *Microbial interspecies electron transfer via electric currents*

through conductive minerals. Proc. Natl. Acad. Sci. USA, 2012. **109**(25): p. 10042-10046.

16. McGlynn, S.E., et al., *Single cell activity reveals direct electron transfer in methanotrophic consortia.* Nature, 2015. **526**(7574): p. 531-5.

17. Dinh, H.T., et al., *Iron corrosion by novel anaerobic microorganisms.* Nature, 2004. **427**(6977): p. 829-32.

18. Enning, D. and J. Garrelfs, *Corrosion of iron by sulfate-reducing bacteria: new views of an old problem.* Appl Environ Microbiol, 2014. **80**(4): p. 1226-36.

19. Tang, H.Y., et al., *Iron Corrosion via Direct Metal-Microbe Electron Transfer.* mBio, 2019. **10**(3).

20. Little, B.J., et al., *Microbially influenced corrosion—Any progress?* Corrosion Science, 2020. **170**.

21. Dou, W., D. Xu, and T. Gu, *Biocorrosion caused by microbial biofilms is ubiquitous around us.* Microb Biotechnol, 2021. **14**(3): p. 803-805.

22. Simonte, F., et al., *Extracellular Electron Transfer and Biosensors.* Adv Biochem Eng Biotechnol, 2019. **167**: p. 15-38.

23. Kim, M., et al., *A novel biomonitoring system using microbial fuel cells.* J Environ Monit, 2007. **9**(12): p. 1323-8.

24. Chang, I.S., et al., *Continuous determination of biochemical oxygen demand using microbial fuel cell type biosensor.* Biosens Bioelectron, 2004. **19**(6): p. 607-13.

25. Dziurkowska, E. and M. Wesolowski, *Solid Phase Extraction Purification of Saliva Samples for Antipsychotic Drug Quantitation.* Molecules, 2018. **23**(11).

26. Locey, K.J. and J.T. Lennon, *Scaling laws predict global microbial diversity.* Proc Natl Acad Sci U S A, 2016. **113**(21): p. 5970-5.

27. Borchers, A. and T. Pieler, *Programming pluripotent precursor cells derived from Xenopus embryos to*

generate specific tissues and organs. Genes (Basel), 2010. **1**(3): p. 413-26.

28. Struzycka, I., *The oral microbiome in dental caries.* Pol J Microbiol, 2014. **63**(2): p. 127-35.

29. Marsh, P.D. and E. Zaura, *Dental biofilm: ecological interactions in health and disease.* J Clin Periodontol, 2017. **44 Suppl 18**: p. S12-s22.

30. Beech, I.B. and J. Sunner, *Biocorrosion: towards understanding interactions between biofilms and metals.* Curr Opin Biotechnol, 2004. **15**(3): p. 181-6.

31. Yang, Y., et al., *Biofilm Formation and Biofouling Development on Different Ultrafiltration Membranes by Natural Anaerobes from an Anaerobic Membrane Bioreactor.* Environ Sci Technol, 2022. **56**(14): p. 10339-10348.

32. Chabert, N., O. Amin Ali, and W. Achouak, *All ecosystems potentially host electrogenic bacteria.* Bioelectrochemistry, 2015. **106**(Pt A): p. 88-96.

33. Lin, X., et al., *Liposoluble quinone promotes the reduction of hydrophobic mineral and extracellular electron transfer of Shewanella oneidensis MR-1.* Innovation (N Y), 2021. **2**(2): p. 100104.

34. Seeliger, S., R. Cord-Ruwisch, and B. Schink, *A periplasmic and extracellular c-type cytochrome of Geobacter sulfurreducens acts as a ferric iron reductase and as an electron carrier to other acceptors or to partner bacteria.* J Bacteriol, 1998. **180**(14): p. 3686-91.

35. Long, X., et al., *Microbial fuel cell-photoelectrocatalytic cell combined system for the removal of azo dye wastewater.* Bioresour Technol, 2017. **244**(Pt 1): p. 182-191.

36. Ucar, D., Y. Zhang, and I. Angelidaki, *An Overview of Electron Acceptors in Microbial Fuel Cells.* Front Microbiol, 2017. **8**: p. 643.

37. Munoz-Cupa, C., et al., *An overview of microbial fuel cell usage in wastewater treatment, resource recovery and energy production.* Sci Total Environ, 2021. **754**: p. 142429.

38. Gavrilov, S.N., et al., *Novel Extracellular Electron Transfer Channels in a Gram-Positive Thermophilic Bacterium.* Front Microbiol, 2020. **11**: p. 597818.

39. Scheller, S., et al., *Artificial electron acceptors decouple archaeal methane oxidation from sulfate reduction.* Science, 2016. **351**(6274): p. 703-7.

40. Gu, T., et al., *Toward a better understanding of microbiologically influenced corrosion caused by sulfate reducing bacteria.* Journal of Materials Science & Technology, 2019. **35**(4): p. 631-636.

41. Kushkevych, I., D. Dordević, and M. Vítězová, *Possible synergy effect of hydrogen sulfide and acetate produced by sulfate-reducing bacteria on inflammatory bowel disease development.* J Adv Res, 2021. **27**: p. 71-78.

42. Venzlaff, H., et al., *Accelerated cathodic reaction in microbial corrosion of iron due to direct electron uptake by sulfate-reducing bacteria.* Corrosion Science, 2013. **66**: p. 88-96.

43. Zhang, P., et al., *Electron mediators accelerate the microbiologically influenced corrosion of 304 stainless steel by the Desulfovibrio vulgaris biofilm.* Bioelectrochemistry, 2015. **101**: p. 14-21.

44. Drake, H.L., K. Küsel, and C. Matthies, *Ecological consequences of the phylogenetic and physiological diversities of acetogens.* Antonie Van Leeuwenhoek, 2002. **81**(1-4): p. 203-13.

45. Saheb-Alam, S., et al., *Effect of Start-Up Strategies and Electrode Materials on Carbon Dioxide Reduction on Biocathodes.* Appl Environ Microbiol, 2018. **84**(4).

46. Aryal, N., et al., *Highly Conductive Poly(3,4-ethylenedioxythiophene) Polystyrene Sulfonate Polymer Coated Cathode for the Microbial Electrosynthesis of Acetate From Carbon Dioxide.* Frontiers in Energy Research, 2018. **6**.

47. Zeppilli, M., et al., *Bioelectrochemical vs hydrogenophilic approach for CO2 reduction into methane and acetate.* Chemical Engineering Journal, 2020. **396**.

48. Sørensen, K.B., K. Finster, and N.B. Ramsing, *Thermodynamic and Kinetic Requirements in Anaerobic Methane Oxidizing Consortia Exclude Hydrogen, Acetate, and Methanol as Possible Electron Shuttles.* Microb Ecol, 2001. **42**(1): p. 1-10.

49. Pancost, R.D., et al., *Biomarker evidence for widespread anaerobic methane oxidation in Mediterranean sediments by a consortium of methanogenic archaea and bacteria. The Medinaut Shipboard Scientific Party.* Appl Environ Microbiol, 2000. **66**(3): p. 1126-32.

50. Lovley, D.R. and E.J. Phillips, *Novel mode of microbial energy metabolism: organic carbon oxidation coupled to dissimilatory reduction of iron or manganese.* Appl Environ Microbiol, 1988. **54**(6): p. 1472-80.

51. Myers, C.R. and K.H. Nealson, *Bacterial manganese reduction and growth with manganese oxide as the sole electron acceptor.* Science, 1988. **240**(4857): p. 1319-21.

52. Shi, L., et al., *Extracellular electron transfer mechanisms between microorganisms and minerals.* Nat Rev Microbiol, 2016. **14**(10): p. 651-62.

53. Lovley, D.R., D.E. Holmes, and K.P. Nevin, *Dissimilatory Fe(III) and Mn(IV) reduction.* Adv Microb Physiol, 2004. **49**: p. 219-86.

54. Jiang, X., et al., *Nanoparticle facilitated extracellular electron transfer in microbial fuel cells.* Nano Lett, 2014. **14**(11): p. 6737-42.

55. Deng, X., et al., *Biogenic Iron Sulfide Nanoparticles to Enable Extracellular Electron Uptake in Sulfate-Reducing Bacteria.* Angew Chem Int Ed Engl, 2020. **59**(15): p. 5995-5999.

56. Deng, X., et al., *Enhancement of cell growth by uncoupling extracellular electron uptake and oxidative stress production in sediment sulfate-reducing bacteria.* Environ Int, 2020. **144**: p. 106006.

57. Gupta, D., et al., *Photoferrotrophs Produce a PioAB Electron Conduit for Extracellular Electron Uptake.*

mBio, 2019. **10**(6).

58. Gupta, D., M.S. Guzman, and A. Bose, *Extracellular electron uptake by autotrophic microbes: physiological, ecological, and evolutionary implications.* J Ind Microbiol Biotechnol, 2020. **47**(9-10): p. 863-876.

59. Schütz, M.K., et al., *Impact of iron-reducing bacteria on the corrosion rate of carbon steel under simulated geological disposal conditions.* Environ Sci Technol, 2015. **49**(12): p. 7483-90.

60. Benck, J.D., et al., *Substrate selection for fundamental studies of electrocatalysts and photoelectrodes: inert potential windows in acidic, neutral, and basic electrolyte.* PloS one, 2014. **9**(10): p. e107942-e107942.

61. Deng, X., et al., *Electron Extraction from an Extracellular Electrode by Desulfovibrio ferrophilus Strain IS5 Without Using Hydrogen as an Electron Carrier.* Electrochemistry, 2015. **83**(7): p. 529-531.

62. Beese-Vasbender, P.F., et al., *Electrochemical characterization of direct electron uptake in electrical microbially influenced corrosion of iron by the lithoautotrophic SRB Desulfopila corrodens strain IS4.* Electrochimica Acta, 2015. **167**: p. 321-329.

63. Uchiyama, T., et al., *Iron-corroding methanogen isolated from a crude-oil storage tank.* Appl Environ Microbiol, 2010. **76**(6): p. 1783-8.

64. Palacios, P.A., et al., *Baltic Sea methanogens compete with acetogens for electrons from metallic iron.* ISME J, 2019. **13**(12): p. 3011-3023.

65. Tsurumaru, H., et al., *An extracellular [NiFe] hydrogenase mediating iron corrosion is encoded in a genetically unstable genomic island in Methanococcus maripaludis.* Sci Rep, 2018. **8**(1): p. 15149.

66. Beese-Vasbender, P.F., et al., *Selective microbial electrosynthesis of methane by a pure culture of a marine lithoautotrophic archaeon.* Bioelectrochemistry, 2015. **102**: p. 50-5.

67. Rowe, A.R., et al., *Methane-Linked Mechanisms of Electron Uptake from Cathodes by Methanosarcina barkeri.* mBio, 2019. **10**(2).

68. Picard, A., A. Gartman, and P.R. Girguis, *What Do We Really Know about the Role of Microorganisms in Iron Sulfide Mineral Formation?* Frontiers in Earth Science, 2016. **4**.

69. Picard, A., et al., *Sulfate-reducing bacteria influence the nucleation and growth of mackinawite and greigite.* Geochimica et Cosmochimica Acta, 2018. **220**: p. 367-384.

70. Eduok, U., E. Ohaeri, and J. Szpunar, *Accelerated corrosion of pipeline steel in the presence of Desulfovibrio desulfuricans biofilm due to carbon source deprivation in CO2 saturated medium.* Materials Science and Engineering: C, 2019. **105**: p. 110095.

71. Chen, Y., et al., *Long-term survival of Desulfovibrio vulgaris on carbon steel and associated pitting corrosion.* Corrosion Science, 2015. **90**: p. 89-100.

72. Viggi, C.C., et al., *Conductive Magnetite Nanoparticles Enhance the Microbial Electrosynthesis of Acetate from CO2 while Diverting Electrons away from Methanogenesis.* Fuel Cells, 2020. **20**(1): p. 98-106.

73. Xu, D. and T. Gu, *Carbon source starvation triggered more aggressive corrosion against carbon steel by the Desulfovibrio vulgaris biofilm.* International Biodeterioration & Biodegradation, 2014. **91**: p. 74-81.

74. Gao, L., et al., *Oral microbiomes: more and more importance in oral cavity and whole body.* Protein Cell, 2018. **9**(5): p. 488-500.

75. Hou, K., et al., *Microbiota in health and diseases.* Signal Transduct Target Ther, 2022. **7**(1): p. 135.

76. Daniluk, T., et al., *Aerobic and anaerobic bacteria in subgingival and supragingival plaques of adult patients with periodontal disease.* Adv Med Sci, 2006. **51 Suppl 1**: p. 81-5.

77. Lovegrove, J.M., *Dental plaque revisited: bacteria associated with periodontal disease.* J N Z Soc

Periodontol, 2004(87): p. 7-21.

78. Mark Welch, J.L., et al., *Biogeography of a human oral microbiome at the micron scale.* Proc Natl Acad Sci U S A, 2016. **113**(6): p. E791-800.

79. van Winkelhoff, A.J., et al., *Porphyromonas gingivalis, Bacteroides forsythus and other putative periodontal pathogens in subjects with and without periodontal destruction.* J Clin Periodontol, 2002. **29**(11): p. 1023-8.

80. Ahn, J., C.Y. Chen, and R.B. Hayes, *Oral microbiome and oral and gastrointestinal cancer risk.* Cancer Causes Control, 2012. **23**(3): p. 399-404.

81. Casanova, L., F.J. Hughes, and P.M. Preshaw, *Diabetes and periodontal disease.* BDJ Team, 2015. **1**(1).

82. Bourgeois, D., et al., *Periodontal Pathogens as Risk Factors of Cardiovascular Diseases, Diabetes, Rheumatoid Arthritis, Cancer, and Chronic Obstructive Pulmonary Disease-Is There Cause for Consideration?* Microorganisms, 2019. **7**(10).

83. Bansal, M., M. Khatri, and V. Taneja, *Potential role of periodontal infection in respiratory diseases - a review.* J Med Life, 2013. **6**(3): p. 244-8.

84. Dong, J., et al., *Relationships Between Oral Microecosystem and Respiratory Diseases.* Front Mol Biosci, 2021. **8**: p. 718222.

85. Jungbauer, G., et al., *Periodontal microorganisms and Alzheimer disease - A causative relationship?* Periodontol 2000, 2022. **89**(1): p. 59-82.

86. Ren, H. and M. Du, *Role of Maternal Periodontitis in Preterm Birth.* Front Immunol, 2017. **8**: p. 139.

87. Nagao, Y. and T. Tanigawa, *Red complex periodontal pathogens are risk factors for liver cirrhosis.* Biomed Rep, 2019. **11**(5): p. 199-206.

88. Yoshizawa, J.M., et al., *Salivary biomarkers: toward future clinical and diagnostic utilities.* Clin

Microbiol Rev, 2013. **26**(4): p. 781-91.

89. Ryder, M.I., *Porphyromonas gingivalis and Alzheimer disease: Recent findings and potential therapies.* J Periodontol, 2020. **91 Suppl 1**(Suppl 1): p. S45-s49.

90. Naradasu, D., et al., *Electrochemical Characterization of Current-Producing Human Oral Pathogens by Whole-Cell Electrochemistry.* ChemElectroChem, 2020. **7**(9): p. 2012-2019.

91. Naradasu, D., et al., *Microbial current production from Streptococcus mutans correlates with biofilm metabolic activity.* Biosens Bioelectron, 2020. **162**: p. 112236.

92. Zhang, S., et al., *A Human Pathogen Capnocytophaga Ochracea Exhibits Current Producing Capability.* Electrochemistry, 2020. **88**(3): p. 224-229.

93. Naradasu, D., W. Miran, and A. Okamoto, *Metabolic Current Production by an Oral Biofilm Pathogen Corynebacterium matruchotii.* Molecules, 2020. **25**(14).

94. Lovley, D., Stolz, J., Nord, G., *Anaerobic production of magnetite by a dissimilatory iron-reducing microorganism.* Nature 1987. **330**: p. 252–254.

95. Hernandez, M., Newman, D., *Extracellular electron transfer.* Cellular and Molecular Life Sciences CMLS, 2001. **58**: p. 1562–1571.

96. Gregory, K.B., D.R. Bond, and D.R. Lovley, *Graphite electrodes as electron donors for anaerobic respiration.* Environ Microbiol, 2004. **6**(6): p. 596-604.

97. Rosenbaum, M., et al., *Cathodes as electron donors for microbial metabolism: which extracellular electron transfer mechanisms are involved?* Bioresour Technol, 2011. **102**(1): p. 324-33.

98. Myers, C.R. and J.M. Myers, *Localization of cytochromes to the outer membrane of anaerobically grown Shewanella putrefaciens MR-1.* J Bacteriol, 1992. **174**(11): p. 3429-38.

99. Okamoto, A., et al., *Bound Flavin Model Suggests Similar Electron-Transfer Mechanisms in Shewanella*

and Geobacter. ChemElectroChem, 2014. **1**(11): p. 1808-1812.

100. Newman, D.K. and R. Kolter, *A role for excreted quinones in extracellular electron transfer.* Nature, 2000. **405**(6782): p. 94-7.

101. Derek R. Lovley, J.D.C., Elizabeth L. Blunt-Harris, Elizabeth J. P. Phillips, Joan C. Woodward *Humic substances as electron acceptors for microbial respiration.* Nature, 1996(382): p. 445–448.

102. You, L.X., et al., *Flavins mediate extracellular electron transfer in Gram-positive Bacillus megaterium strain LLD-1.* Bioelectrochemistry, 2018. **119**: p. 196-202.

103. Edwards, M.J., et al., *The Crystal Structure of a Biological Insulated Transmembrane Molecular Wire.* Cell, 2020. **181**(3): p. 665-673 e10.

104. Watanabe, H.C., Y. Yamashita, and H. Ishikita, *Electron transfer pathways in a multiheme cytochrome MtrF.* Proc Natl Acad Sci U S A, 2017. **114**(11): p. 2916-2921.

105. Tanaka, K., et al., *Extracellular Electron Transfer via Outer Membrane Cytochromes in a Methanotrophic Bacterium Methylococcus capsulatus (Bath).* Front Microbiol, 2018. **9**: p. 2905.

106. Castelle, C., et al., *A new iron-oxidizing/O2-reducing supercomplex spanning both inner and outer membranes, isolated from the extreme acidophile Acidithiobacillus ferrooxidans.* J Biol Chem, 2008. **283**(38): p. 25803-11.

107. Keffer, J.L., et al., *Iron Oxidation by a Fused Cytochrome-Porin Common to Diverse Iron-Oxidizing Bacteria.* mBio, 2021. **12**(4): p. e0107421.

108. Okamoto, A., et al., *Cell-secreted Flavins Bound to Membrane Cytochromes Dictate Electron Transfer Reactions to Surfaces with Diverse Charge and pH.* Sci. Rep., 2014. **4**: p. 5628.

109. Okamoto, A., et al., *Uptake of Self-secreted Flavins as Bound Cofactors for Extracellular Electron Transfer in Geobacter Species.* Energy Environ. Sci., 2014. **7**: p. 1357-1361.

110. Okamoto, A., et al., *Rate enhancement of bacterial extracellular electron transport involves bound flavin semiquinones.* Proc Natl Acad Sci U S A, 2013. **110**(19): p. 7856-61.

111. Reguera, G., et al., *Extracellular electron transfer via microbial nanowires.* Nature, 2005. **435**(7045): p. 1098-1101.

112. Gorby, Y.A., et al., *Electrically conductive bacterial nanowires produced by Shewanella oneidensis strain MR-1 and other microorganisms.* Proc Natl Acad Sci U S A, 2006. **103**(30): p. 11358-63.

113. Deng, X., et al., *Multi-heme cytochromes provide a pathway for survival in energy-limited environments.* Science advances, 2018. **4**(2): p. eaao5682.

114. Wong, G.C.L., et al., *Roadmap on emerging concepts in the physical biology of bacterial biofilms: from surface sensing to community formation.* Phys Biol, 2021. **18**(5).

115. Malvankar, N.S., et al., *Tunable metallic-like conductivity in microbial nanowire networks.* Nat Nanotechnol, 2011. **6**(9): p. 573-9.

116. Filman, D.J., et al., *Cryo-EM reveals the structural basis of long-range electron transport in a cytochrome-based bacterial nanowire.* Communications Biology, 2019. **2**(1): p. 219.

117. Wang, F., et al., *Structure of Microbial Nanowires Reveals Stacked Hemes that Transport Electrons over Micrometers.* Cell, 2019. **177**(2): p. 361-369.e10.

118. Summers, Z.M., et al., *Direct Exchange of Electrons Within Aggregates of an Evolved Syntrophic Coculture of Anaerobic Bacteria.* Science, 2010. **330**(6009): p. 1413-1415.

119. Yalcin, S.E. and N.S. Malvankar, *The blind men and the filament: Understanding structures and functions of microbial nanowires.* Curr Opin Chem Biol, 2020. **59**: p. 193-201.

120. Gu, Y., et al., *Structure of Geobacter pili reveals secretory rather than nanowire behaviour.* Nature, 2021. **597**(7876): p. 430-434.

121. Yalcin, S.E., et al., *Electric field stimulates production of highly conductive microbial OmcZ nanowires.* Nat Chem Biol, 2020. **16**(10): p. 1136-1142.

122. Pirbadian, S., et al., *Shewanella oneidensis MR-1 nanowires are outer membrane and periplasmic extensions of the extracellular electron transport components.* Proc Natl Acad Sci U S A, 2014. **111**(35): p. 12883-8.

123. Liang, D., et al., *Extracellular Electron Exchange Capabilities of Desulfovibrio ferrophilus and Desulfopila corrodens.* Environ Sci Technol, 2021.

124. Light, S.H., et al., *A flavin-based extracellular electron transfer mechanism in diverse Gram-positive bacteria.* Nature, 2018. **562**(7725): p. 140-144.

125. Li, X., et al., *Electron transfer capacity dependence of quinone-mediated Fe(III) reduction and current generation by Klebsiella pneumoniae L17.* Chemosphere, 2013. **92**(2): p. 218-24.

126. Rhodes, Z., et al., *Using structure-function relationships to understand the mechanism of phenazine-mediated extracellular electron transfer in Escherichia coli.* iScience, 2021. **24**(9): p. 103033.

127. Hu, M., et al., *Nano-Fe(3)C@PGC as a novel low-cost anode electrocatalyst for superior performance microbial fuel cells.* Biosens Bioelectron, 2019. **142**: p. 111594.

128. Rawson, F.J., A.J. Downard, and K.H. Baronian, *Electrochemical detection of intracellular and cell membrane redox systems in Saccharomyces cerevisiae.* Scientific Reports, 2014. **4**.

129. Marsili, E., et al., *Shewanella secretes flavins that mediate extracellular electron transfer.* Proceedings of the National Academy of Sciences, 2008. **105**(10): p. 3968-3973.

130. You, L.X., et al., *Extracellular electron transfer of Enterobacter cloacae SgZ-5T via bi-mediators for the biorecovery of palladium as nanorods.* Environ Int, 2019. **123**: p. 1-9.

131. Lovley, D.R., et al., *Reduction of humic substances and Fe(III) by hyperthermophilic microorganisms.*

Chemical Geology, 2000. **169**(3-4): p. 289-298.

132. Gupta, V.K., et al., *Equilibrium and Thermodynamic Studies on the Removal and Recovery of Safranine-T Dye from Industrial Effluents.* Separation Science and Technology, 2011. **46**(5): p. 839-846.

133. Okamoto, A., et al., *Proton Transport in the Outer-Membrane Flavocytochrome Complex Limits the Rate of Extracellular Electron Transport.* Angewandte Chemie International Edition, 2017. **56**(31): p. 9082-9086.

134. Tokunou, Y., et al., *Basicity of N5 in semiquinone enhances the rate of respiratory electron outflow in Shewanella oneidensis MR-1.* bioRxiv, 2019: p. 686493.

135. Lusk, B.G., et al., *pH Dependency in Anode Biofilms of Thermincola ferriacetica Suggests a Proton-Dependent Electrochemical Response.* Journal of the American Chemical Society, 2018. **140**(16): p. 5527-5534.

136. Vieira Lemos, R., et al., *Extracellular electron transfer by Microcystis aeruginosa is solely driven by high pH.* Bioelectrochemistry, 2021. **137**: p. 107637.

137. Li, S.L., et al., *Chemical Characteristics of Electron Shuttles Affect Extracellular Electron Transfer: Shewanella decolorationis NTOU1 Simultaneously Exploiting Acetate and Mediators.* Front Microbiol, 2019. **10**: p. 399.

138. Rowe, A.R., et al., *Tracking Electron Uptake from a Cathode into Shewanella Cells: Implications for Energy Acquisition from Solid-Substrate Electron Donors.* mBio, 2018. **9**(1).

139. Liu, X., L. Shi, and J.D. Gu, *Microbial electrocatalysis: Redox mediators responsible for extracellular electron transfer.* Biotechnol Adv, 2018. **36**(7): p. 1815-1827.

140. Ueki, T., *Cytochromes in Extracellular Electron Transfer in Geobacter.* Appl Environ Microbiol, 2021. **87**(10).

141. Zhang, Y.-C., Z.-H. Jiang, and Y. Liu, *Application of Electrochemically Active Bacteria as Anodic Biocatalyst in Microbial Fuel Cells.* Chinese Journal of Analytical Chemistry, 2015. **43**(1): p. 155-163.

142. Santoro, C., et al., *Microbial fuel cells: From fundamentals to applications. A review.* J Power Sources, 2017. **356**: p. 225-244.

143. Mathuriya, A.S., D.A. Jadhav, and M.M. Ghangrekar, *Architectural adaptations of microbial fuel cells.* Appl Microbiol Biotechnol, 2018. **102**(22): p. 9419-9432.

144. Grattieri, M. and S.D. Minteer, *Microbial fuel cells in saline and hypersaline environments: Advancements, challenges and future perspectives.* Bioelectrochemistry, 2018. **120**: p. 127-137.

145. Beyenal, H., et al., *Microbial fuel cells: Current trends and emerging applications.* Bioresour Technol, 2021. **324**: p. 124687.

146. Zhang, Q., J. Hu, and D.J. Lee, *Microbial fuel cells as pollutant treatment units: Research updates.* Bioresour Technol, 2016. **217**: p. 121-8.

147. Li, W.W. and G.P. Sheng, *Microbial fuel cells in power generation and extended applications.* Adv Biochem Eng Biotechnol, 2012. **128**: p. 165-97.

148. Van Hees, W., *A bacterial methane fuel cell.* Journal of the Electrochemical Society, 1965. **112**(3): p. 258–262.

149. Cohen, B., *The bacterial culture as an electrical half-cell.* Journal of Bacteriology, 1931. **21**: p. 18-19.

150. Yu, F., C. Wang, and J. Ma, *Applications of Graphene-Modified Electrodes in Microbial Fuel Cells.* Materials (Basel), 2016. **9**(10).

151. Yuan, H. and Z. He, *Graphene-modified electrodes for enhancing the performance of microbial fuel cells.* Nanoscale, 2015. **7**(16): p. 7022-9.

152. Zhang, Y., et al., *Analysis of functional genomes from metagenomes: Revealing the accelerated electron*

transfer in microbial fuel cell with rhamnolipid addition. Bioelectrochemistry, 2018. **119**: p. 59-67.

153. Yong, X.Y., et al., *Enhancement of bioelectricity generation by manipulation of the electron shuttles synthesis pathway in microbial fuel cells.* Bioresour Technol, 2014. **152**: p. 220-4.

154. Zhou, L., et al., *Soft-template assisted synthesis of Fe/N-doped hollow carbon nanospheres as advanced electrocatalysts for the oxygen reduction reaction in microbial fuel cells.* Journal of Materials Chemistry A, 2017. **5**(36): p. 19343-19350.

155. Wu, X., et al., *Anode modification by biogenic gold nanoparticles for the improved performance of microbial fuel cells and microbial community shift.* Bioresour Technol, 2018. **270**: p. 11-19.

156. Wang, R., et al., *FeS(2) Nanoparticles Decorated Graphene as Microbial-Fuel-Cell Anode Achieving High Power Density.* Adv Mater, 2018. **30**(22): p. e1800618.

157. Cheng, S., et al., *Biodegradation of metal complex Naphthol Green B and formation of iron-sulfur nanoparticles by marine bacterium Pseudoalteromonas sp CF10-13.* Bioresour Technol, 2019. **273**: p. 49-55.

158. Cui, Y., et al., *Biosynthesized iron sulfide nanoparticles by mixed consortia for enhanced extracellular electron transfer in a microbial fuel cell.* Bioresour Technol, 2020. **318**: p. 124095.

159. Vu, M.T., M.T. Noori, and B. Min, *Conductive magnetite nanoparticles trigger syntrophic methane production in single chamber microbial electrochemical systems.* Bioresour Technol, 2020. **296**: p. 122265.

160. Su, L., et al., *Synergistic improvement of Shewanella loihica PV-4 extracellular electron transfer using a TiO(2)@TiN nanocomposite.* Bioelectrochemistry, 2020. **134**: p. 107519.

161. Jiang, Y., et al., *Trifunctional modification of individual bacterial cells for magnet-assisted bioanodes with high performance in microbial fuel cells.* Journal of Materials Chemistry A, 2020. **8**(46): p. 24515-

24523.

162. Wang, C., et al., *Biochar facilitates rapid restoration of methanogenesis by enhancing direct interspecies electron transfer after high organic loading shock.* Bioresour Technol, 2021. **320**(Pt A): p. 124360.

163. Xian, J., et al., *α-FeOOH nanowires loaded on carbon paper anodes improve the performance of microbial fuel cells.* Chemosphere, 2021. **273**: p. 129669.

164. Cao, B., et al., *Silver nanoparticles boost charge-extraction efficiency in Shewanella microbial fuel cells.* Science, 2021. **373**(6561): p. 1336-1340.

165. Li, Z., et al., *Biosynthetic FeS/BC hybrid particles enhanced the electroactive bacteria enrichment in microbial electrochemical systems.* Sci Total Environ, 2021. **762**: p. 143142.

166. Bian, B., et al., *Microbial electrosynthesis from CO(2): Challenges, opportunities and perspectives in the context of circular bioeconomy.* Bioresour Technol, 2020. **302**: p. 122863.

167. Dessì, P., et al., *Microbial electrosynthesis: Towards sustainable biorefineries for production of green chemicals from CO(2) emissions.* Biotechnol Adv, 2021. **46**: p. 107675.

168. Prévoteau, A., et al., *Microbial electrosynthesis from CO(2): forever a promise?* Curr Opin Biotechnol, 2020. **62**: p. 48-57.

169. Liang, P., et al., *Carbon nanotube powders as electrode modifier to enhance the activity of anodic biofilm in microbial fuel cells.* Biosensors & Bioelectronics, 2011. **26**(6): p. 3000-3004.

170. Zou, L., et al., *Bacterial extracellular electron transfer: a powerful route to the green biosynthesis of inorganic nanomaterials for multifunctional applications.* J Nanobiotechnology, 2021. **19**(1): p. 120.

171. Kimber, R.L., et al., *Biosynthesis and Characterization of Copper Nanoparticles Using Shewanella oneidensis: Application for Click Chemistry.* Small, 2018. **14**(10).

172. Tian, L.J., et al., *Directed Biofabrication of Nanoparticles through Regulating Extracellular Electron*

Transfer. J Am Chem Soc, 2017. **139**(35): p. 12149-12152.

173. Stark, W.J., *Nanoparticles in biological systems.* Angew Chem Int Ed Engl, 2011. **50**(6): p. 1242-58.

174. Ijaz, I., et al., *Detail review on chemical, physical and green synthesis, classification, characterizations and applications of nanoparticles.* Green Chemistry Letters and Reviews, 2020. **13**(3): p. 223-245.

175. Koch, G., *1 - Cost of corrosion*, in *Trends in Oil and Gas Corrosion Research and Technologies*, A.M. El-Sherik, Editor. 2017, Woodhead Publishing: Boston. p. 3-30.

176. Koch, G.H., et al., *Chapter 1 - Cost of corrosion in the United States*, in *Handbook of Environmental Degradation of Materials*, M. Kutz, Editor. 2005, William Andrew Publishing: Norwich, NY. p. 3-24.

177. Nedeljkovic, I., *Effect of Oral Biofilms on Dental Materials: Biocorrosion and Biodeterioration*, in *Oral Biofilms and Modern Dental Materials : Advances Toward Bioactivity*, A.C. Ionescu and S. Hahnel, Editors. 2021, Springer International Publishing: Cham. p. 85-97.

178. Mystkowska, J., *Biocorrosion of dental alloys due to Desulfotomaculum nigrificans bacteria.* Acta Bioeng Biomech, 2016. **18**(4): p. 87-96.

179. Keller, M.K. and S. Twetman, *Acid production in dental plaque after exposure to probiotic bacteria.* BMC Oral Health, 2012. **12**: p. 44.

180. Takahashi, N., T. Sato, and T. Yamada, *Metabolic pathways for cytotoxic end product formation from glutamate- and aspartate-containing peptides by Porphyromonas gingivalis.* J Bacteriol, 2000. **182**(17): p. 4704-10.

181. Contuzzi, N., et al., *Metals Biotribology and Oral Microbiota Biocorrosion Mechanisms.* J Funct Biomater, 2022. **14**(1).

182. Hirasawa, M., K. Takada, and S. Otake, *Inhibition of acid production in dental plaque bacteria by green tea catechins.* Caries Res, 2006. **40**(3): p. 265-70.

183. Wang, Y.X., et al., *Advances in interfacial engineering for enhanced microbial extracellular electron transfer.* Bioresour Technol, 2022. **345**: p. 126562.

184. Zhou, T., et al., *Microbial Fuels Cell-Based Biosensor for Toxicity Detection: A Review.* Sensors (Basel), 2017. **17**(10).

185. Do, M.H., et al., *Challenges in the application of microbial fuel cells to wastewater treatment and energy production: A mini review.* Sci Total Environ, 2018. **639**: p. 910-920.

186. Do, M.H., et al., *Microbial fuel cell-based biosensor for online monitoring wastewater quality: A critical review.* Sci Total Environ, 2020. **712**: p. 135612.

187. Deng, X., D. Luo, and A. Okamoto, *Defined and unknown roles of conductive nanoparticles for the enhancement of microbial current generation: A review.* Bioresour Technol, 2022. **350**: p. 126844.

188. Lowe, C.R., *Biosensors.* Philos Trans R Soc Lond B Biol Sci, 1989. **324**(1224): p. 487-96.

189. Cesewski, E. and B.N. Johnson, *Electrochemical biosensors for pathogen detection.* Biosens Bioelectron, 2020. **159**: p. 112214.

190. Naresh, V. and N. Lee, *A Review on Biosensors and Recent Development of Nanostructured Materials-Enabled Biosensors.* Sensors (Basel), 2021. **21**(4).

191. Yoda, I., et al., *Effect of surface roughness of biomaterials on Staphylococcus epidermidis adhesion.* BMC Microbiol, 2014. **14**: p. 234.

192. Ammar, Y., et al., *Influence of surface roughness on the initial formation of biofilm.* Surface and Coatings Technology, 2015. **284**: p. 410-416.

193. Ding, C.M., et al., *Wettability-regulated extracellular electron transfer from the living organism of Shewanella loihica PV-4.* Angew Chem Int Ed Engl, 2015. **54**(5): p. 1446-51.

194. Zheng, S., et al., *Implication of Surface Properties, Bacterial Motility, and Hydrodynamic Conditions on*

Bacterial Surface Sensing and Their Initial Adhesion. Front Bioeng Biotechnol, 2021. **9**: p. 643722.

195. Artyushkova, K., et al., *Relationship between surface chemistry, biofilm structure, and electron transfer in Shewanella anodes.* Biointerphases, 2015. **10**(1): p. 019013.

196. Song, F., H. Koo, and D. Ren, *Effects of Material Properties on Bacterial Adhesion and Biofilm Formation.* J Dent Res, 2015. **94**(8): p. 1027-34.

197. Deng, X., et al., *Multi-heme cytochromes provide a pathway for survival in energy-limited environments.* Science Advances, 2018. **4**(2).

198. Deng, X., et al., *Enhancement of cell growth by uncoupling extracellular electron uptake and oxidative stress production in sediment sulfate-reducing bacteria.* Environment International, 2020. **144**.

199. Ding, C.M., et al., *Wettability-Regulated Extracellular Electron Transfer from the Living Organism of Shewanella loihica PV-4.* Angewandte Chemie-International Edition, 2015. **54**(5): p. 1446-1451.

200. Zhao, C., et al., *Hydrophilicity boosted extracellular electron transfer in Shewanella loihica PV-4.* Rsc Advances, 2016. **6**(27): p. 22488-22493.

201. Krasowska, A. and K. Sigler, *How microorganisms use hydrophobicity and what does this mean for human needs?* Frontiers in Cellular and Infection Microbiology, 2014. **4**(112).

202. Song, S., et al., *Characterization of Cytochrome-C Alkanethiolate Structures Prepared by Self-Assembly on Gold.* Journal of Physical Chemistry, 1993. **97**(24): p. 6564-6572.

203. Sender, R., S. Fuchs, and R. Milo, *Revised Estimates for the Number of Human and Bacteria Cells in the Body.* PLoS Biol, 2016. **14**(8): p. e1002533.

204. Zhang, Y.J., et al., *Impacts of gut bacteria on human health and diseases.* Int J Mol Sci, 2015. **16**(4): p. 7493-519.

205. Martin, R.M. and M.A. Bachman, *Colonization, Infection, and the Accessory Genome of Klebsiella*

pneumoniae. Front Cell Infect Microbiol, 2018. **8**: p. 4.

206. How, K.Y., K.P. Song, and K.G. Chan, *Porphyromonas gingivalis: An Overview of Periodontopathic Pathogen below the Gum Line.* Front Microbiol, 2016. **7**: p. 53.

207. Nazir, M.A., *Prevalence of periodontal disease, its association with systemic diseases and prevention.* Int J Health Sci (Qassim), 2017. **11**(2): p. 72-80.

208. Zimmermann, H., et al., *Pocket depth and bleeding on probing and their associations with dental, lifestyle, socioeconomic and blood variables: a cross-sectional, multicenter feasibility study of the German National Cohort.* BMC Oral Health, 2015. **15**: p. 7.

209. Jiang, Y., et al., *Comparison of Red-Complex Bacteria Between Saliva and Subgingival Plaque of Periodontitis Patients: A Systematic Review and Meta-Analysis.* Front Cell Infect Microbiol, 2021. **11**: p. 727732.

210. Suzuki, N., M. Yoneda, and T. Hirofuji, *Mixed red-complex bacterial infection in periodontitis.* Int J Dent, 2013. **2013**: p. 587279.

211. da Silva-Boghossian, C.M., et al., *Association of red complex, A. actinomycetemcomitans and non-oral bacteria with periodontal diseases.* Arch Oral Biol, 2011. **56**(9): p. 899-906.

212. Chigasaki, O., et al., *A cross-sectional study on the periodontal status and prevalence of red complex periodontal pathogens in a Japanese population.* J Oral Sci, 2018. **60**(2): p. 293-303.

213. Papapanou, P.N., et al., *Subgingival microbiota in adult Chinese: prevalence and relation to periodontal disease progression.* J Periodontol, 1997. **68**(7): p. 651-66.

214. Kugaji, M.S., et al., *Quantitative Evaluation of Porphyromonas gingivalis in Indian Subjects With Chronic Periodontitis by Real-Time Polymerase Chain Reaction.* Journal of Advanced Oral Research, 2019. **10**(2): p. 137-144.

215. Riggio, M.P., et al., *Comparison of polymerase chain reaction and culture methods for detection of Actinobacillus actinomycetemcomitans and Porphyromonas gingivalis in subgingival plaque samples.* J Periodontal Res, 1996. **31**(7): p. 496-501.

216. O'Brien-Simpson, N.M., et al., *Rapid Chair-Side Test for Detection of Porphyromonas gingivalis.* J Dent Res, 2017. **96**(6): p. 618-625.

217. O'Brien-Simpson, N.M., et al., *Development and evaluation of a saliva-based chair-side diagnostic for the detection of Porphyromonas gingivalis.* J Oral Microbiol, 2015. **7**: p. 29129.

218. Dong, T., et al., *Advances in Electrochemical Biosensors Based on Nanomaterials for Protein Biomarker Detection in Saliva.* Adv Sci (Weinh), 2023. **10**(6): p. e2205429.

219. Hendrickson, E.L., et al., *Pathway analysis for intracellular Porphyromonas gingivalis using a strain ATCC 33277 specific database.* BMC Microbiol, 2009. **9**: p. 185.

220. Naito, M., et al., *Determination of the genome sequence of Porphyromonas gingivalis strain ATCC 33277 and genomic comparison with strain W83 revealed extensive genome rearrangements in P. gingivalis.* DNA Res, 2008. **15**(4): p. 215-25.

Chapter 2. Electrode hydrophilicity enhanced the rate of extracellular electron uptake in *Desulfovibrio ferrophilus* IS5

2.1 Introduction

Anaerobic iron corrosion, which deteriorates iron materials in anaerobic environments (such as oil and gas pipelines and storage tanks buried underground), is predominantly caused by the metabolic activities of microbes. Microbially induced corrosion (MIC) severely pollutes environments and causes enormous economic losses by causing oil spill and gas or waste leakage. It has been estimated that the cost of MIC is 20-30% of total corrosion costs [1], which are equivalent to 3%–4% of each nation's gross domestic product [2]. Therefore, studying MIC mechanisms has attracted substantial attention in the industry.

SRB have long been considered to corrode iron by producing corrosive hydrogen sulfide during dissimilatory sulfate reduction coupled with the oxidation of an organic or gaseous electron donor, or by consuming hydrogen that accumulates on the iron surface. However, in 2004, novel iron-corroding SRB such as *Desulfovibrio ferrophilus* IS5 were isolated using metal iron as the sole electron donor [3]. These SRB corrode iron significantly faster than conventional hydrogenotrophic or organotrophic SRB, and therefore, it was suggested that direct bacterial extracellular electron uptake (EEU) from metal iron, rather than hydrogen consumption or hydrogen sulfide production, accounts for rapid biocorrosion [4]. Hence, it is important to elucidate the mechanisms mediating direct EEU in SRB.

Though EEU in SRB was proposed for iron, this metal is unsuitable for analyses of the electrochemical interactions between SRB and solids. Versatile side redox reactions, including hydrogen generation, occur on iron, which may serve as an EEU electron mediator. By contrast, bioelectrochemical measurements of the EEU process by SRB are feasible using inert cathodes with large hydrogen evolution overpotential such as indium-tin doped oxide (ITO) electrodes [5]. Stable ITO electrode systems have enabled the identification of EEU capability in the absence of hydrogen evolution [6] and EEU-coupled metabolic activation in SRB [7, 8]. Therefore, they are vital platforms for clarifying the mechanisms underlying EEU and providing valuable insights into EEU-driven processes.

However, despite multiple investigations into the mechanism underlying EEU in *D. ferrophilus* IS5, it remains unclear whether this bacterium uses direct EEU. It was proposed that *D. ferrophilus* IS5 uses

outer-membrane cytochromes (OMCs) for EEU [7, 8]. Direct EEU was proposed based on the observation that the current immediately increased in response to the addition of IS5 cells collected from liquid culture by centrifugation, which should not contain redox mediators, to the electrodes [7]. Direct EEU also gained support based on the observation that the washed IS5 biofilm attached on an ITO electrode, after being transferred into a new reactor containing fresh sterile medium, quickly recovered current production to a comparable level (80% within 2 hours) in the previous reactor [9]. However, because some considerable extent amount of current decrease was observed by the biofilm wash and transfer, and the presence of redox species in the spent supernatant was not analyzed, it still remains unclear whether direct EEU via cell attachment without soluble mediator is the mechanism. Furthermore, given it is challenging to construct a mutant IS5 strain lacking OMCs, direct EEU via OMCs has not yet been fully confirmed.

A few recent studies have demonstrated that electrode hydrophilicity alters the interactions between OMCs and electrodes and also enhances current generation by the iron-reducing bacterium *Shewanella loihica* PV-4 on anodes [10, 11]. Electrode wettability can also affect cell attachment on electrodes [12] and redox properties of proteins [13]. Hydrophilicity has been recognized as a critical surface property that can directly influence cell attachment [14]. Cell attachment is initiated by the protein adsorption to the material surface [15]. Meanwhile, the surface hydrophilicity can modify the conformation of adsorbed proteins, thereby influencing cell-substrate interactions [16]. As there must be a cell-electrode interface for direct EEU to occur, it is probable that wettability affects direct EEU occurring in the absence of mediator shuttles.

In this chapter, the author investigated how electrode wettability affects EEU in IS5. The author used a dip-coating method to deposit various hydrophilic and hydrophobic ligands on ITO electrodes and measured IS5 cell current generation by amperometry. Differential pulse (DP) voltammetry and scanning electron microscopy (SEM) were utilized to examine the electrochemical activity of IS5 OMCs on the electrodes and enumerate the cells attached to the electrodes, respectively. The author then discussed the mechanisms underlying direct and wettability regulated EEU in IS5.

2.2 Experimental

2.2.1 ITO modification

ITO electrodes were precleaned by sequential sonication in detergent solution, acetone, ethanol, and ultrapure water for 15 min, as previously described [10]. They were then immersed in a 1:1:5 (v/v) $H_2O_2/NH_4OH/H_2O$ solution at 80 °C for 30 min to distribute the OH groups uniformly over the ITO surfaces. The electrodes were then rinsed with ultrapure water and dried under a fume hood at a room temperature of 24 °C. They were then immersed either in 5 mM trichloro(propyl)silane or (3-mercaptopropyl) trimethoxysilane dissolved in hexane or 0.01% filter-sterilized poly-*L*-lysine solution at room temperature for 1 h. The electrodes were covered with a glass Petri dish on a clean bench. They were then rinsed with chloroform and water to remove any physically absorbed chemicals from their surfaces and dried at room temperature on a clean bench. The trichloro(propyl)silane, (3-mercaptopropyl) trimethoxysilane, and poly-*L*-lysine-treated ITO electrodes were named CH_3-ITO, SH-ITO, and PLL-ITO, respectively. For untreated ITO, a brand-new electrode surface was wiped with 70% ethanol solution for sterilization prior to constructing the reactor.

2.2.2 Water contact angle measurements

The water contact angles of the electrodes were measured with VCA Optima-XE (AST Products Inc., Billerica, MA, USA). Then, 2 μL ultrapure water was placed onto the surface of each electrode using a microsyringe in preparation for the water contact angle measurement. Three points across the electrode were measured (**Figure 2.1**).

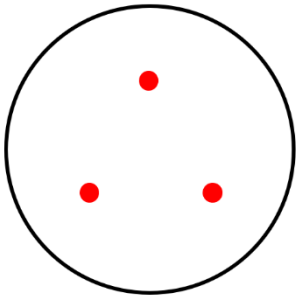

Figure 2.1 Indication of points used for the measurement of water contact angles of ITO electrodes, which have a circle working region with a diameter of 2 cm.

2.2.3 Bacterial cultivation

Desulfovibrio ferrophilus IS5 was precultured in vials containing 100 mL anoxic Deutsche Sammlung von Mikroorganismen und Zellkulturen (DSMZ) 195c medium containing 22.3 mM Na-*L*-lactate and 21.1 mM Na_2SO_4 as the electron donor and acceptor, respectively. The vials were sealed with butyl rubber stoppers and the bacterial cells were incubated at 28 °C for 5 d, as previously reported [17].

2.2.4 Electrochemical characterization

The IS5 was centrifuged at 12,850 × *g* and 28 °C for 15 min inside a COY anaerobic chamber filled with 100% N_2. The supernatant was discarded and the pellet was washed and resuspended in an anoxic salt medium [17] comprising (per liter) 457 mM NaCl, 47 mM $MgCl_2$, 7 mM KCl, 30 mM $NaHCO_3$, 1 mM $CaCl_2$, 1 mM K_2HPO_4, 1 mM NH_4Cl, 25 mM Na^+-HEPES (pH 7.4), 1 mL selenite-tungstate solution (12.5 mM NaOH, 11.4 mM $Na_2SeO_3 \cdot 5H_2O$, and 12.1 mM $Na_2WO_4 \cdot 2H_2O$), 1 mL SL-10 (trace element solution), 1 mM acetate (carbon source), and 21 mM Na_2SO_4 (electron acceptor). The medium was rendered anoxic by N_2 purging for 30 min, autoclaving, and N_2 purging for another 30 min. It was then used as the electrolyte for the electrochemical measurements, which were conducted at 28 °C in single-chamber, three-electrode reactors inside a COY anaerobic chamber filled with 100% N_2. ITO, CH_3-ITO, SH-ITO, and PLL-ITO served as the working electrodes. Platinum wire and Ag/AgCl (saturated KCl) were used as counter- and reference electrodes, respectively. The electrolyte used was 5.5 mL sterile anoxic salt medium. For chronoamperometry (CA), the electrode potential was set to -0.4 V (vs. SHE). The background current was measured for 3.5 h and the anoxically accumulated and washed IS5 cells were introduced using a syringe into each reactor until a final OD_{600} = 0.3. DP voltammetry was conducted with an automatic polarization system (VMP3; Bio-Logic SAS Instruments, Paris, France) using the following parameters: pulse increment, 5.0 mV; pulse amplitude, 50 mV; pulse width, 300 ms; and pulse period, 5.0 s. The potential was scanned from the positive to the negative direction. Baseline subtraction of the DP voltammogram was performed using Qsoas [18].

2.2.5 Scanning electron microscopy (SEM) and cell counting

After the electrochemical measurements, the ITO electrodes were removed from the reactors and gently rinsed with 0.1 M phosphate buffer (pH = 7) to remove unattached cells that precipitated near the

electrode surfaces; the cells were immediately fixed with 2.5% (v/v) glutaraldehyde in 0.1 M phosphate buffer (pH = 7) for 1 h. The ITO electrodes were then washed thrice by immersing in 50 mM Na-HEPES buffer (pH 7.4) for 5 min per wash. The samples were dehydrated with an ethanol concentration gradient of 25% (v/v), 50% (v/v), and 75% (v/v) prepared in ultrapure water and 100% ethanol for 10 min per concentration. The 100% ethanol was exchanged thrice with *tert*-butanol, chilled at -20 °C for 10 min, and then freeze-dried under vacuum. The dried samples were coated with evaporated platinum with a Quick Coater SC-701 (Sanyu Denshi KK, Nishi-ku Nagoya, Japan) and viewed under a KEYENCE VE-9800 microscope (Keyence Corp., Osaka, Japan). To avoid the bias in cell counting caused by heterogenous cell distributions on the ITO electrodes, 13 areas (~10,000 μm^2) at the center, middle, and edge of each ITO electrode were imaged. The selected viewing areas and those adjacent to them all had similar cell densities. The cell counts of the 13 points were averaged to estimate the total cell number per electrode. The working area was 3.14 cm^2. ImageJ software (National Institutes of Health, Bethesda, MD, USA) was used for cell counting [19].

2.3 Results

ITO electrodes with different degrees of wettability were fabricated by dip-coating them in trichloro(propyl)silane with a hydrophobic methyl (CH_3-) group, (3-mercaptopropyl) trimethoxysilane with a hydrophilic thiol (SH-) group [10], or poly-*L*-lysine with a hydrophilic amino (NH_2-) group. These modified ITO electrodes were named CH_3-ITO, SH-ITO, and PLL-ITO, respectively. Unmodified ITO electrodes served as the control. The flat ITO electrode surface and the full immersion coating method ensured that the chemical coating layers on the electrode were uniform. The water contact angles of the modified and unmodified ITO electrodes measured for three different locations across the ITO electrode (**Figure 2.1**) showed that PLL-ITO was the most hydrophilic (43.3 ± 1.8°), followed by the untreated ITO (46.1 ± 2.5°) and SH-ITO (52.9 ± 2.1°). By contrast, CH_3-ITO (106.1 ± 1.8°) was hydrophobic (**Figure 2.2**). Hence, ITO electrodes with modified wettability were successfully obtained by the dip-coating method.

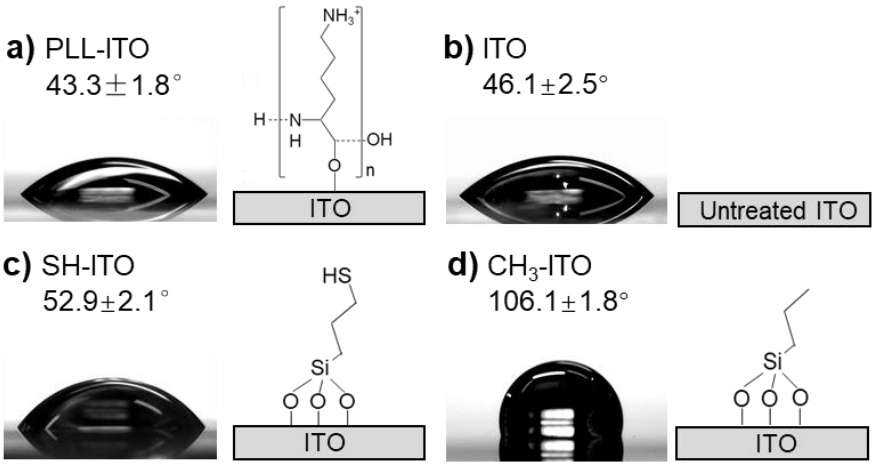

Figure 2.2 Contact angle measurements for water droplets on the surfaces of modified and unmodified ITO electrodes. (a) Poly-*L*-lysine (PLL)-ITO. (b) untreated ITO. (c) (3-Mercaptopropyl)trimethoxysilane (SH)-ITO. (d) Trichloro(propyl)silane (CH_3)-ITO.

To investigate whether electrode wettability affects EEU in *D. ferrophilus* IS5, the author performed electrochemical measurements in single-chamber, three-electrode reactors. To confirm that the ligand coatings on the ITO electrodes did not affect their redox properties or electron transport, the author performed cyclic voltammetry measurements on all electrodes in a standard sterile potassium ferricyanide solution. The cyclic voltammograms were identical for wettability-modified and -unmodified ITO electrodes and each displayed a pair of ferricyanide redox peaks (**Figure 2.3**). Thus, the chemical coatings on the electrode surfaces had minimal steric hindrance and did not markedly impact electron transfer resistance.

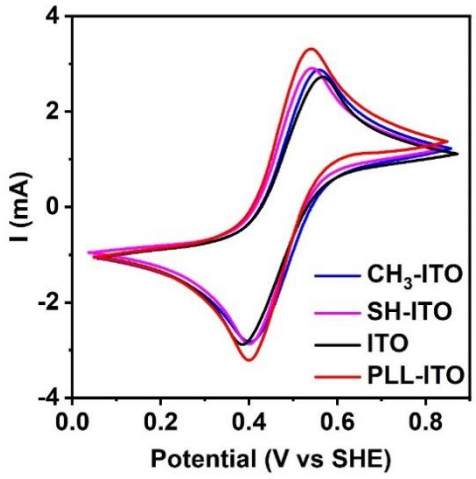

Figure 2.3 Cyclic voltammograms of 0.2 M sterile potassium ferricyanide solution prepared in 1 M KCl on various ITO electrodes with modified surface wettability. Scan rate = 0.1 mV/s.

The author then used the ITO electrodes to measure current generation in *D. ferrophilus* IS5 cells. The ITO electrodes had > 0.5 V overpotential for hydrogen evolution [5, 6] and were poised at −0.4 V (vs. SHE) to prevent hydrogen formation at pH = 7.4. They served as the sole electron donors for the cells. The sterile electrolyte generated background currents that sharply declined after the initiation of current measurement, which was most likely due to the reaction of electrolyte components with the electrode (**Figure 2.4a-c**). The control current production (only electrolyte and sterilized cells) was also measured and no significant current was observed (**Figure 2.4a and b**). The active IS5 cells were added at ~3 h and the background current immediately decreased from −0.1 to −0.2 μA and then to approximately −0.025 μA under all conditions (**Figure 2.4c**). Addition of the IS5 cells to the electrode surfaces might have blocked side reactions between the electrolyte and the electrodes. Thereafter, the current continuously increased with time but to varying degrees depending on the electrode type, whereas the current on the hydrophobic CH_3-ITO only slightly increased to approximately −0.03 μA after 50 h; there was significantly more current generation on the hydrophilic SH-ITO (−0.09 μA at 50 h). Current generation was further enhanced on the hydrophilic untreated ITO (−0.17 μA at 50 h) and the most strongly hydrophilic PLL-ITO (−0.3 μA at 50 h). These observations were repeatable (**Figure 2.5**). The foregoing results showed that the hydrophilic electrodes promoted current generation in *D. ferrophilus* IS5 by as much as nine-fold compared to the hydrophobic CH_3-ITO.

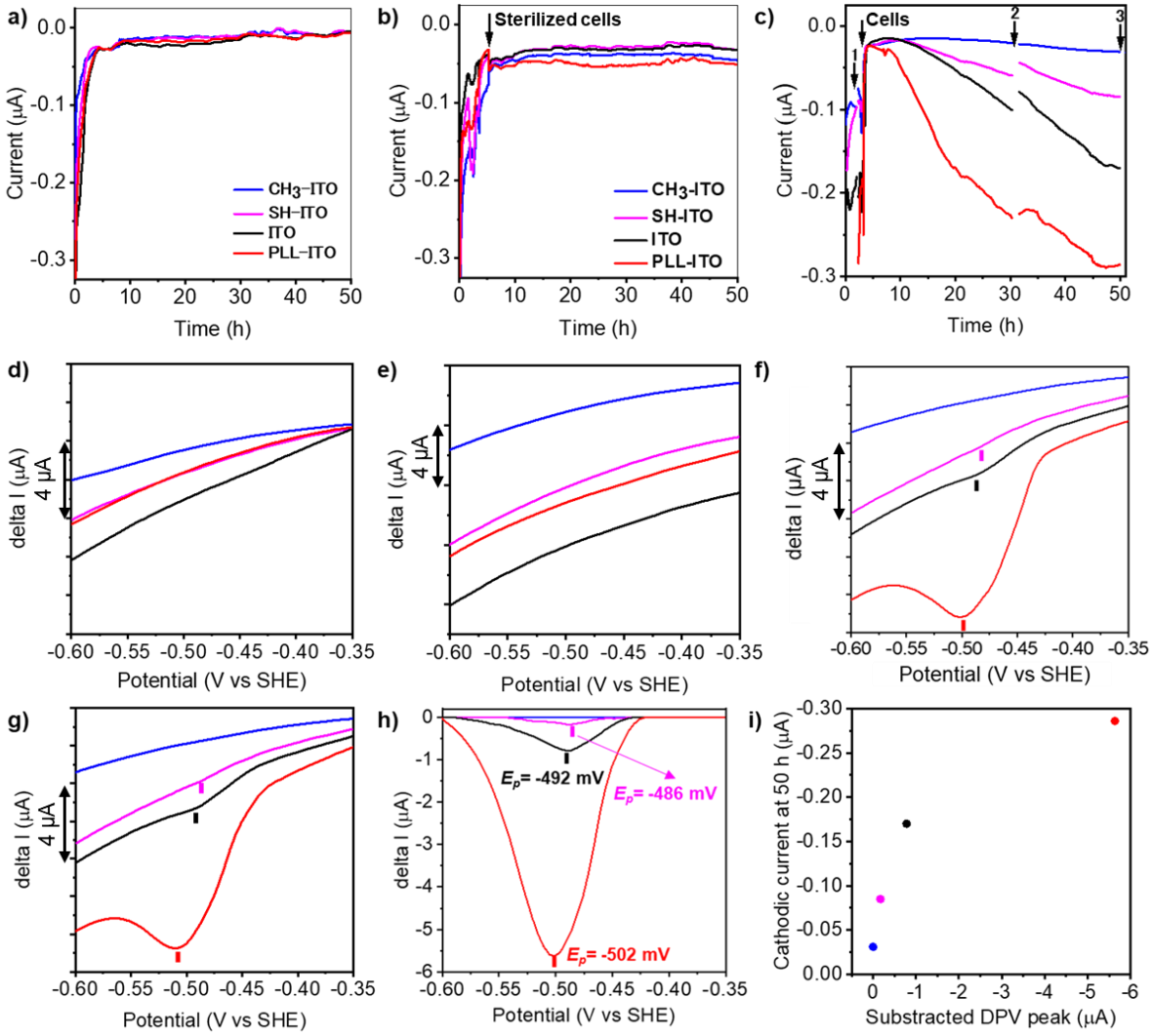

Figure 2.4 Electrochemical measurements of *Desulfovibrio ferrophilus* IS5 cells on PLL-ITO (red), untreated ITO (black), SH-ITO (pink), and CH_3-ITO (blue) electrodes. (a-c) Plot of cathodic current vs. time of sterile medium (a), sterilized IS5 cells (b), and live IS5 cells (c) poised at −0.4 V vs. SHE. Arrows 1, 2, and 3 in panel (c) indicate timing at which differential pulse (DP) voltammograms were recorded. (d-g) DP voltammograms measured with sterilized IS5 cells (d), before (e), and after (f, g) adding live IS5 cells. DP voltammograms of panel e, f, g were recorded at timings indicated by arrows 1, 2, and 3 in panel c. (h) DP voltammogram of live IS5 cells in panel (g) after baseline subtraction. The short bars indicate the peak potentials (E_p). (i) Plot of current production by IS5 cells at 50 h in panel c versus the corresponding redox peak height of baseline-subtracted DP voltammogram in panel e.

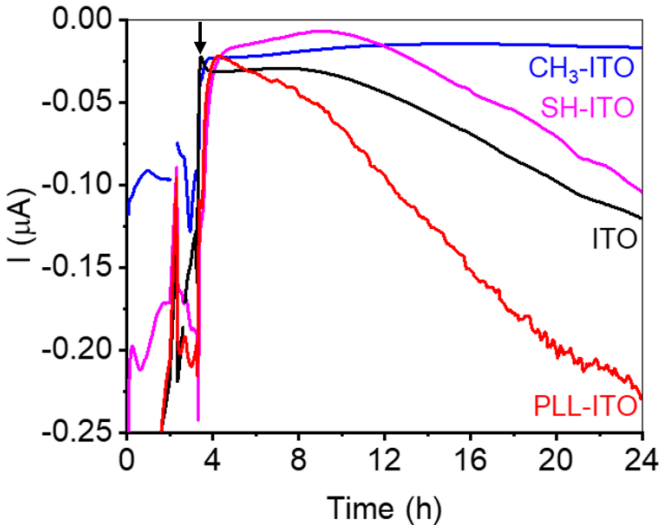

Figure 2.5 Cathodic current generation by *Desulfovibrio ferrophilus* IS5 cells on -0.4 V (vs. SHE)-poised ITO electrodes with modified surface wettability. The black arrow indicates the cell addition timing.

To clarify the mechanism by which hydrophilic electrodes augment the current, the author performed DP voltammetry measurements using both the modified and unmodified electrodes. The DP voltammograms of the sterilized IS5 cells (**Figure 2.4d**) and electrolyte (dpv1; **Figure 2.4e**) revealed no redox signals on any electrode. However, the DP voltammograms for PLL-ITO, untreated ITO, and SH-ITO in the presence of live IS5 cells measured at 30 h disclosed a single peak within the −0.35 to −0.6 V region. The half-peak width was ~100 mV and no significant redox peaks were detected for CH_3-ITO (dpv2; **Figure 2.4f**). Moreover, the DP voltammograms measured at 50 h presented with nearly identical peaks for PLL-ITO, untreated ITO, and SH-ITO (dpv3; **Figure 2.4g**), indicating that the detected species was stable on the electrode surfaces. Although the peak potential (around −0.48 V measured with uncoated ITO) was slightly more negative than that previously reported for IS5 OMCs (around −0.45 V) [7, 8], the overall potential region and the half-peak width for the detected species were consistent with those reported for IS5 OMCs. Hence, the detected redox peak within the potential region of −0.35 to −0.6 V was most assignable to IS5 OMCs. Importantly, the redox potential of the OMCs slightly shifted from −492 mV for ≤ 16 mV in the negative direction with increasing hydrophilicity of SH-ITO, untreated ITO, and PLL-ITO (**Figure 2.4f–h**). This finding suggests that the

electrode surface wettability affected the redox property of the IS5 OMCs and that the OMCs and electrodes directly interacted.

The observed reductive peak significantly increased on the more hydrophilic electrodes (**Figure 2.4f–g**). Plotting the current recorded at 50 h (immediately before the dpv3 measurement) against the redox peak intensity calculated according to the baseline-subtracted dpv3 (**Figure 2.4h**) revealed that the cathodic current generation was positively correlated with the redox peak intensity (**Figure 2.4i**). The relatively higher redox peaks of the OMCs on hydrophilic electrodes suggest that comparatively more OMCs were present on the electrode surfaces and/or the electrical interactions between the OMCs and the hydrophilic electrode surfaces differed. To determine which mechanism enhanced current generation on the hydrophilic electrodes, the author examine the electrodes under a SEM and observed whether their wettability affected cell attachment. To exclusively observe the cells attached to the electrodes, the electrodes were briefly rinsed to remove precipitated cells that were not attached to the electrodes. A previous study showed that most *Shewanella* cells transporting electrons to an electrode would not detach from it [20]. SEM revealed that the number of IS5 cells attached to an electrode significantly increased with electrode hydrophilicity (**Figure 2.6a**). The author estimated the numbers of cells on each electrode (3.14 cm^2) according to SEM images uniformly distributed across 13 locations on the ITO electrode (**Figure 2.7;** Materials and Methods). The cell counts on PLL-ITO, untreated ITO, SH-ITO, and CH_3-ITO were estimated to be 8.2×10^6, 4.4×10^6, 1.8×10^6, and 0.8×10^6, respectively. Thus, electrode hydrophilicity promoted IS5 cell attachment (**Figure 2.6b**). Greater cell attachment on the hydrophilic electrodes was consistent with their relatively higher reductive peaks detected by DP voltammetry. Moreover, a plot of the total electrical charge extracted by the cells from the electrode (**Figure 2.4c**) against the numbers of cells attached to the electrodes exhibited a nearly linear relationship (**Figure 2.6c**). These results indicated that enhanced cell attachment substantially explains the observed augmented current generation by IS5 on hydrophilic electrodes. These findings also strongly suggest that only the IS5 cells that were tightly attached to the electrode surface were responsible for current generation. Therefore, IS5 cells most likely perform direct EEU via OMCs without redox mediators.

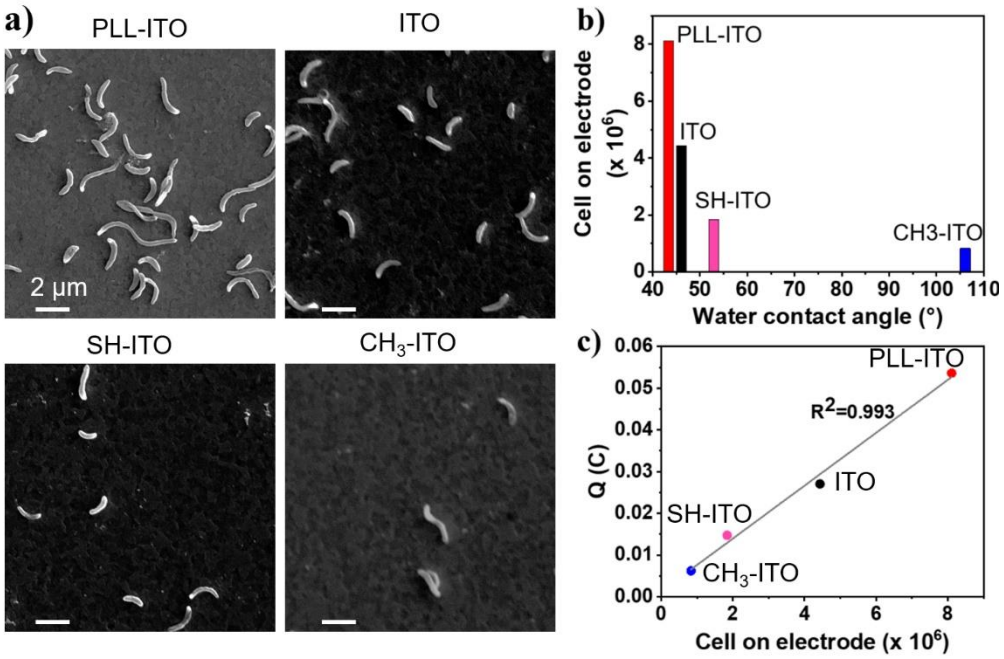

Figure 2.6 Impact of ITO electrode wettability on numbers of *D. ferrophilus* IS5 cells attached to electrodes. (a) Representative scanning electron microscopic (SEM) image of ITO electrode surface after electrochemical measurements of *D. ferrophilus* IS5 cells. (b) Association between numbers of cells on electrode surfaces and water contact angles. Cell numbers were estimated by multiplying electrode surface area (3.14 cm^2) by average cell density. The latter was calculated based on cell counting using 13 SEM images of 10000 μm^2 across the electrode (Figure 2.7). (c) Plot of electrical charge (Q) extracted by IS5 cells vs. number of cells on electrode.

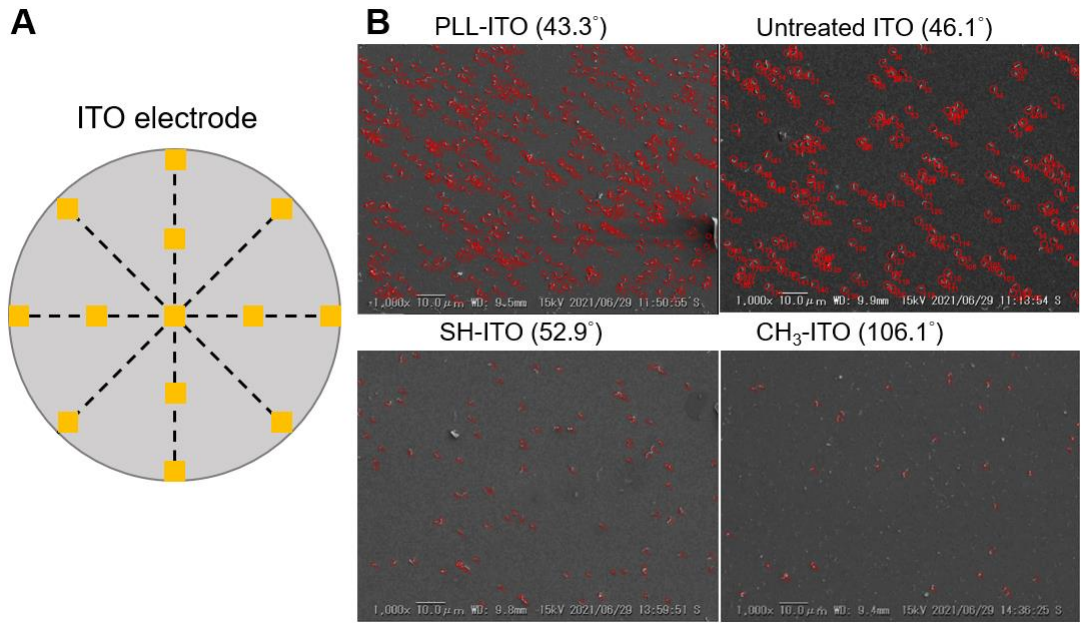

Figure 2.7 Scanning electron microscopy (SEM)-based cell counting on ITO electrodes. (A) Schematic image showing 13 SEM imaging points used to estimate the average cell density and total cell number per electrode. (B) Representative SEM image of PLL-ITO, untreated ITO, SH-ITO, and CH_3-ITO. Red circles were drawn using the ImageJ software and used for cell counting.

The author further analyzed the reductive peaks in the DP voltammograms for electrodes with different wettability. According to the amperometry, the total electrical charge linearly increased with cell number (**Figure 2.6c**). For this reason, the average current (EEU rate) per cell should be nearly identical for all electrodes. Hence, there should be similar numbers of OMCs among individual IS5 cells. The redox peak height per cell could thus be an indicator of the intensity of the electrical interactions between OMCs and electrodes. The redox peak height for the CH_3-ITO electrode was too low to be analyzed. Nevertheless, the redox peak heights per cell increased significantly with electrode hydrophilicity **(Figure 2.8a)**. In fact, the peak height per cell on the most hydrophilic PLL-ITO was more than three-fold and six-fold higher than those for the less hydrophilic untreated ITO and SH-ITO electrodes, respectively. Combined with the observation that the OMCs became slightly more reduced on hydrophilic electrodes (**Figure 2.4f–h and 2.8b**), these results indicate that the electrical interactions were enhanced between the OMCs and more hydrophilic electrodes. Together, the author proposes that hydrophilicity significantly improved IS5 cell attachment to the electrodes and strengthened the

electrical interactions between the OMCs and the electrodes. And the increase in IS5 cell attachment is the predominant reason for the significant increases observed in current generation on hydrophilic electrodes (**Figure 2.8c**).

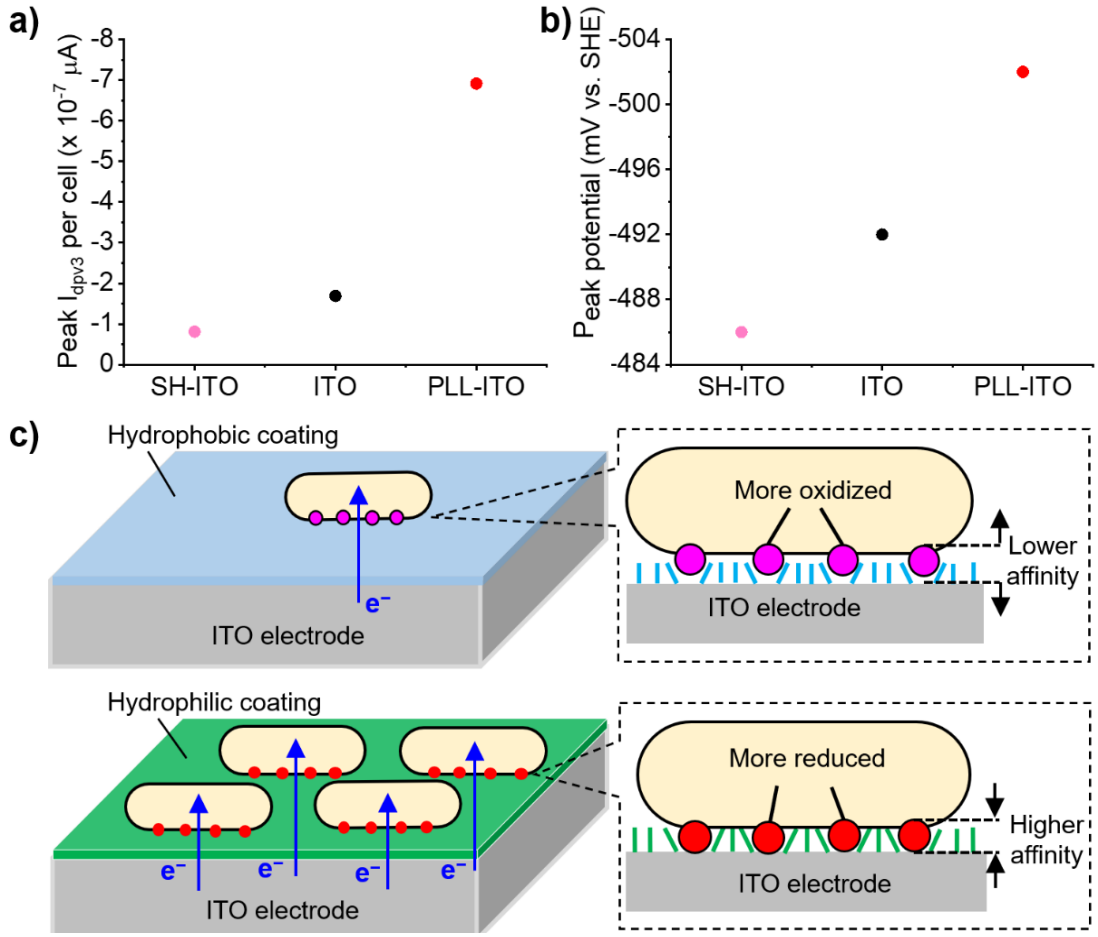

Figure 2.8 Impact of electrode wettability on electrochemical properties of surfaces of bacterial redox species *Desulfovibrio ferrophilus* IS5. (a) Cathodic redox peak current (I) per cell on various electrodes. Calculated based on dpv3 shown in Figure 2.4h and cell numbers shown in Figure 2.6b. Redox signal on CH_3-ITO electrode was too low (Figure 2.4g) and was omitted from the figure. EEU currents per cell were comparable for all electrodes and indicated similar numbers of OMCs among them. Hence, peak I_{dpv3} per cell most likely reflects electrical interactions between IS5 cell-surface redox proteins and electrode surface. (b) Redox peak potentials (Figure 2.4g-h) on various ITO electrodes. (c) Schematic diagram of electrode wettability regulated EEU performance in *D. ferrophilus* IS5 including impact on macroscopic cell attachment to electrodes and nanoscale affinity between OMCs and electrode surfaces.

2.4 Discussion

Several studies have attempted to elucidate the biological mechanisms of EEU and EEU-coupled metabolic activity in *Desulfovibrio ferrophilus* IS5 [6-9]. While it has been clearly demonstrated that the hydrogen did not involve as an electron mediator for IS5 current production on ITO electrodes poised at −0.4 V, it remains unclear whether the EEU of IS5 involves soluble redox shuttles as well as OMCs. Here, the author evaluated the impact of electrode wettability on current generation, OMC redox properties, and cell attachment on the electrode surfaces. To the best of our knowledge, the author demonstrated for the first time that the IS5 OMCs directly interact with electrode surfaces. The author also showed that current generation by IS5 is linearly correlated with the number of cells attached to the electrodes. These findings strongly indicate that IS5 utilizes direct EEU via OMCs without using redox shuttles. Consistently, the IS5 genome lacks the gene region encoding riboflavin biosynthesis and secretion [7]. Riboflavin is a common redox mediator used by other EEU-capable bacterial genera such as *Shewanella* and *Geobacter* [21, 22]. This information helps us clarify the electrical iron corrosion mechanism in IS5 cells. Direct cell attachment to iron is essential for IS5 to corrode iron electrochemically.

Hydrophobic coatings have been applied to inhibit the SRB corrosion in several studies [23, 24]. However, due to different bacterial surface have varied hydrophilicity, an increase in surface hydrophobicity may not necessarily be associated with less corrosion in case of bacterial mixture [23]. Nevertheless, this study demonstrated for the first time that hydrophilic electrodes promoted current generation by IS5 to a far greater extent than hydrophobic electrodes, because of enhanced IS5 cell attachment on hydrophilic electrodes and strong electrical interactions between OMCs and hydrophilic electrodes. Therefore, the use of a hydrophobic coating on iron material may inhibit IS5 attachment and the associated electrical corrosion. However, certain SRB such as *D. vulgaris* Hildenborough have hydrophobic surfaces and would, therefore, more effectively attach to other hydrophobic surfaces [25]. *D. vulgaris* Hildenborough has been reported to perform EEU via electroconductive iron sulfide nanoparticles that self-synthesize on the cell surface [26], thus hydrophobic iron surface might enhance EEU and cause more electrical corrosion in *D. vulgaris* Hildenborough. Also, when considering real

application of using coatings to inhibit corrosion, complex environmental substances such as organic substrates, salts, and other microorganisms that further alter material wettability must be taken into consideration. It remains to be determined how wettability and various environmental factors influence the EEU of other SRB species and mixed microbial consortia. The coating method is also difficult to be applied to already existing iron structures. Hence, the application of wettability-modified materials to inhibit corrosion by SRB may not be simple in practice except in certain special cases where the corrosion environment is dominated by SRB species with similar surface properties.

Though the author empirically demonstrated the importance of electrode wettability in regulating the EEU rate of SRB, other electrode properties such as electrical conductivity, surface charge, and nanostructures should also impact EEU performance. Identification of the factors regulating EEU will help us develop materials and methods regulating the rates of EEU-driven reactions.

References

1. Koch, G.H., et al., *Chapter 1 - Cost of corrosion in the United States*, in *Handbook of Environmental Degradation of Materials*, M. Kutz, Editor. 2005, William Andrew Publishing: Norwich, NY. p. 3-24.
2. Koch, G., *1 - Cost of corrosion*, in *Trends in Oil and Gas Corrosion Research and Technologies*, A.M. El-Sherik, Editor. 2017, Woodhead Publishing: Boston. p. 3-30.
3. Dinh, H.T., et al., *Iron corrosion by novel anaerobic microorganisms.* Nature, 2004. **427**(6977): p. 829-32.
4. Enning, D., et al., *Marine sulfate-reducing bacteria cause serious corrosion of iron under electroconductive biogenic mineral crust.* Environmental microbiology, 2012. **14**(7): p. 1772-1787.
5. Benck, J.D., et al., *Substrate selection for fundamental studies of electrocatalysts and photoelectrodes: inert potential windows in acidic, neutral, and basic electrolyte.* PloS one, 2014. **9**(10): p. e107942-e107942.

6. Deng, X., et al., *Electron Extraction from an Extracellular Electrode by Desulfovibrio ferrophilus Strain IS5 Without Using Hydrogen as an Electron Carrier.* Electrochemistry, 2015. **83**(7): p. 529-531.

7. Deng, X. and A. Okamoto, *Electrode Potential Dependency of Single-Cell Activity Identifies the Energetics of Slow Microbial Electron Uptake Process.* Frontiers in Microbiology, 2018. **9**.

8. Deng, X., et al., *Enhancement of cell growth by uncoupling extracellular electron uptake and oxidative stress production in sediment sulfate-reducing bacteria.* Environment International, 2020. **144**.

9. McCully, A.L. and A.M. Spormann, *Direct cathodic electron uptake coupled to sulfate reduction by Desulfovibrio ferrophilus IS5 biofilms.* Environ Microbiol, 2020. **22**(11): p. 4794-4807.

10. Ding, C.M., et al., *Wettability-Regulated Extracellular Electron Transfer from the Living Organism of Shewanella loihica PV-4.* Angewandte Chemie-International Edition, 2015. **54**(5): p. 1446-1451.

11. Zhao, C., et al., *Hydrophilicity boosted extracellular electron transfer in Shewanella loihica PV-4.* Rsc Advances, 2016. **6**(27): p. 22488-22493.

12. Krasowska, A. and K. Sigler, *How microorganisms use hydrophobicity and what does this mean for human needs?* Frontiers in Cellular and Infection Microbiology, 2014. **4**(112).

13. Song, S., et al., *Characterization of Cytochrome-C Alkanethiolate Structures Prepared by Self-Assembly on Gold.* Journal of Physical Chemistry, 1993. **97**(24): p. 6564-6572.

14. Zheng, S., et al., *Implication of Surface Properties, Bacterial Motility, and Hydrodynamic Conditions on Bacterial Surface Sensing and Their Initial Adhesion.* Frontiers in Bioengineering and Biotechnology, 2021. **9**.

15. Ferrari, M., F. Cirisano, and M.C. Morán, *Mammalian Cell Behavior on Hydrophobic Substrates: Influence of Surface Properties.* Colloids and Interfaces, 2019. **3**(2): p. 48.

16. Chen, H., et al., *Biocompatible polymer materials: Role of protein–surface interactions.* Progress in

Polymer Science, 2008. **33**(11): p. 1059-1087.

17. Nevin, K.P., et al., *Electrosynthesis of Organic Compounds from Carbon Dioxide Is Catalyzed by a Diversity of Acetogenic Microorganisms.* Applied and Environmental Microbiology, 2011. **77**(9): p. 2882-2886.

18. Fourmond, V., *QSoas: A Versatile Software for Data Analysis.* Analytical Chemistry, 2016. **88**(10): p. 5050-5052.

19. Schneider, C.A., W.S. Rasband, and K.W. Eliceiri, *NIH Image to ImageJ: 25 years of image analysis.* Nature Methods, 2012. **9**(7): p. 671-675.

20. Harris, H.W., et al., *Electrokinesis is a microbial behavior that requires extracellular electron transport.* Proceedings of the National Academy of Sciences of the United States of America, 2010. **107**(1): p. 326-331.

21. Marsili, E., et al., *Shewanella secretes flavins that mediate extracellular electron transfer.* Proceedings of the National Academy of Sciences, 2008. **105**(10): p. 3968.

22. Okamoto, A., et al., *Uptake of self-secreted flavins as bound cofactors for extracellular electron transfer in Geobacter species.* Energy & Environmental Science, 2014. **7**(4): p. 1357-1361.

23. Arukalam, I.O., et al., *Inhibition of sulfate-reducing bacteria influenced corrosion on hydrophobic poly(dimethylsiloxane) coatings.* Journal of Materials Science & Technology, 2020. **52**: p. 198-206.

24. Mahalakshmi, P.V., et al., *Enhancing corrosion and biofouling resistance through superhydrophobic surface modification.* Current Science, 2011. **101**(10): p. 1328-1336.

25. Tran, T.T.T., et al., *A study of bacteria adhesion and microbial corrosion on different stainless steels in environment containing Desulfovibrio vulgaris.* Royal Society Open Science, 2021. **8**(1).

26. Deng, X., et al., *Biogenic Iron Sulfide Nanoparticles to Enable Extracellular Electron Uptake in Sulfate-*

Reducing Bacteria. Angewandte Chemie-International Edition, 2020. **59**(15): p. 5995-5999.

Chapter 3. A histidine metabolism-based electrochemical sensor for early-stage detection of *Porphyromonas gingivalis*

3.1 Introduction

Periodontal diseases are a global health concern, particularly among the elderly population, as they not only result in dental pain and tooth damage but also have been linked to various systemic ailments including rheumatoid arthritis, atherosclerosis, Alzheimer's disease, and preterm birth [1-4]. Chronic periodontitis is a slow developing pathogenesis which is difficult to diagnose and challenging to treat at later stages. Clinical detection of oral diseases is usually probing pocket depth or bleeding-on-probing, which is difficult for instant diagnosis [5]. Thus, point-of-care diagnosis for home care is critical to human health. It has been concluded that periodontitis is mainly caused by high-risk periodontal pathogens including *Aggregatibacter actinomycetemcomitans* (Aa), *Porphyromonas gingivalis* (*P. gingivalis*), *Tannerella forsythia*, *Treponema denticola* and *Fusobacterium nucleatum* [6-10]. Moreover, the red complex bacteria (*P. gingivalis*, *T. forsythia* and *T. denticola*) exhibit higher activity as the periodontal disease progresses [11]. Identifying these pathogens can serve as an indicator of periodontitis-associated illness, aiding in the selection of appropriate targeted therapeutic interventions, as well as facilitating the prediction of oral disease status for potential oral treatments. Consequently, a significant body of research has been dedicated to the detection of these microorganisms, with *P. gingivalis* being the most commonly utilized marker for the diagnosis of both chronic and aggressive periodontitis [12-16]. Conventional techniques for detection *P. gingivalis* provide culturing, polymerase chain reaction (PCR), DNA probe and enzyme-linked immunosorbent assay (ELISA), which are too complex and time-consuming to be easily executed at home [17-19]. In the context of home care, the analysis of microbiota was limited to the collection of saliva samples, which were subsequently sent to a specialized agency for 16s rRNA sequencing [20-22]. This approach is associated with high costs and time requirements. Biosensor provides a promising avenue for point-of-care diagnosis of *P. gingivalis*. Various biosensors utilizing antibodies, DNA, and PCR technologies have been developed and employed to detect of *P. gingivalis*. [23, 24]. Nonetheless, the application of these biosensors is impeded by factors such

as their low sensitivity and specificity, instability, requirement for pretreatment, and high cost, and the activity of *P. gingivalis* is challenging to detect. Hence, there is an urgent need for a simple and sensitive biosensor that can facilitate the early diagnosis of periodontitis in a home-care setting.

Recent research has revealed the electrogenicity of some well-known human pathogens, such as *P. gingivalis*, and showed links between metabolic activity and electrochemical signals [25-27], which could lead to the development of a real-time assay for drug assessment by directly measuring the current production associated with cellular metabolism. Meanwhile, microbial current production is measurable using reusable, low-cost screen-printed electrode systems and single-potential amperometry (SA) techniques [28]. Electrochemical detection of *P. gingivalis* is possible on-site without any electrode modification. However, *P. gingivalis* generated too limited amount of current production (*Ic*) coupled with glucose oxidation to be used for a sensitive biosensor [26]. It is noticed that *P. gingivalis* prefers different nutrients to reduce competition in the oral biofilm [29], however, the pathogen's substrate specificity for current production capability was not studied so far.

In this chapter, the author examined the effect of different substrates (amino acids, peptides and sugars) on current production of *P. gingivalis*. It was found that with histidine, *P. gingivalis* can generate extremely higher current than other substrates. Furthermore, the current production of *P. gingivalis* was compared with reported oral electroactive bacteria, Aa, *Streptococcus mutans* (Sm), *Corynebacterium matruchotii* (Cm) and *Capnocytophaga ochracea* (Co) with histidine as sole electron and carbon source. Surprisingly, *P. gingivalis* generated significant current compared to other oral pathogens. The potential metabolic models were simulated to compare the metabolic pathways among pathogens by using metabolic flux analysis such as NADH and ATP. The author also examined the impact of electrode wettability on EET activity and the electron transfer mechanism at the interfaces between *P. gingivalis* cells and electrodes. With increasing electrode hydrophilicity, current generation coupled with histidine oxidation increased and displayed a

positive correlation with the outer-membrane redox proteins with more reduced state attached to the electrodes, which support the hypothesis that *P. gingivalis* utilizes outer-membrane redox proteins to mediate direct EET mechanism. The author further electrochemically analyzed human saliva collected from a healthy (without *P. gingivalis*) and un-healthy (with high percentage of *P. gingivalis*) volunteer using a three-electrode electrochemical system with three substrates, glucose, lactate and histidine. As expected, the patient sample containing higher counts of *P. gingivalis* produced a significantly higher current only with histidine, while the healthy sample generated a similar current with all substrates. The results presented here are the first steps in developing a sensing methodology that could be used for the accurate early-stage detection of pathogens implicated in the pathogenicity of periodontitis and associated systemic diseases that occur in locations other than the oral cavity, such as the heart and brain. The author report an independent culturing method that allows for the quick, specific, and selective detection of *P. gingivalis.*

3.2 Experimental

3.2.1 Cell culture preparation

Porphyromonas gingivalis W83 strain was grown anaerobically in Gifu anaerobic medium, while *Capnocytophaga ochracea* were grown in DSMZ 340 medium supplied with 1 g/L sodium bicarbonate. *Aggregatibacter actinomycetemcomitans* y4 (anaerobically) and *Corynebacterium matruchotii* ATCC 14266 (aerobically) were grown in brain heart infusion (BHI) medium supplemented with 1% yeast extract in falcon tubes. *Streptococcus mutans* UA159 was grown in only BHI medium with 5% CO_2 [25-27]. All cultures were grown at 37°C till the growth reached the late exponential phase. Cells were then centrifuged at 7200 rpm and 37 °C for 10 min, and the resultant cell pellet was washed with defined medium (DM) twice to remove the cell secreted metabolites of the preculture medium. Cell cultures were handled in COY anaerobic chamber

filled with 100% N_2. DM was prepared according to previously described methods [30] with some modification. DM contained (per liter) the following components: $NaHCO_3$, 2.5 g; $CaCl_2 \cdot 2H_2O$, 0.09 g; NH_4Cl, 1.0 g; $MgCl_2 \cdot 6H_2O$, 0.2 g; NaCl, 10 g; HEPES, 7.2 g.

3.2.2 Substrates screening using high-throughput 96-well screen-printed electrode system

To find out the best substrate for higher current generation by *P. gingivalis*, different substrates were tested in 96-well plate screen-printed carbon electrode system with carbon as working and counter electrode, and Ag/AgCl as reference electrodes (SPCE, purchased from *Metrohm DropSens*, surface area of each electrode in 96-well plate is 7.07 mm^2, **Figure 3.1a**). Amino acids (L-histidine, L-aspartate, L-glutamate, L-leucine, L-threonine and L-arginine), peptides (His-His, Asp-Asp, Glu-Glu, Lys-Ala-MCA, AC-Asp-Glu-Thr-Asp-MCA, AC-Asp-Glu-Val-Asp-MCA, Boc-Leu-Ser-Thr-Arg-MCA), glucose and lactate were screened for current production with *P. gingivalis*. The DM solution without any substrate was used as control and all substrates were dissolved in DM solution which purged N_2 for more than 30 minutes to remove oxygen. Firstly, different substrates were added to each well in 4-8 replicates (100 µL volume). 100 µL freshly prepared DM washed *P. gingivalis* cells (OD_{600} = 2.0) were injected into each well to make total volume up to 200 µL and reach the final OD_{600} = 1.0. The final concentration of each amino acid, glucose and lactate was 10 mM, while the peptides concentration was 10/n mM (n is the number of amino acids in each peptide). All solution in each well was mixed with pipette for several times to become homogeneous. Tin foil tape was used to cover the whole 96-well plate for preventing evaporation. The 96-well plate was poised at +0.4 V vs standard hydrogen electrode (SHE) by high-throughput potentiostat to measure the single potential amperometry of each well. All procedures were handled in COY anaerobic chamber filled with 100% N_2 at 37 °C.

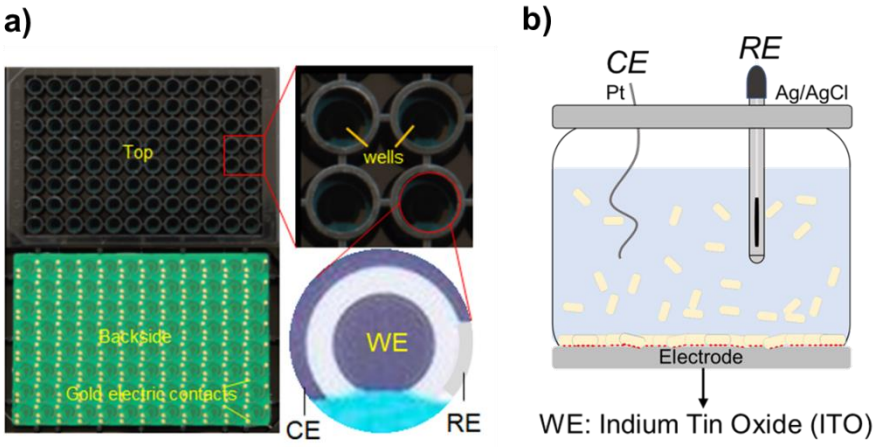

Figure 3.1 (a) The 96-well carbon electrode plate for substrate-scanning experiment, working and counter electrode are carbon and reference electrode is Ag/AgCl. (b) The electrochemical reactor for detail analysis with glass coated indium tin oxide (ITO) as working electrode, platinum wire as counter electrode and Ag/AgCl (3 M KCl) as reference electrode. WE, working electrode; CE, counter electrode; RE, reference electrode.

3.2.3 Whole-cell electrochemical analysis of pure strains

Electrochemical measurements were conducted in single-chamber, three-electrode reactors (**Fig 3.1b**). indium tin-doped oxide (ITO) grown on a glass substrate by spray pyrolysis deposition (SPD Laboratory, Inc., Japan) was used as the working electrode (resistance, 8 Ω/square; thickness, 1.1 mm; and surface area, 3.14 cm^2) and was placed at the bottom of the reactor. Platinum wire and Ag/AgCl (sat. KCl) were used as counter and reference electrodes, respectively. DM containing 10 mM histidine/glucose/glutamate (4.5 mL) was injected into the electrochemical cell as an electrolyte, and the solution was purged with N_2 gas for at least 15 min to remove the dissolved oxygen. Single-potential amperometry (SA) was started to detected the current under potentiostatic condition of +0.4 V vs a SHE. Meanwhile open-circuit voltage (OCV) of *P. gingivalis* was also detected. After the background current became stable, 0.5 mL of freshly prepared cell suspension of *P. gingivalis/ Aggregatibacter actinomycetemcomitans* /

Streptococcus mutans / *Corynebacterium matruchotii* / *Capnocytophaga ochracea* pre-washed with DM having an optical density of X at 600 nm was injected into the electrochemical cell to reach a final OD_{600} of X/10. During the electrochemical measurements, the reactor temperature was maintained at 37 °C, and the reactor was operated without agitation. Single-potential amperometry (SA) was measured with an automatic polarization system (VMP3, Bio Logic Company, France) **[31]**. Histidine concentrations from three replicate experiments were measured using Micromolar Histidine Assay Kit according to manufacturer's instructions. After SA and OCV measurement of *P. gingivalis* with histidine, the protein concentration of cells attached on electrode surface and in the supernatant was measured using Pierce™ BCA Protein Assay Kit according to manufacturer's instructions. The coulombic efficiency (CE) was calculated by the formula as followed:

$$\mathrm{CE} = \frac{\int I\, dt}{F \cdot n \cdot V \cdot \Delta C_{mol}}$$

Where $\int \boldsymbol{I\, dt}$ calculated the number of electrons (Q), t is the measurement time (s), I is the current (A), F is Faraday's constant (96,485 C/mol), n is the number of electrons, V is the volume of anolyte (L), and ΔC is the concentration difference of the substrate (mol/L) during t time.

3.2.4 Scanning electron microscopy (SEM)

For the scanning electron microscopy, ITO electrodes were removed from the reactors after performing the electrochemical measurements and slightly washed with 0.1 M phosphate buffer (pH 7.4) to remove the cells suspended on electrode surface. Microbial fixation on electrodes was carried out with 2.5% glutaraldehyde diluted in 0.1 M phosphate buffer for more than one hour in dark at room temperature. This was followed by washing three times in 0.1 M phosphate buffer for 15 min each. These washed samples were then dehydrated in 25%, 50%, 75% and 100% ethanol gradients for 15 min each. Ethanol gradient dehydrated samples were exchanged thrice with 100 % t-butanol and finally freeze-dried under vacuum. The dried samples were coated with platinum and then observed using a Keyence VE-9800 microscope.

3.2.5 Genome-scale metabolic model simulation of histidine metabolism in *P. gingivalis*

A genome-scale metabolic model of *Porphyromonas gingivalis* W83 (*P. gingivalis*) was constructed [32]. Briefly, the author performed homology search of each coding region in *P. gingivalis* bacterial genome (GCF_000007585.1) against all genes posted on BiGG database [33] (those amino acid sequences were used as reference). The alignment scores of the homology search described certainty that each reaction is included in *P. gingivalis*. Finally, *P. gingivalis* metabolic model is constructed by removing reactions from bacterial universal model based on the estimated alignment score to maximize certainty of the presence of reactions in *P. gingivalis* while existing no gap in the metabolic network for biomass production by CarveMe using IBM ILOG CPLEX Optimizer version 12.9.0. The carving process was conducted under the condition that the *P. gingivalis* model can produce the biomass in the presence of following metabolites: ca2_e, cl_e, cobalt2_e, cu2_e, fe2_e, fe3_e, h2O_e, h_e, k_e, mg2_e, mn2_e, mobd_e, na1_e, nh4_e, ni2_e, pi_e, so4_e, zn2_e, and his__L_e. Then the constructed *P. gingivalis* model by CarveMe was further modified based on experimental results from published literature. Acetate transport reaction (ACt2rpp) was added to the model to enable acetate secretion [29, 34], and lower bounds of propionate transport reaction (PPAt4pp) and butyrate transport reaction (BUTt4pp) were changed to –1000 mmol×gDW-1×h-1 to allow the model to secrete propionate and butyrate [29, 34]. The lower bound of Acetyl-CoA: butyrate-CoA transferase (BUTCT) was also set to –1000 mmol×gDW-1×h-1 allow the butyrate production in the simulation [29, 34]. The lower bound of Formate-tetrahydrofolate ligase (FTHFLi) was set to –1000 mmol×gDW-1×h-1 because this reaction is reported to be reversible in bacteria [35]. The proton-pumping cytochrome bd oxydase (CYTB2pp) was removed because of the lack of evidence of the activity.

The author also introduced a demand reaction of NADH, DMnadh: NADH → NAD+ + H+, for mimicking the extracellular electron transport to the electrode. Flux distribution of the metabolic network in Pg was estimated by flux balance analysis (FBA) using cobrapy package [36]. The author set the following metabolites were unlimited (i.e. the lower bounds of EX

reactions for those metabolites were set to –1000 mmol× gDW-1×h-1): ca2_e, cl_e, cobalt2_e, cu2_e, fe2_e, fe3_e, h2O_e, h_e, k_e, mg2_e, mn2_e, mobd_e, na1_e, nh4_e, ni2_e, pi_e, so4_e, zn2_e. The author performed the simulation under anoxic condition like experiments (the lower bound of EX reaction for o2_e was set to 0 mmol× gDW-1×h-1). For L-histidine (his_L_e), a lower bound for its EX-reaction was set to –10 mmol× gDW-1×h-1 in accordance with the experimental condition. The author set ATPM: ATP + H_2O →ADP + H^+ + Pi as an objective function for optimization.

3.2.6 Flux sensitive analysis

The author estimated the impact of flux-changes in each metabolic reaction on flux in EET (i.e. flux in DM_nadh reaction, *F* in Figure 3.10A) by changing the flux in each reaction from its lower to upper bound. Upper and lower limits of flux in each reaction were determined by Flux variability analysis (F.V.A.) under the constraint that the model can generate the flux in ATPM at least 30 % of the maximal value. Then flux-changes in EET (ΔF in Figure 3.10B) is estimated by calculating absolute value of the difference between the minimum and maximum fluxes of the EET when the flux amount of the reaction of interest (*J* in Figure 3.10B) is altered from its lower to upper limit. Then the author computed Spearman's correlation (*r*) between *J* and *F* and multiplied the sign of *r* to ΔF. Therefore, if *F* decreased by changing *J* from its lower to upper bound, ΔF becomes negative.

3.2.7 Transcriptome analysis

The *P. gingivalis* cells attached on electrode surface after single potential amperometry (SA) and open circuit voltammetry (OCV) long-term measurements for one day with histidine as a substrate were collected to a sterile microtube and centrifuged at 6000 rpm and 4 °C to get pellets. The supernatant was discarded and 0.1 mL lysozyme (1 mg/mL) was added to resuspend the pellets by vigorous vortex. Subsequently, the cells were incubated 10 min at 37 °C and proceeded to the RNA extraction procedure using the NucleoSpin® RNA kit (Takara Bio) following the manufacturer's instructions. The collected RNA was sent to analysis agency Macrogen Japan.

Ribo-zero RNA removal Kit was used to purify RNA and a complementary DNA (cDNA) library was prepared for sequencing using the TruSeq Stranded Total RNA Library Prep Gold Kit following the manufacturer's guidelines. The cDNA library was sequenced by Illumina platform. In order to map cDNA fragments obtained from RNA sequencing, ASM758v1 was used as a reference genome. To compare relative expression patterns of *Porphyromonas gingivalis* W83 cells under SA and OCV conditions, read count per gene was extracted from known gene annotations with HTSeq program.

3.2.8 Estimation of transcriptional changes in metabolic genes corresponding to a metabolic reaction in the model

In the case of some metabolic reactions, the coding gene(s) on the genome does not correspond in one-to-one basis (e.g., metabolic reactions accomplished by complex of multiple proteins). Then, the author calculated the geometric mean of the fold changes in corresponding genes in each reaction and estimated the transcription-level regulation of each reaction. The author first checked gene-reaction-rule in the metabolic model. If a reaction of interest (*reactionX*) needs *gene1, gene2, …,* and *geneN* (this is described as (*gene1* and *gene2* and, …, and *geneN*)), then the author computed the geometric mean of the fold changes in read count per gene as follows:

$$fc_{reactionX} = \sqrt[N]{fc_{gene1} \cdot fc_{gene2} \cdot \cdots \cdot fc_{geneN}}$$

Here, $fc_{reactionX}$ is the estimated transcription-level control in the reaction X, and fc_{geneN} is the fold change in read per gene in *geneN*. In some reactions, there are multiple candidates for gene-reaction-rule (e.g., (*gene1* and *gene2*) or (*gene1* and *gene2* and *gene3*)), and the author calculated $fc_{reactionX}$ in each case and used the maximum value as a representative metric for transcriptional control in each reaction.

3.2.9 Electrochemical incubation of human saliva sample

This study was approved by the Kyushu dental university Ethics Committee (ethical approval number: 19-61 and 21-23). Saliva samples were obtained from a healthy volunteer

having history of no tooth problems, a moderate-healthy volunteer have minor tooth problems and an unhealthy person having severe tooth problems. A 1 mL of saliva sample was collected in an Eppendorf tube and diluted up to 3 mL with DM. The sample was centrifuged, and pellet was resuspended in 3 mL DM. The electrochemical incubation in an ITO based three electrode system was initiated using DM containing 10 mM histidine, glucose and lactate with 1 mL of diluted microbial consortium to each substrate condition and temperature was maintained at 37 °C. Controlled voltage conditions were maintained throughout the electrochemical analysis and corresponding current was measured with an automatic polarization system (VMP3, Bio-Logic Science Instruments).

3.2.10 DNA isolation and 16s r RNA sequencing of real saliva samples

The fresh saliva microbiome samples were analyzed by 16S rRNA gene sequencing. The forward and reverse primers for PCR were 27 F (5-AGA GTT TGA TCC TGG CTC AG-3) and 1492 R (5'-GGT TAC CTT GTT ACG ACT T-3). The 16S rRNA gene sequences were compared with the sequences of closely related strains by using the BLAST program in the GenBank database.

3.3 Results and Discussion

3.3.1 Substrate screening for current enhancement by *P. gingivalis*

Substrate effect on current production of *P. gingivalis* (Pg) was initially screened with different substrates by using a high-throughput system with 96-well screen-printed carbon electrode (SPCE) containing of carbon as working electrode (WE) with potential poised at +0.4 V vs standard hydrogen electrode (SHE), carbon as counter electrode (CE) and Ag/AgCl as reference electrode (RE) connected to a 96 channel potentiostat (**Figure 3.1a** and **3.2a**). The experimental setup was maintained anaerobically in an anaerobic gas chamber (100% N_2) and temperature was maintained at 37 °C. A 100 microliter of defined medium (DM) added to the SPCE well and *P. gingivalis* was spiked into the medium to reach a final optical density of 1.0 at

600 nm (OD_{600}). Single-potential amperometry (SA) was conducted with *P. gingivalis* using different substrates as electron and carbon sources, including amino acids which were previously reported to be tested for *P. gingivalis* metabolism [29] (L-histidine, L-leucine, L-threonine, L-arginine, L-aspartate, L-glutamate), peptides (His-His, Asp-Asp, Glu-Glu, Lys-Ala-MCA, AC-Asp-Glu-Thr-Asp-MCA, AC-Asp-Glu-Val-Asp-MCA, Boc-Leu-Ser-Thr-Arg-MCA), and commonly used sugar substrates glucose and lactate. The final concentration of each amino acids, glucose and lactate is 10 mM, while peptides concentration was 10/n mM (n is the number of amino acids in each peptide). Each condition had more than four replicates which have good reproducibility (**Figure 3.3a**). The screening experiments were separately conducted in two 96-well plates and the average current production versus time curves are showed in **Figure 3.3b-c**. The maximum current of each I-t curve was selected as peak current. The peak currents of all substrates were normalized based on the peak current of histidine taken from two replicate experiments (**Figure 3.2b**). The comparation of average peak currents of all substrates clearly demonstrates that the current production of *P. gingivalis* with histidine was significantly higher than other substrates (**Figure 3.2**). Histidine, among all the substrates, exhibited a progressive rise in current production with the maximum net current of about 3.50 nA when microorganisms were present (**Figure 3.3b**). *P. gingivalis* also generated high current of 2.56 nA with lactate. Among all the peptides, His-His shows the highest peak current of 2.43 nA, which is the third best substrate produced comparatively higher current. The current generation of *P. gingivalis* with other substrates was in the range of 1-2 nA, however, no significant current production was observed with sterilized defined medium, glutamate amino acid and glucose. Given that glutamate is a by-product of the histidine metabolism pathway (KEGG map) and that their respective processing pathways should mostly overlap, but the low current generation with glutamate monomer appears strange. Although *P. gingivalis* did produce current using glutamate dipeptide as a substrate (**Figure 3.2b**, Gluta-Gluta), this may be explained by the fact that *P. gingivalis* ATCC 33277 and *P. gingivalis* W83 strains have previously been found to significantly metabolize

glutamate dipeptides rather than monomers of glutamate [29, 37].

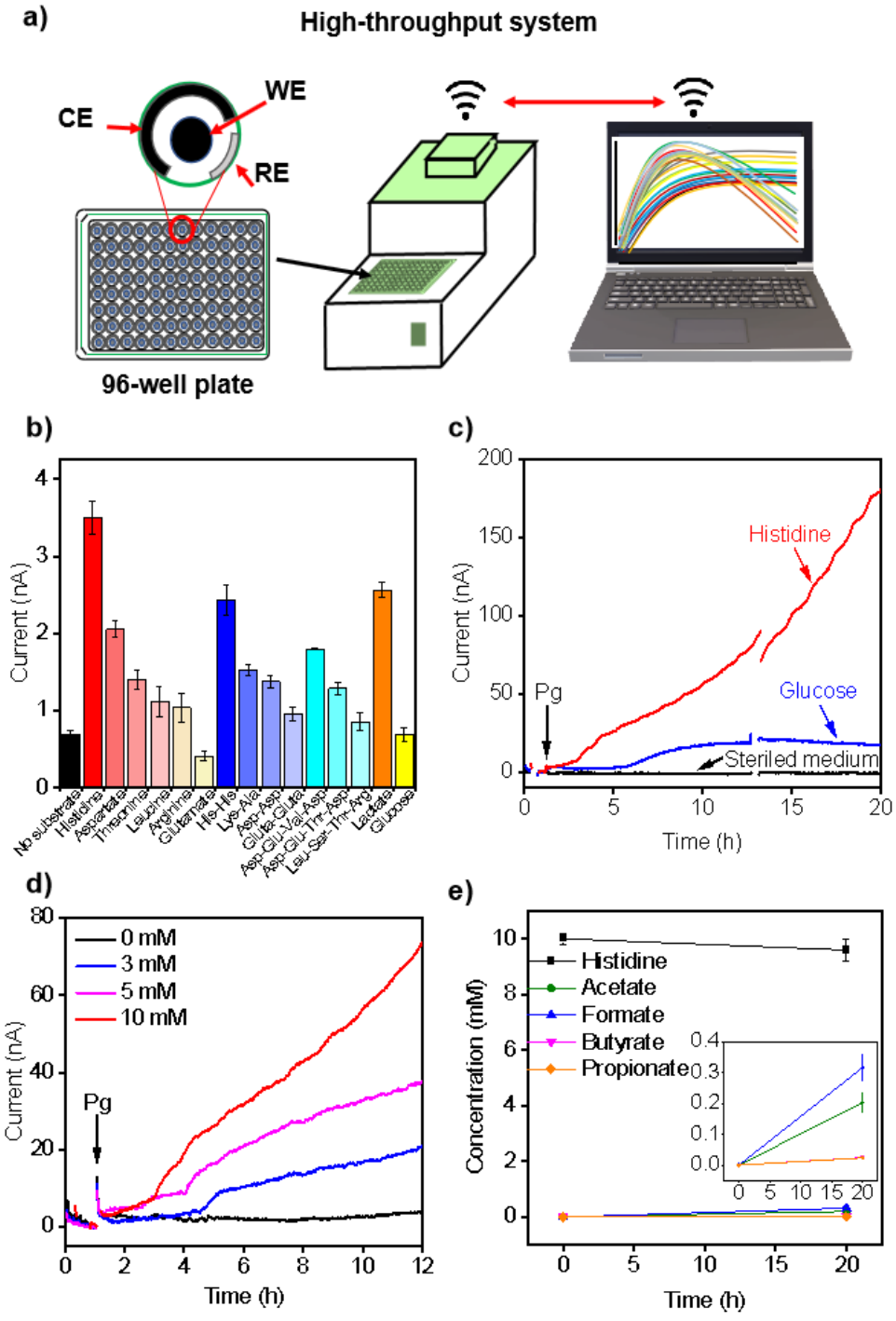

Figure 3.2 (a) The 96 well high-throughput SPCE system used for substrate screening with working electrode (WE) and counter electrode are carbon, reference electrode (RE) is Ag/AgCl. (b) Comparation of average peak current generated by *P. gingivalis* with all substrates in 96-well

plate, data presented are taken from 4-5 replicates. (c) Representative current production versus time measurements of *P. gingivalis* (Pg) in the presence of histidine or glucose conducted in an anaerobic reactor equipped with indium tin-doped oxide (ITO) electrodes. Similar tendency was observed in more than two individual experiments. (d) Representative current production versus time measurements by *P. gingivalis* (Pg) with different histidine concentration (0, 3, 5, 10 mM) measured in the ITO electrode system. (e) Histidine consumption and metabolites of *P. gingivalis* before and after the single-potential amperometry (SA) measurement of Figure 3.2c.

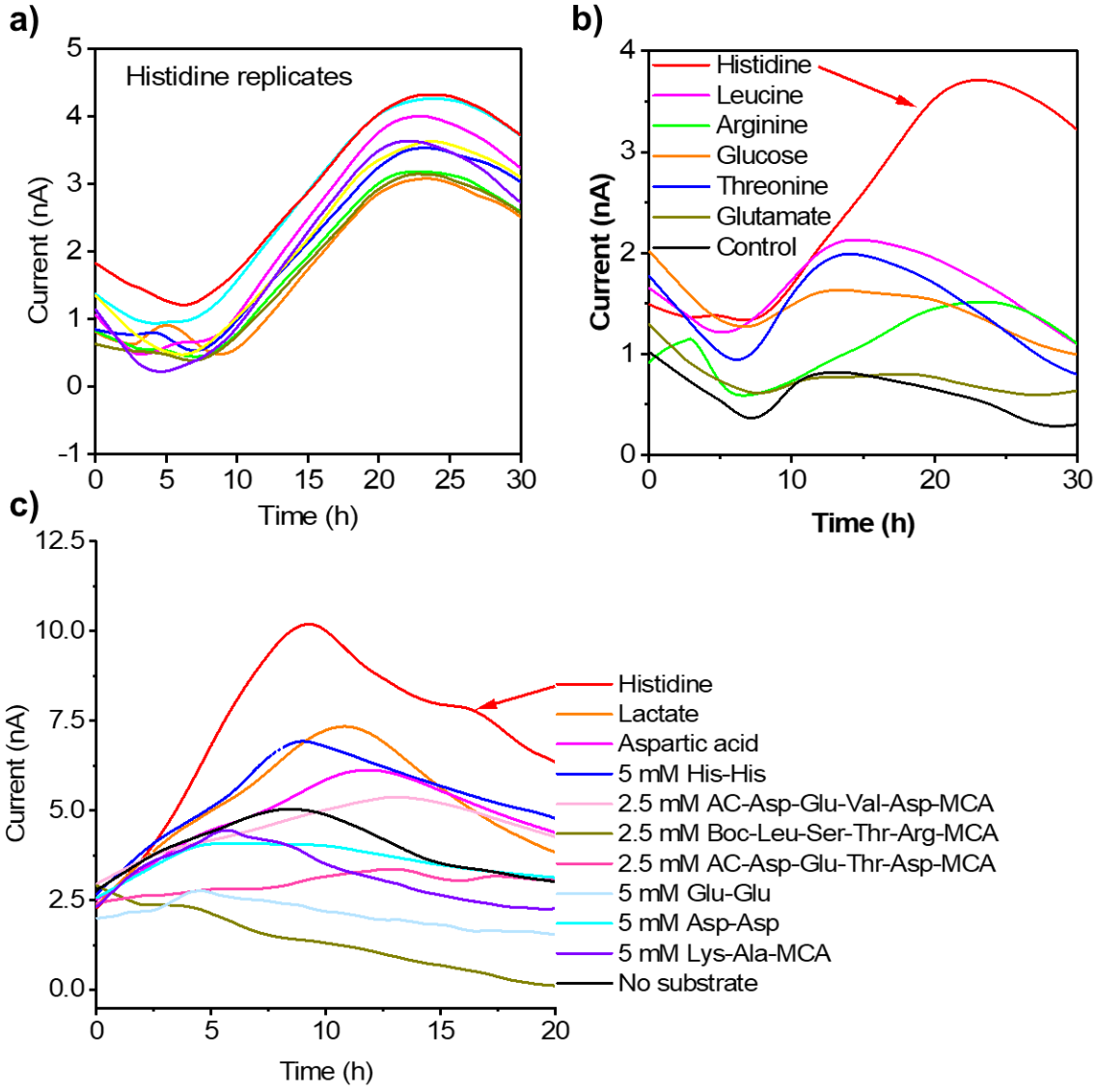

Figure 3.3 (a) Single-potential amperometry (SA) results of corresponding 10 replicates of histidine. (b) Average current production of *P. gingivalis* using different amino acids (histidine, leucine, threonine, arginine, glutamate) and common substrates glucose as electron and carbon sources. (c) Average current production of *P. gingivalis* using different amino acids (histidine, aspartate), peptides (His-His, Asp-Asp, Glu-Glu, Lys-Ala-MCA, AC-Asp-Glu-Thr-Asp-MCA, AC-Asp-Glu-Val-Asp-MCA, Boc-Leu-Ser-Thr-Arg-MCA), and common substrates lactate as electron and carbon sources. Each substrate had a final concentration of 10 mM and ≥4 replicates by using 96-well channel SPCE.

To further comprehend the significance of *P. gingivalis*' enhanced electron transfer with histidine, its current production with histidine and glucose was compared, and further analyzed whether current production was correlated with histidine concentration, SA measurements were conducted with various histidine concentrations (0–10 mM) in an indium tin oxide (ITO, WE) based electrochemical system with platinum wire as counter and Ag/AgCl as reference electrodes, respectively, and a total reactor volume of 5 mL (**Figure 3.1b**). The background current of sterilized medium without microbe was measured within the first hour, and there was no current generation with only defined medium with/without histidine and glucose (**Figure 3.2c**). With glucose, the current started increasing slowly after 4 hours of adding *P. gingivalis* cells and reached to a maximum of 22.6 nA at around 14 hours, while the current raised instantaneously with histidine and continue to increase during 20 hrs of measurement to reach a net current of 181.0 nA. In comparison to glucose, *P. gingivalis*' peak current increased by 8 times with histidine (**Figure 3.2c**). The current measured with different concentrations of histidine showed that the higher histidine concentration generated the higher current production (**Figure 3.2d**), similarly total charge (Q) generated by *P. gingivalis* with different histidine concentration has showed a good correlation with histidine concentration (**Figure 3.4**, R^2=0.972), strongly suggesting that the electron transfer of *P. gingivalis* with histidine is associated with its catabolism. After SA

measurement, the cells on electrode surface were collected and their morphology was analyzed using scanning electron microscopy (SEM) (**Figure 3.5**). With higher histidine concentration (10 mM) *P. gingivalis* cells showed intact cellular structure and clear cell shape; while 0 mM, 1 mM and 3 mM histidine conditions showed a relatively damaged cell shape, indicating the cell inactivity on electrode surface. These results strongly suggests that histidine was an essential substrate for current generation of *P. gingivalis* and highly increased the current generation as the electron and carbon source.

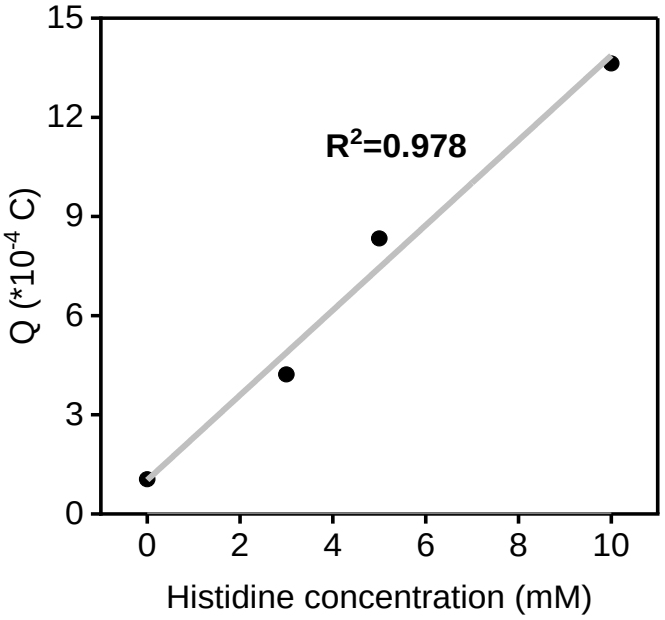

Figure 3.4 Correlation between histidine concentration and total charge (Q) produced by *P. gingivalis* taken from Figure 3.2d.

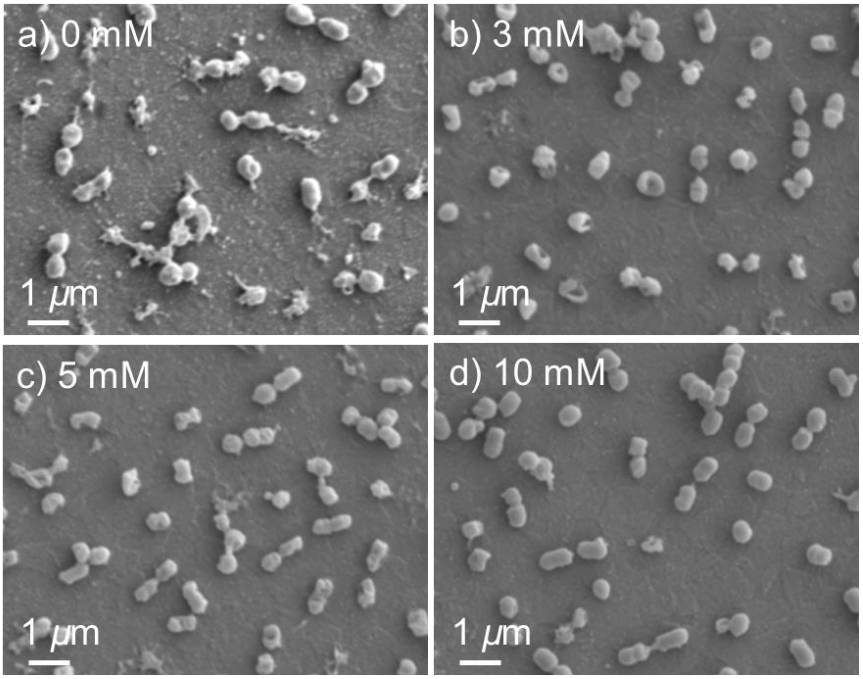

Figure 3.5 The scanning electron microscopy (SEM) images of *P. gingivalis* cells after single-potential amperometry (SA) measurement in ITO system with different a) 0 mM, b) 3 mM, c) 5 mM and d) 10 mM (Figure 3.2d).

Moreover, as glutamate is the first substrate created following histidine oxidation (KEGG), the author contrasted the histidine-based current of *P. gingivalis* with glutamate, which generated the lowest current in substrate-screening experiments (**Figure 3.2b**). With glutamate *P. gingivalis* generated a significantly less current compared to histidine (**Figure 3.6c**). After SA measurement, the morphology of cells on electrode surface was analyzed by using SEM. The cellular morphology of *P. gingivalis* with histidine supplementation exhibited a plump appearance and lacked observable signs of cellular damage, as depicted in **Figure 3.6a**. Conversely, in the presence of glucose or glutamate the cells appeared shrunken, and substantial amounts of cellular debris were evident (**Figure 3.6b** and **d**). These findings indicate that *P. gingivalis* cells remained active on the electrode surface during EET facilitated by histidine, whereas the cells supplemented with glutamate or glucose became inactive over prolonged testing periods, as evidenced by

reduced current production.

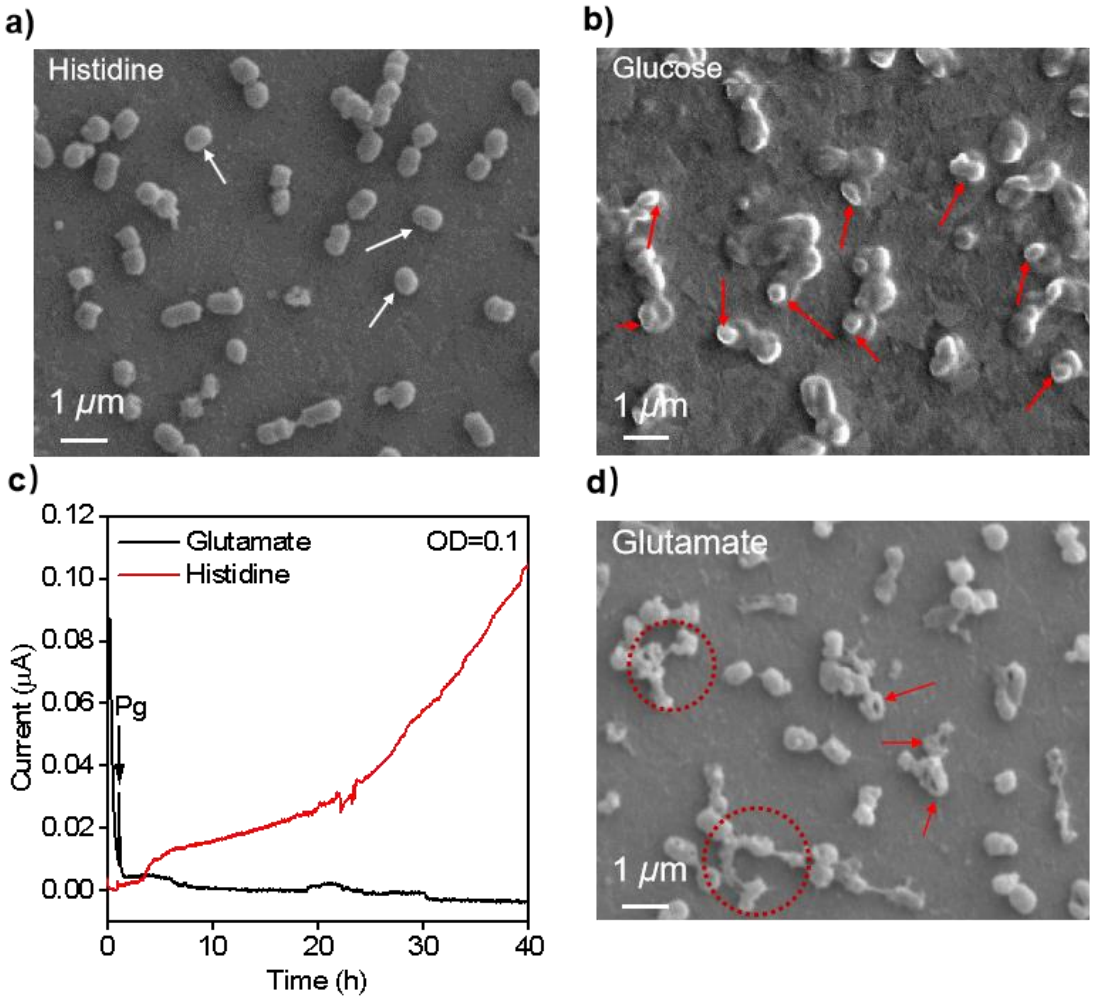

Figure 3.6 The corresponding scanning electron microscopy (SEM) images of *P. gingivalis* cells attached on electrode surface after single-potential amperometry (SA) in indium tin-doped oxide (ITO) system (Figure 3.2c) with (a) histidine or (b) glucose as the substrate. (c) Current production of *P. gingivalis* with glutamate as sole electron and carbon sources in ITO electrode system. (d) The corresponding SEM image of *P. gingivalis* cells after SA measurement with glutamate as the substrate.

The current generation of *P. gingivalis* displayed glucose metabolism when using glucose as the only substrate in previous research [26]. The author analyzed the histidine consumption and

metabolites produced throughout the SA measurement using a histidine assay kit and Ion-chromatography to determine whether the current production by histidine was associated with its metabolic utilization. An open circuit voltage (OCV) condition was also employed to compare the metabolic pathway of histidine under EET and non-EET conditions. As a result, as shown in **Figure 3.2e**, the less decrease in histidine concentration (0.41 mM) resulted in the production of acetate, butyrate, and formate, indicating that the fermentation of histidine occurred simultaneously with the current production of *P. gingivalis*. The SA measurement revealed increased concentrations of acetate and formate, while butyrate and propionate production were at a lower level than OCV (**Figure 3.7**). Acetate alone was released during SA measurement of *P. gingivalis* with glucose [26], suggesting that the specific fermentative metabolism would be coupled with the current production. While *P. gingivalis* cells did not grow in the supernatant during SA and OCV measurements, as shown in OD_{600} measurements (**Figure 3.8a**). Furthermore, there was little to no difference in the concentration of total protein after SA and OCV measurements (**Figure 3.8b**), which indicates that electron transfer cannot accelerate *P. gingivalis* cell growth. However, the cells attached to the electrode surface and formed a biofilm during SA measurement (**Figure 3.8c**). These results highlight the possibility that histidine oxidation and electron transfer may not support microbial growth but rather their metabolism in the biofilm, which would account for the low consumption of histidine despite the increased current production. This possibility suggests a thorough examination of the histidine metabolic pathway discussed in later sections.

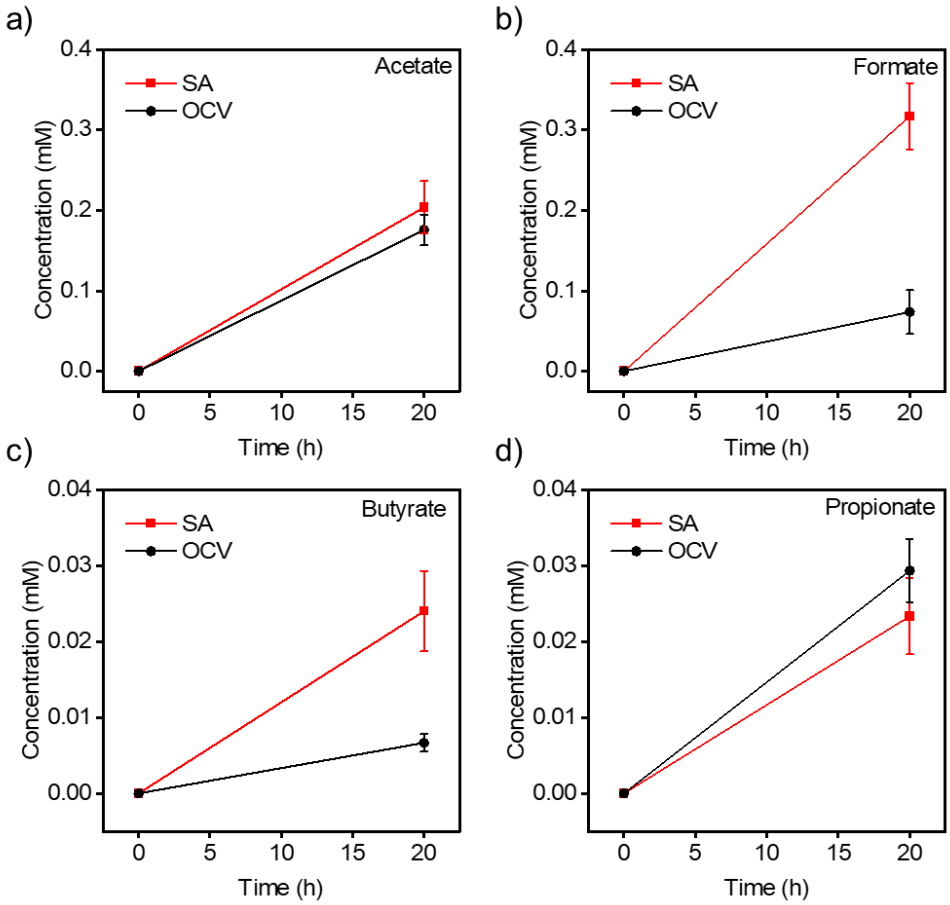

Figure 3.7 The metabolite concentration of *P. gingivalis* after keeping single-potential amperometry (SA) or open circuit voltage (OCV) condition for 50 h in the presence of 10 mM histidine.

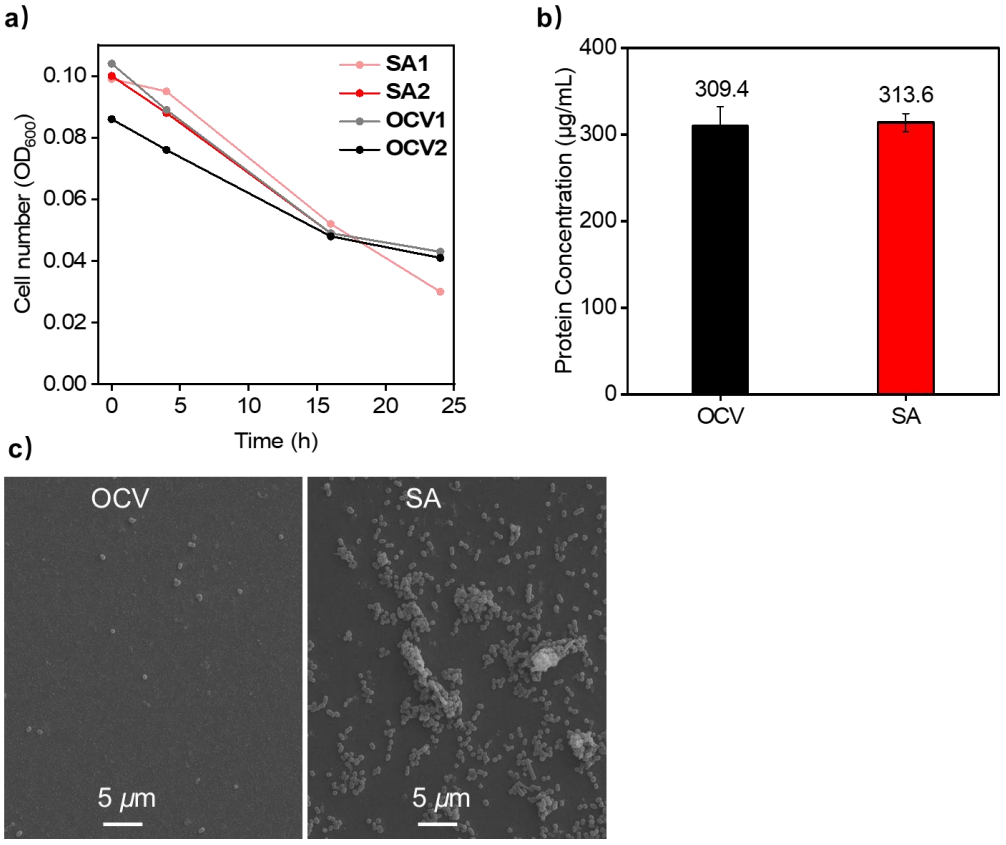

Figure 3.8 a) Growth of *P. gingivalis* in the supernatant analyzed by OD_{600} measurements under single-potential amperometry (SA) and open circuit voltammetry (OCV) condition in the presence of 10 mM histidine in an ITO based electrochemical systems. b) Total protein concentration (supernatant and electrode) of *P. gingivalis* measured after OCV and SA measurements. c) Scanning electron microscopy images of *P. gingivalis* on electrode surface after OCV and SA measurements.

In order to further assess the amount of *P. gingivalis* mRNA present on the ITO electrode during the SA measurement to indicate cellular activity, the author calculated the ratio of total mRNA to 16S rRNA [11]. This ratio serves as an indicator of single-cell gene expression since total mRNA levels reflect overall gene expression, while 16S rRNA is a measure of cell number. Therefore, the total mRNA/16S rRNA ratio provides a means to estimate the level of cellular activity. However, this method always works for community analysis to figure out the activity of

each species [11]. It is difficult to direct calculate the mRNA/16S rRNA ratio of pure culture. Housekeeping genes are genes that are consistently expressed in cells and are necessary for fundamental cellular processes [38]. They are often utilized as internal controls to standardize mRNA levels across diverse samples [39]. In this research, the infB gene was selected as the housekeeping gene for *P. gingivalis* [40]. The ratio of total mRNA to the infB housekeeping gene was employed as a measure of cellular activity. The data presented in **Figure 3.9** indicates that the ratio of mRNA to housekeeping gene in *P. gingivalis* cells supplemented with histidine is over two-fold higher than that in cells supplemented with glucose. This finding is in agreement with our previous observations of both current production and cell activity. Therefore, our results suggest that current production can serve as a more accurate and easier indicator of cell activity. A potential biosensor for periodontitis could be developed using the electrogenicity of *P. gingivalis*, which would not only detect the presence of the bacteria but also their metabolic activity. Additionally, this biosensor could be used to assess the effectiveness of drugs in biofilm monitoring.

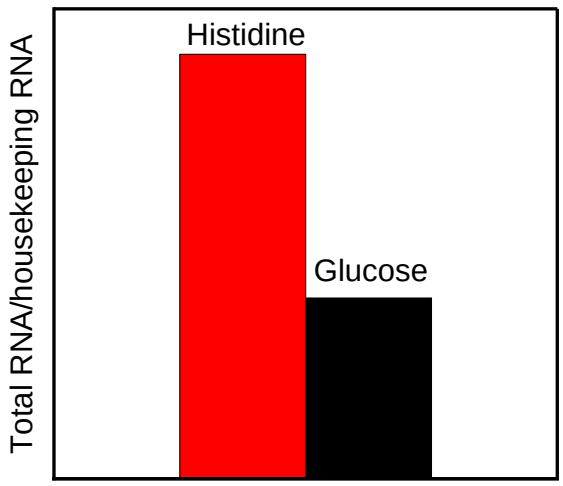

Figure 3.9 The total mRNA/housekeeping gene ratio analyzed by gene expression of *P. gingivalis* cells attached on electrode surface after electrochemical measurement in indium tin-doped oxide (ITO) system with a) histidine or b) glucose as the substrate.

The physiological role of EET associated with amino acid is somehow distinct from that of glucose fermentation coupled EET as reported previously in the same strain of *P. gingivalis* [41]. Amino acids and carbohydrates are both metabolized by dental plaque. The former is primarily capable of being broken down into acids like lactic acid though fermentation, whereas the latter is capable of being broken down into a variety of metabolites, including ammonia, acids, and amines, and is connected to tissue inflammation, oral malodor, and acid-neutralization [42]. It is well known that dental plaque contains abundant amounts of amino acids [43], pathogens like *P. gingivalis* could utilize available histidine for their energy generation and survival in oral biofilms.

3.3.2 Metabolic simulation proposed possible current producing metabolic pathways in *P. gingivalis* and their uniqueness

Next, the author explored what kind of metabolic reactions are responsible for current production by utilizing histidine. To this end, the author constructed genome-scale metabolic model of *P. gingivalis* based on the genomic information (see Materials and Methods). Current production was proposed to be associated with the level of intracellular excess reducing equivalents (e.g., NADH) and NAD^+/NADH balance greatly affect the rate of extracellular electron transfer in the case of other well-studied electricity-producing bacteria [44-46]. Therefore, the author introduced the artificial demand reaction DMnadh: $NADH \rightarrow NAD^+ + H^+$ and used its flux as an approximation for potential capability to produce current (**Figure 3.10a**). Besides, the author did not observe the growth of *P. gingivalis* under histidine available condition as a sole carbon source (**Figure 3.8a-b**), although they formed a monolayer under SA condition (**Figure 3.8c**). The author estimated optimal flux distribution of *P. gingivalis* on L-histidine by optimizing ATP maintenance requirement reaction (ATPM: $ATP + H_2O \rightarrow ADP + H^+ + Pi$) instead of their biomass function and checked how the flux in conversion of excess NADH to NAD^+ change by other intracellular metabolic fluxes under histidine available condition. Of 620 annotated metabolic reactions, flux changes in 430 reactions caused the changes in current production level (showing impact of the flux on the current production ($\Delta F > 0$) (**Figure 3.10b**). Since the increase

in butyrate and formate production were primary signatures in fermentation metabolism upon shift to current-producible condition (SA condition) (**Figure 3.7**), the metabolic reaction responsible for current production should also have a great impact on production of those metabolites in the same manner. Then, the author also explored the impact of each metabolic reaction on butyrate and formate efflux (**Figure 3.10a-b**). Many of the 430 reactions also changed the efflux of those two metabolites, but most of those exhibited opposite effect to the case of current production (**Figure 3.10c**). Next, the author screened the reactions whose flux-changes can drive the increase (or decrease) in both the current production and the production of butyrate and formate. Among 430 reactions, only 18 reactions exhibited the impact on those 3 fluxes in the same direction (**Figure 3.10d**, **3.11**, and **3.12**). Those metabolic reactions are located on particularly histidine, folate, acetate, butyrate, and inosine-monophosphate (IMP) metabolism (**Figure 3.10e**). The positive effects of reactions in histidine metabolism (HISDr, URCN, and IZPN_1) would be reasonable because this pathway is essential for conversion to glutamate and the metabolism in downstream. The author found 1 reaction in folate metabolism, glycine hydroxymethyltransferase (GHMT2r), exhibited positive impact on all fluxes (**Figure 3.10e**). Folate metabolism is closely linked to histidine metabolism and potentially can produce NADH and formate (**Figure 3.10e**), and thus this pathway could explain both current production and the changes in metabolic profiles. The redox reaction in butyrate metabolism, butanoyl-CoA dehydrogenase (ACOAD1f) was also screened as the positively affecting reactions. On the other hand, the reactions in acetate metabolism (HACD1, PTAr, and ACKr) all negatively affected current, formate, and butyrate productions, suggesting that activation of acetate metabolism would potentially decrease the current production level (**Figure 3.10d-e**). The reactions in IMP biosynthesis also screened as negatively affecting because up-regulation of this pathway would cause the consumption of 10-Formyltetrahydrofolate and glutamate, both are important for energy production in folate and amino-acid fermentation metabolism (**Figure 3.10e**). The author also found that metabolic reactions that can work as FAD: NAD oxidoreductase (NADFADOR)

showed the strong impact on the current generation and production of butyrate and formate. However, the consumption of histidine (**Figure 3.2e**, 0.41 mM) was much less compared with histidine provided (10 mM), as *P. gingivalis* is more likely to survive and persist within in dental biofilm and utilizes amino acids as energy and carbon sources [47-49]. The histidine oxidation efficiency of *P. gingivalis* (considering oxidation of histidine to acetate) is measured by its coulombic efficiency (CE), which is remarkably high at 2.8% (**Figure 3.13**). This value is approximately 1000 times greater than the reported CE for glucose oxidation by *P. gingivalis* in a previous study (0.003%) [26]. This finding is of great significance and is notably surprising for EET of *P. gingivalis*.

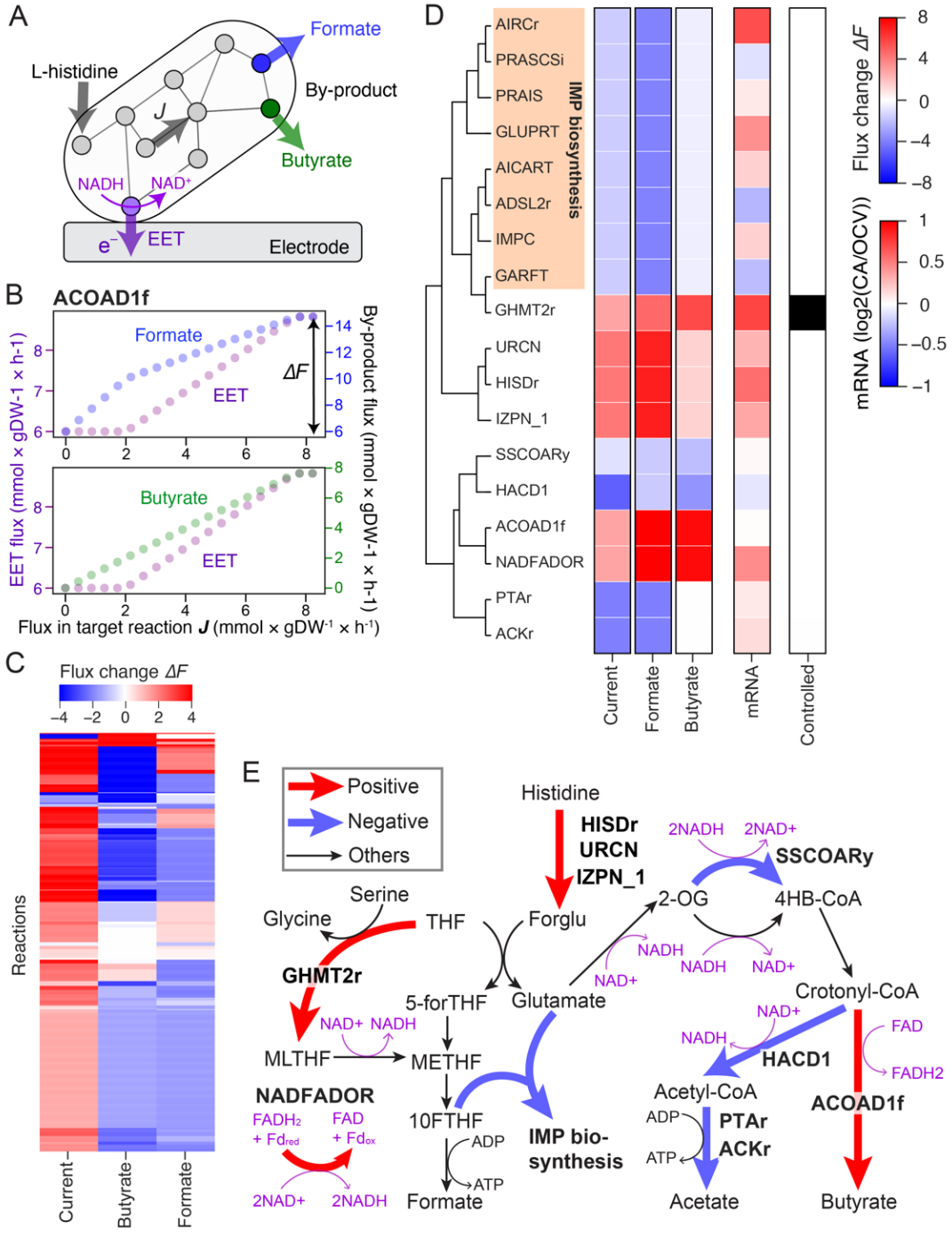

Figure 3.10 Proposed metabolic pathways responsible for current production from histidine in *P. gingivalis* by metabolic simulation and transcriptome analysis. (a) A schematic diagram for analyzing the impact of each metabolic reaction (gray arrow) on current production using a genome-scale metabolic model. The author altered flux in a target reaction (*J*) and checked level of flux change in NADH oxidizing reaction (DMnadh), which was used as a proxy for EET rate.

(b) Representative flux change in EET by altering flux in one of metabolic reactions. Here, the author altered the flux in ACOAD1f (butanoyl-CoA dehydrogenase) from its lower to upper limits (see Materials and Methods) and monitored the change in EET flux. Then the difference between minimum and maximum flux of current calculated (ΔF). If the flux in EET positively or negatively correlates to that in target reaction, ΔF becomes positive or negative, respectively. (c) Heatmap of ΔF in metabolic reactions showing significant effect on the flux in EET. Red and blue in heatmaps showed increase and decrease of flux in the displayed reactions when a flux in target reaction was forcibly changed. (d) Heatmap of ΔF in the reactions whose impact on the metabolic fluxes (current, butyrate, and formate production) was consistent to those observed in the experiments. Each reaction was represented by BiGG ID [33]. The author also showed a level of transcriptional change in a corresponding gene to each metabolic reaction which is calculated from RNA-seq data. Metabolic reactions that were transcriptionally controlled and have a consistent effect on current generation is filled in black in the rightmost side (labeled "Controlled" in the panel). Proposed metabolic pathway map of key metabolic reactions for current production. Metabolic reactions listed on the panel d is colored by red or blue depending on whether those reactions showed positive or negative effects. The author also colored redox reactions with purple.

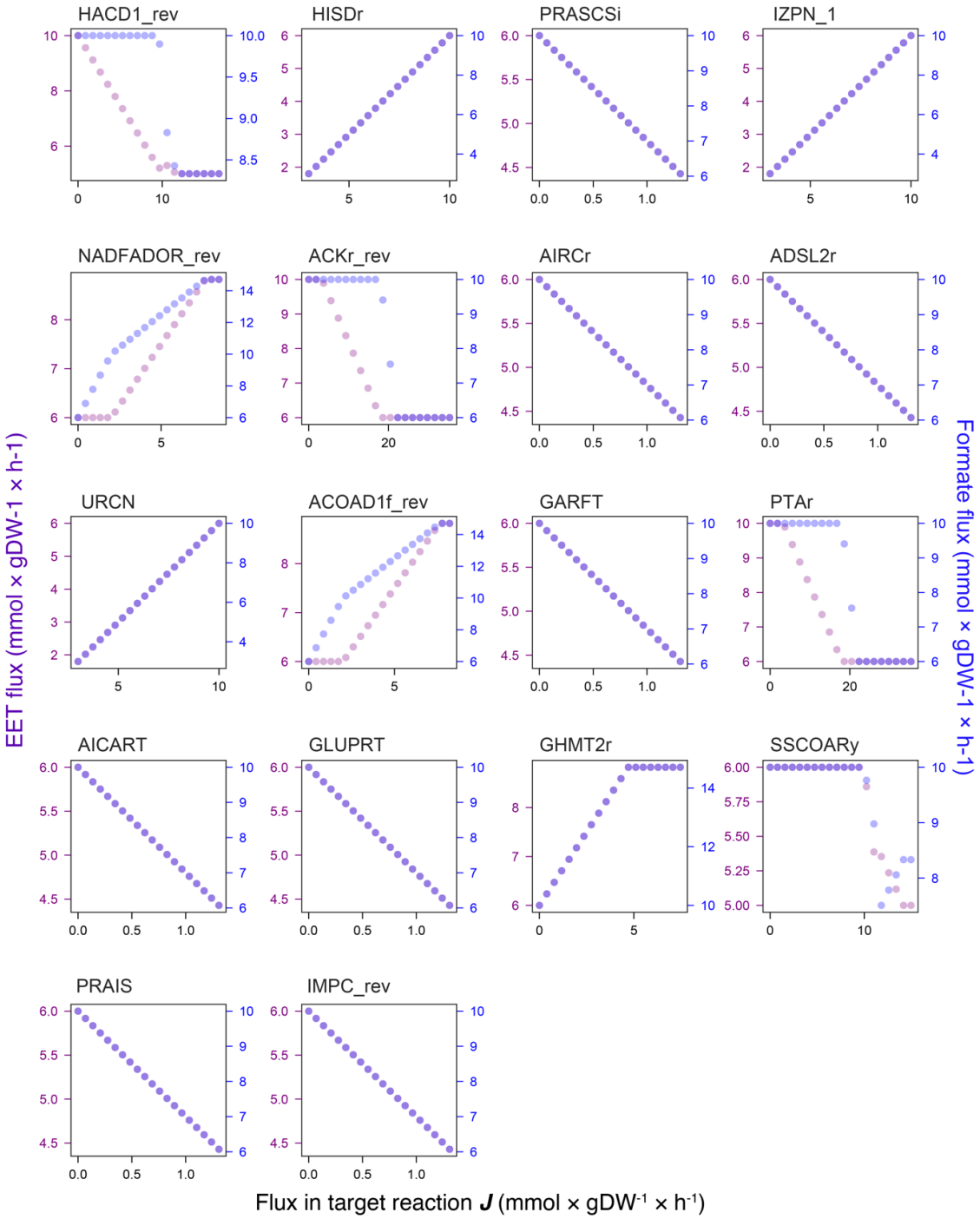

Figure 3.11 Flux changes in current (purple) and formate (blue) production by altering flux in one of metabolic reactions. The author altered the flux in a displayed reaction from its lower to upper bounds and monitored the change in EET flux.

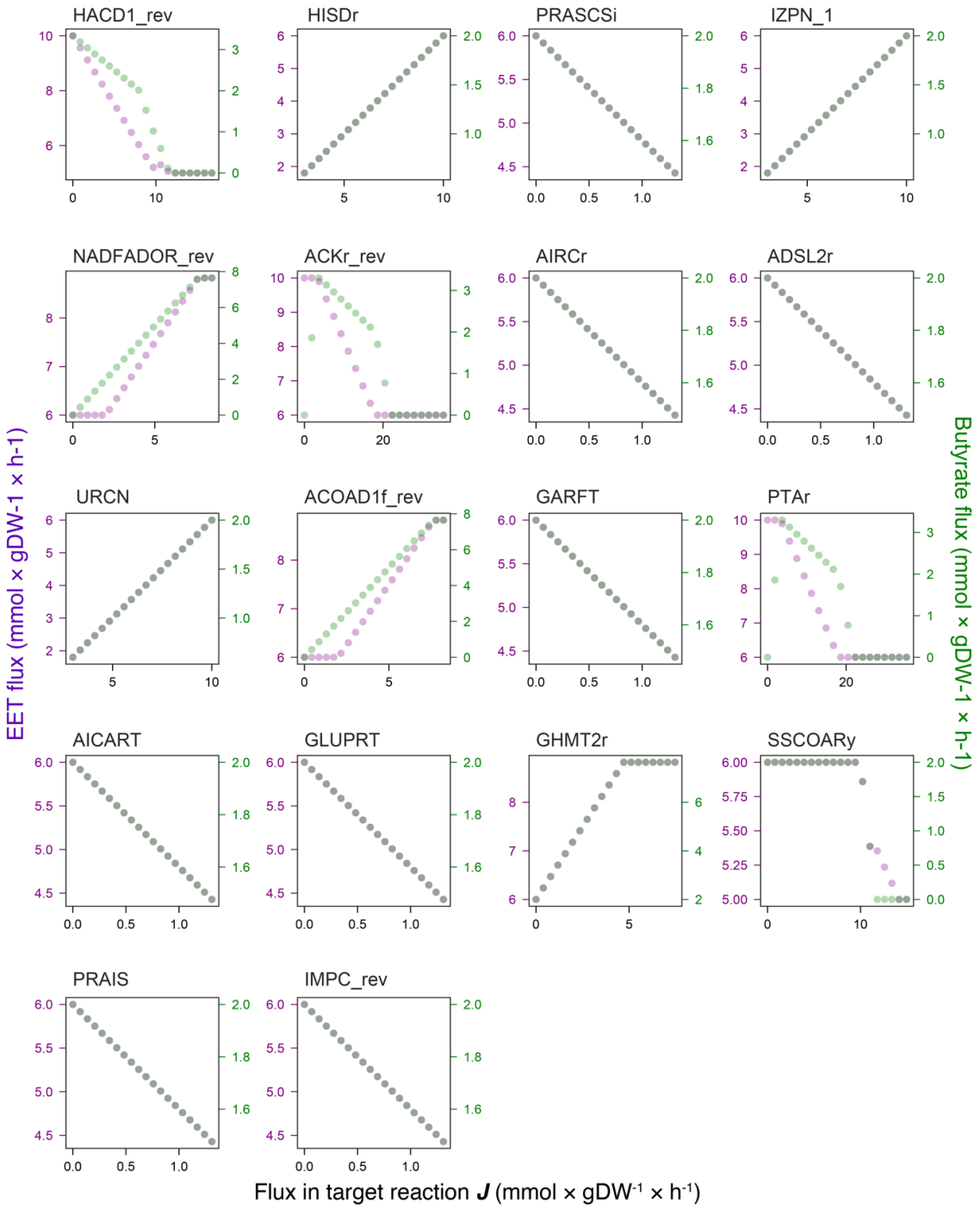

Figure 3.12 Flux changes in current (purple) and butyrate (green) production by altering flux in a displayed reaction. The procedure is same as Figure 3.11.

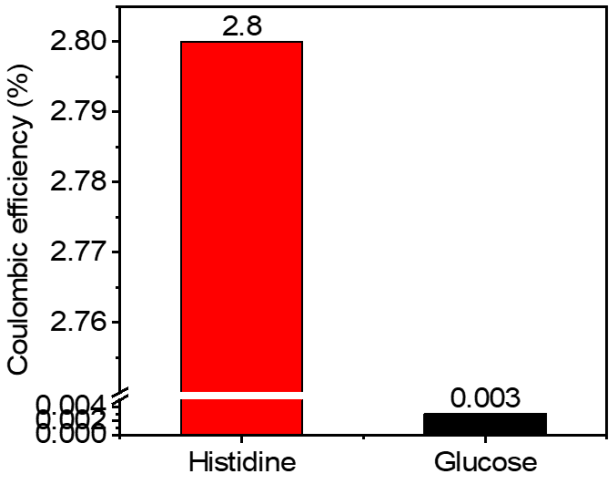

Figure 3.13 The coulombic efficiency (CE) of current production of *P. gingivalis* cells coupled with histidine or glucose oxidation.

In previous studies using other electricity-producing bacteria, key metabolic genes for current generation exhibit different expression levels depending on the electrode potentials [50-53]. Therefore, the author assumed that some of the screened metabolic reactions showing significant effect on the current production would also exhibit altered transcription level by changing electrode potentials. To explore this possibility, the author performed RNA sequencing (RNA-seq) of *P. gingivalis* cells collected from the surface of the electrode. The author compared transcriptional profiles between SA and OCV (where current production was maintained at zero) conditions. The author found 288 genes that were differentially expressed between those two conditions (with a fold change greater than 1.5, almost equivalent to $|\log2(SA/OCV)| > 0.585$), and 72 genes were up-regulated, and 216 down-regulated in SA. Of those, the author found only 39 metabolic reactions encoded by one of those differentially expressed metabolic genes (12 were up-regulated and 27 were down-regulated), suggesting that transcriptional regulation of metabolism is quite limited. Among the screened reactions which have significant effect on the production of current and other metabolites, GHMT2r were transcriptionally controlled (a fold

change greater than 1.5), but no other reactions did not exhibit significant difference in mRNA level (**Figure 3.10d**). Given that this reaction is located specifically in the downstream of histidine (and not other amino acids such as glutamate), the up-regulation of this reaction and folate metabolism would be one possible mechanisms of higher current production level with histidine compared to other amino acids. Overall, our analysis using metabolic models supported the presence of metabolic reactions responsible for current production and unique fermentation metabolism under current producible condition.

3.3.3 Histidine specifically enhanced the current production in *P. gingivalis* among other oral pathogens.

Recent reports indicated that oral pathogens such as *Aggregatibacter actinomycetemcomitans* (Aa)*, Streptococcus mutans* (Sm)*, Corynebacterium matruchotii* (Cm) and *Capnocytophaga ochracea* (Co) has generated significantly higher current production with glucose or lactate compared to *P. gingivalis* [54]. In order to determine if *P. gingivalis* can specifically create a high current with histidine, the author examined the impact of histidine on the current production of Aa, Sm, Cm, and Co and contrasted it with that of *P. gingivalis* (Pg). The current production was measured by SA with a working electrode of indium tin-doped oxide (ITO) at +0.4 V vs SHE. Upon addition of cells to a final concentration of 0.3 OD_{600} into the electrochemical reactor containing 10 mM histidine, current production was gradually increased during initial hours with *P. gingivalis* as shown in time vs current profile measurements (**Figure 3.14a**). Maximum current was reached to approximately 67 nA between 15-20 hrs time period (**Figure 3.14a**, Pg-red line) and started to decrease in next hours either due to histidine unavailability at the bottom of biofilm on electrode surface or cell activity was reduced after 20 hours operation. Similarly, Aa, Sm, Cm and Co were tested with histidine with an initial cell density of OD_{600}=0.3. Clearly, *P. gingivalis* has generated significantly higher current with histidine than the other oral pathogens. Current production of Cm with histidine reached about

~9.1 nA at 7-8 hours (**Figure 3.14a**, Cm- green line), however no significant current production was observed with Aa, Co and Sm in the presence of histidine (**Figure 3.14a**). Similarly, the current production of three strains with glucose were tested as well (**Figure 3.15**), in concurrence with previous reports all three strains have showed significant current generation on electrode surface with glucose [54]. However, with histidine *P. gingivalis* was specifically producing higher current. The histidine metabolic pathway of all five strains was next examined, and the author found that only *P. gingivalis* has all of the enzymes necessary to convert L-histidine into urocanate, 4-Imidazolone-5-propanoate, and N-Fomimino-L-glutamate and L-glutamate (**Figure 3.14b**). The enzymes responsible for L-histidine degradation leading to glutamate production were presented only in *P. gingivalis* (**Figure 3.14b**) whereas Aa, Sm, Cm and Co do not contain all the enzymes of histidine metabolism, thus the current production with histidine was significantly lesser compared to Pg. The elevated currents with histidine shown here further demonstrate the substrate-dependent EET ability of pathogens to derive cellular energy from non-fermenting carbon sources in nutrient-deficient biofilm environments like oral plaque. It is crucial to investigate in greater detail how this method of obtaining energy from external substrates functions physiologically.

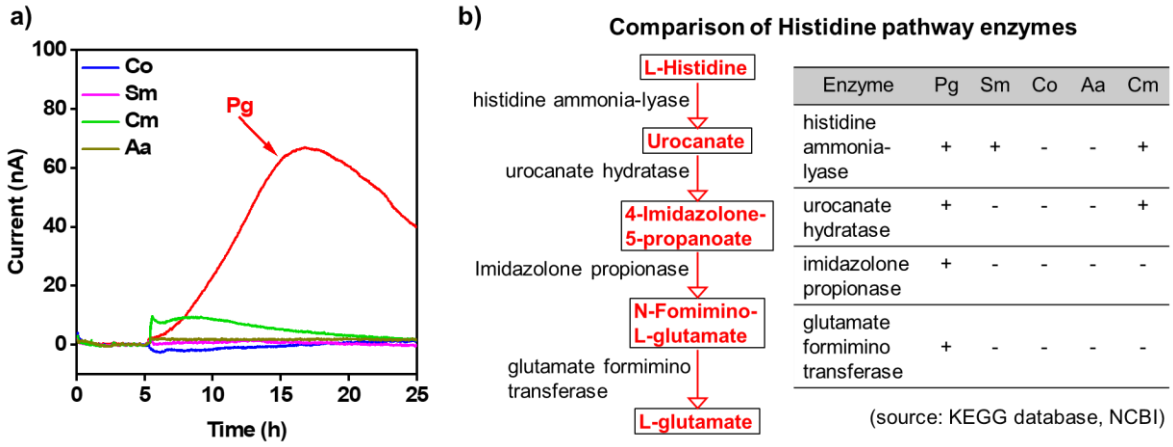

Enzyme	Pg	Sm	Co	Aa	Cm
histidine ammonia-lyase	+	+	-	-	+
urocanate hydratase	+	-	-	-	+
imidazolone propionase	+	-	-	-	-
glutamate formimino transferase	+	-	-	-	-

Figure 3.14 (a) Representative current production versus time measurements conducted in an anaerobic reactor equipped with indium tin-doped oxide (ITO) electrodes in the presence of

histidine by *P. gingivalis* (Pg), *C. matruchotii* (Cm), *A. actinomycetemcomitans* (Aa), *S. mutans* (Sm) and *C. ochracea* (Co). Similar tendency was observed in more than two individual experiments. (b) L-histidine catabolic pathway and enzymes that regulate the pathway present in *P. gingivalis* and comparison analysis of L-histidine pathways enzymes among Pg, Sm, Co, Aa and Cm (source: KEGG database).

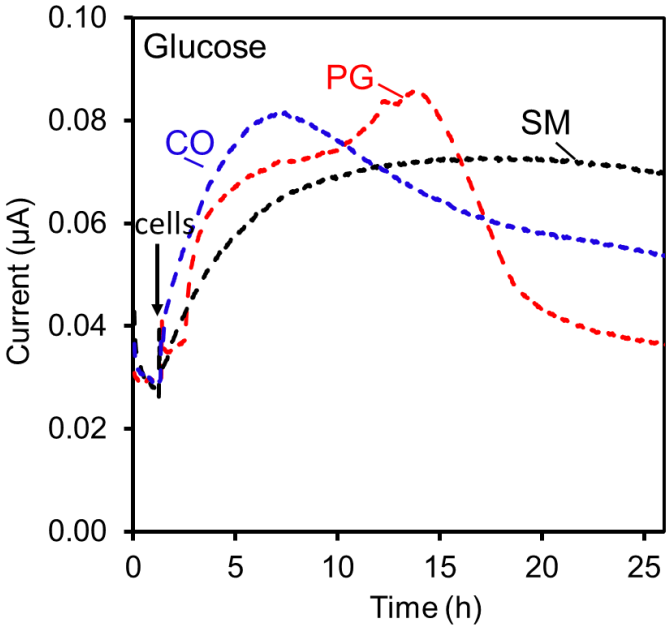

Figure 3.15 Current production versus time measurements conducted in an anaerobic reactor equipped with indium tin-doped oxide (ITO) electrodes (surface area: 3.14 cm^2) poised at +0.4 V (versus SHE) in the presence of histidine and glucose by *P. gingivalis* (PG), *S. mutans* (SM) and *C. ochracea* (CO).

3.3.4 Electron transfer mechanism study of *P. gingivalis* by using electrodes with different wettability

It is expected that outer-membrane cytochromes (OMCs) of *P. gingivalis* mediated EET based on the redox peaks observed in differential pulse (DP) voltammograms [26]. However, the outer-membrane redox proteins haven't been proved in *P. gingivalis*, it is still unclear whether it is OMCs that mediates electron transfer from intracellular to extracellular. The wettability of

electrode affected the redox state of OMCs protein which can be used to study the extracellular electron transfer (EET) process of electrogenic bacteria [55, 56]. Therefore, this study examined the impact of electrode wettability on EET activity and the electron transfer mechanism at the interfaces between *P. gingivalis* cells and electrodes. DP voltammograms were measured with a working electrode of modified indium tin-doped oxide (ITO). Firstly, ITO electrodes' surface was modified by dip-coating them with hydrophobic CH_3- (CH_3-ITO) or hydrophilic SH- (SH-ITO) ligands, respectively. The modification method and water contact angles were showed in **Chapter 2 (Figure 2.2)**. SA was conducted with an applied potential of +0.4 V vs SHE as showed in **Figure 3.16a**. With increasing electrode hydrophilicity, current generation coupled with histidine oxidation increased which is similar with reported. The current production of *P. gingivalis* with hydrophobic electrode quickly decreased after three hours, while the current sustained for more than 9 hours with hydrophilic electrode. To study the potential electron transport pathway, DP voltammograms were measured before and after *P. gingivalis* cells and two grey arrows in **Figure 3.16a** indicates the time point to conduct DP voltammograms. The DP voltammograms of the sterile electrolyte (**Figure 3.16b**) revealed no redox signals on any electrode. However, the DP voltammograms for untreated ITO, CH_3-ITO and SH-ITO in the presence of *P. gingivalis* cells measured at 7 h disclosed two peaks within the −0.5 to −0.2 V region which was consistent with the reported [26] (**Figure 3.16c**). Hence, the detected redox peaks within the potential region were most assignable to the redox agents of *P. gingivalis* that potentially mediate electron transport to the electrode surface, probable OMCs. But no evidence has been reported till now that *P. gingivalis* has OMCs. The two peaks were separated as showing **Figure 3.17**, which can clearly reflect the peak width and height of each peak. The half-peak width of left redox peak was more than 200 mV, which was consistent with one-electron transfer process by outer-membrane redox protein. The half-peak width of more positive redox peak was ~79 mV, which was more like two-electron transport process such as shuttles. This result was consistent with the reported paper that *P. gingivalis* may secrete redox shuttle [26]. Besides, the redox peak current, which stands for the

amount of redox agents, at around −151 mV increased with increasing hydrophilicity, while the peak current at around −23 mV was stable (**Figure 3.16c**). The result indicates the amount of outer-membrane redox proteins (cell number) on hydrophilic electrode was more than that on the hydrophobic electrode [55]. While the cells secreted similar number of redox shuttle due to the same number of cells in two reactors. Importantly, the redox potentials of the OMRPs slightly shifted from −151 mV and −23 mV for ≤ 24 mV and ≤ 13 mV, respectively, in the negative direction with increasing hydrophilicity (**Figure 3.16c** and **Figure 3.17**). This finding suggests that the electrode surface wettability affected the redox property of the outer-membrane redox proteins as well as secreted redox shuttle of *P. gingivalis*. The current production displayed a positive correlation with the DPV redox peak current at around −151 mV and with more reduced state attached to the electrodes, which support the hypothesis that *P. gingivalis* utilizes a significant cell surface bound redox proteins in association with a redox shuttling mediated EET mechanism [26]. To identify the outer-membrane redox proteins and redox shuttles would be an important direction of future study.

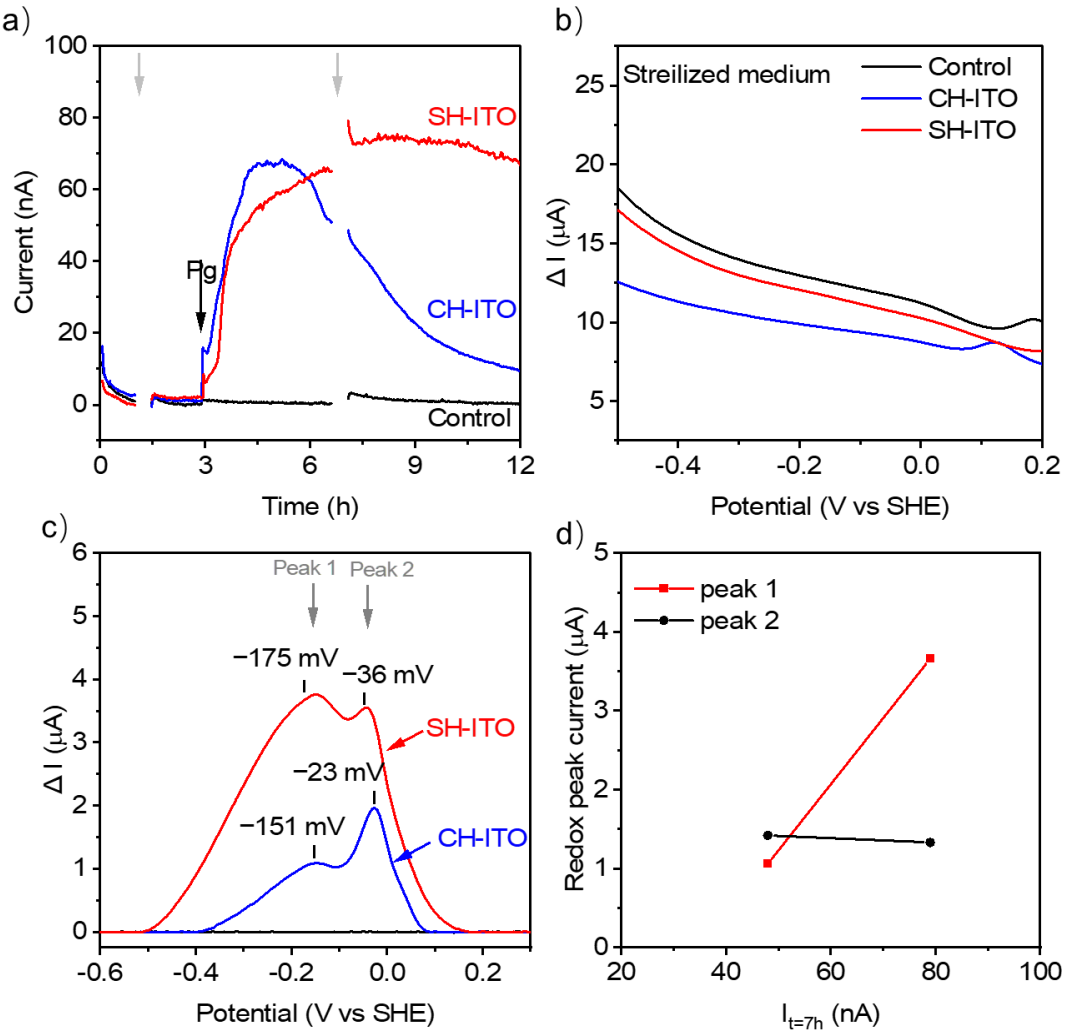

Figure 3.16 Electrochemical measurements of *P. gingivalis* (Pg) cells on SH-ITO (red) and CH_3-ITO (blue) electrodes. (a) Plot of current vs. time of sterile medium and live cells poised at +0.4 V vs. SHE. Arrows in panel (a) indicate timing at which differential pulse (DP) voltammograms were recorded. (b) DP voltammograms measured with sterilized medium before adding live Pg cells. (c) DP voltammogram of live Pg cells after baseline subtraction. The short bars indicate the peak potentials (E_p). (d) Plot of current production by Pg cells at 7 h in panel (a) versus the corresponding redox peak height of baseline-subtracted DP voltammogram in panel (c).

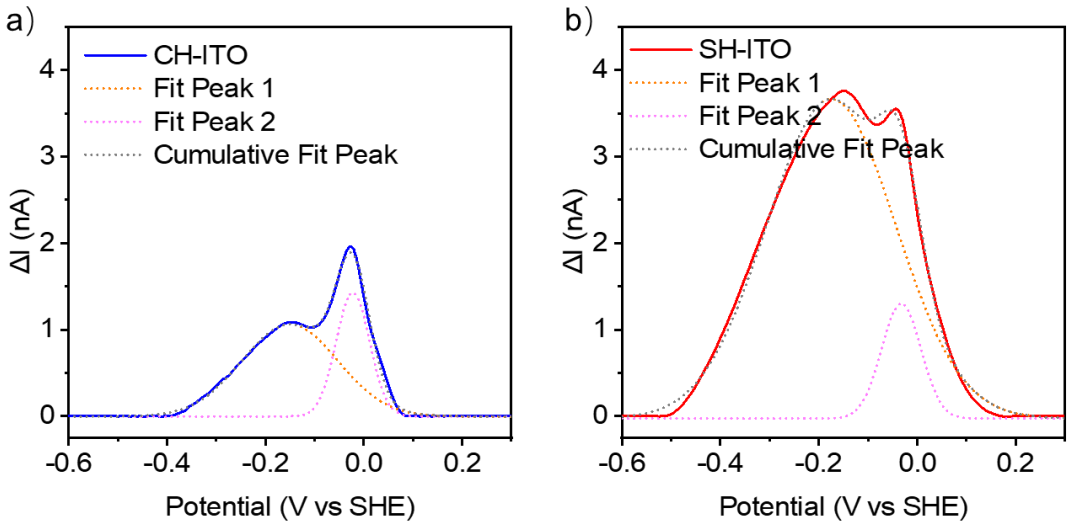

Figure 3.17 Two peaks fitting of DP voltammogram of live *P. gingivalis* cells on (a) CH-ITO and (b) SH-ITO electrode.

3.3.5 Electrochemical incubation of saliva pathogens

It is well known that *P. gingivalis* is asaccharolytic and has ability to utilize amino acids for their metabolism [57]. Based on the results above, *P. gingivalis* showed the ability to produce much higher current with histidine compared with glucose. *P. gingivalis* acts as one of the important periodontitis biomarkers for biosensing of *P. gingivalis* in dental biofilm. Thus, the author further tested the possibility of extracellular electron transfer capability of human saliva microbiome on electrode surface with histidine as substrate. Saliva samples were collected from a healthy person (H-saliva), a moderate-healthy (Mh-saliva) person and an unhealthy (Un-h-saliva) person and were tested for substrate specific EET capability of pathogens with histidine, glucose, and lactate. Saliva samples from each volunteer were initially centrifuged and the pellet was washed with nitrogen sparged defined medium to remove oxygen and any trace carbon sources. Resuspended pellet was diluted with 3 mL of defined medium and 1 mL of saliva is added to each

condition into the three electrode electrochemical reactors containing 10 mM histidine, glucose, and lactate at indicated times with arrow. The current generated by three saliva samples with histidine (**Figure 3.18a**), glucose (**Figure 3.18b**), and lactate (**Figure 3.19**) were measured in the first 16 hours. Surprisingly, with histidine current production from unhealthy saliva was gradually increased and reached to ~180 nA at 16 hrs, which is much higher than from moderately healthy (50 nA) or healthy saliva (20 nA) samples (**Figure 3.18a**). The microbiome of saliva samples generated different currents when exposed to glucose (**Figure 3.18b**) or lactate (**Figure 3.19**), but these currents did not show any correlation with health conditions. The current produced by Mh-saliva was higher than that produced by H-saliva, while the current produced by H-saliva was higher than that produced by Un-h-saliva with glucose or lactate (**Figure 3.18b, 3.19**). Un-healthy salivary microbiome has generated significantly higher current with histidine rather than with glucose or lactate implicating to the presence of *P. gingivalis* and associated current production with histidine.

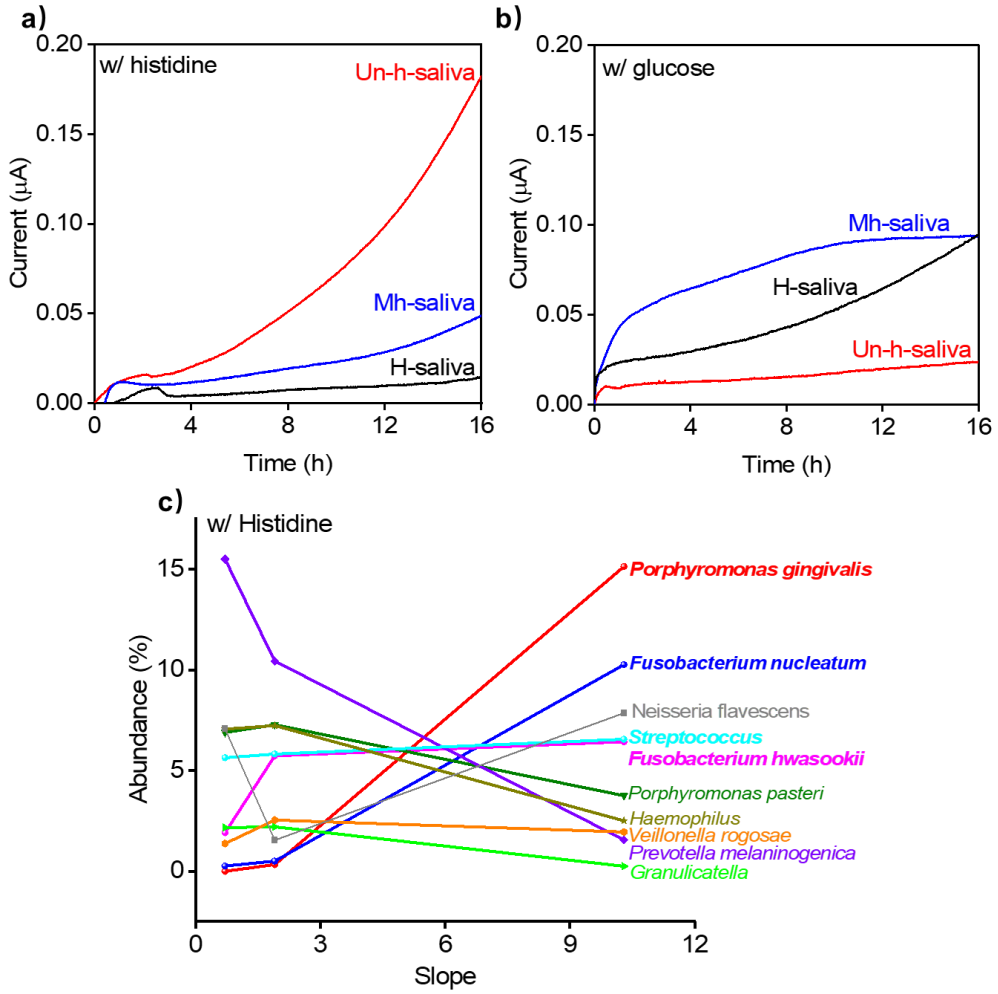

Figure 3.18 Current production versus time measurements conducted in an anaerobic reactor equipped with indium tin-doped oxide (ITO) electrodes (surface area: 3.14 cm^2) poised at +0.4 V (versus SHE) in the presence of (a) histidine and (b) glucose with healthy (H-saliva), moderate-healthy (Mh-saliva) and patient (Un-h-saliva) samples. (c). The potential correlation between the composition of abundant oral microbiota (>1%) determined by 16s rRNA sequencing and the maximum current slope of I*t*-t curves of H-saliva, Mh-saliva and Un-h-saliva with histidine, as an indicator of the bacterial species' association with current production by using histidine as the substrate.

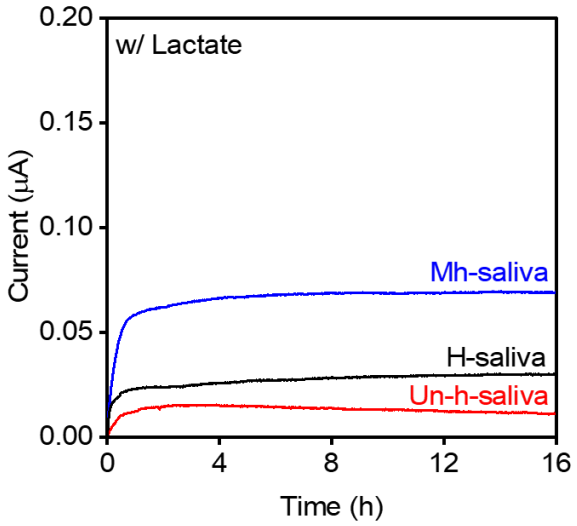

Figure 3.19 Current production versus time measurements conducted in an anaerobic reactor equipped with indium tin-doped oxide (ITO) electrodes (surface area: 3.14 cm^2) poised at +0.4 V (versus SHE) in the presence of lactate with healthy (H-saliva), moderate-healthy (Mh-saliva) and patient (Un-h-saliva) samples.

Electrode attached salivary microbes' biofilm under each condition was collected from the reactors after the operation in order to identity the species that were enriched pertaining to specific substrate. A 16s rRNA sequencing analysis of raw saliva samples and cell enrichment on the electrode surface was conducted and relative abundance of each strain at species level was displayed as shown in **Figure 3.20**. *P. gingivalis* was not detected in healthy saliva sample (**Figure 3.20**, H-saliva, red bar). In all three saliva samples *Streptococcus* was commonly observed. However, in unhealthy saliva, *P. gingivalis* (15%) and *Fusobacterium nucleatum* (*F. nucleatum*, 10%) along with another *fusobacterium* species *F. hwasooki* (6%) were the most abundant species associated with subtypes of colorectal cancer [58]. *F. nucleatum* and *P. gingivalis* are commonly found together and both have been shown to contribute to the development of periodontitis [59]. It is reported that coinfection with *F. nucleatum* can extremely increase the invasion of host cells by *P. gingivalis* [60]. However, *F. hwasooki* was also present

in healthy saliva sample, related higher current production from unhealthy saliva with histidine can be attributed to higher abundance of *P. gingivalis* and *F. nucleatum* (**Figure 3.20**), suggesting histidine associated enhanced current production can be used as a tool to specifically detect the pathogens. By analyzing the potential correlation between the oral microbiota composition (abundance >1%) determined via 16s rRNA sequencing (**Figure 3.20**) and the maximum current slope of current production curves in the presence of histidine (**Figure 3.18a**), glucose (**Figure 3.18b**) and lactate (**Figure 3.19**), it was found that *P. gingivalis* and *F. nucleatum* are primarily associated with current production in saliva microbiota with histidine (**Figure 3.18c**), which indicates *F. nucleatum* is a potential electrochemically active bacteria (EAB) with histidine metabolism, and *Porphyromonas pasteri*, *Haemophilus* and *Granulicatella* are potential EABs associated with sugars metabolism (**Figure 3.21**). The enrichment of *P. gingivalis* and *F. nucleatum* on electrode surface after electrochemical measurements in the presence of histidine is also observed in three saliva samples (**Figure 3.20**), which further proved the current production source with histidine. Although *F. hwasooki* and *Streptococcus* also exhibited a positive correlation with current generation in the presence of histidine, their presence in all three saliva samples and low correlation suggests that these species may only generate a small amount of current in the presence of histidine. 15% abundance of *Prevotella melanlnogenica* in healthy and relatively less (2%) abundance in unhealthy saliva suggest it might be dominated by the *P. gingivalis* under given conditions, however *Bacteroides melaninogenicus* is found to show the enhanced growth with L-aspartate [61]. This further suggest that histidine selectively can generate current from *P. gingivalis*, nonetheless further individual electrochemical analyses is required in future to characterize the other abundant microbiome such as *F. nucleatum, F. hwasooki* and *Neiseeria.* Given substrate availability creates a growth competition in a polymicrobial microbiome [62], thus pathogenic species such as *Streptococcus, Heamophilus, Granulicatella* species showed a variation in all saliva samples (**Figure 3.20**). The collective function of microbial communities is a major driver of homeostasis or dysbiosis and ultimately health or

disease. Advances in isolation studies, pathogenesis, omics technologies and improved database curation and bioinformatics have improved the identification of active microbial social networks and their products (genes, proteins and metabolites) [63]. However, to move beyond correlations and begin to address fundamental bacteria survival mechanism, further refinement of these technologies is needed. Integration of electrochemical properties combined with microorganism substrate specific-pathogenicity association, may be a powerful strategy to address the possible mechanism of pathogenicity.

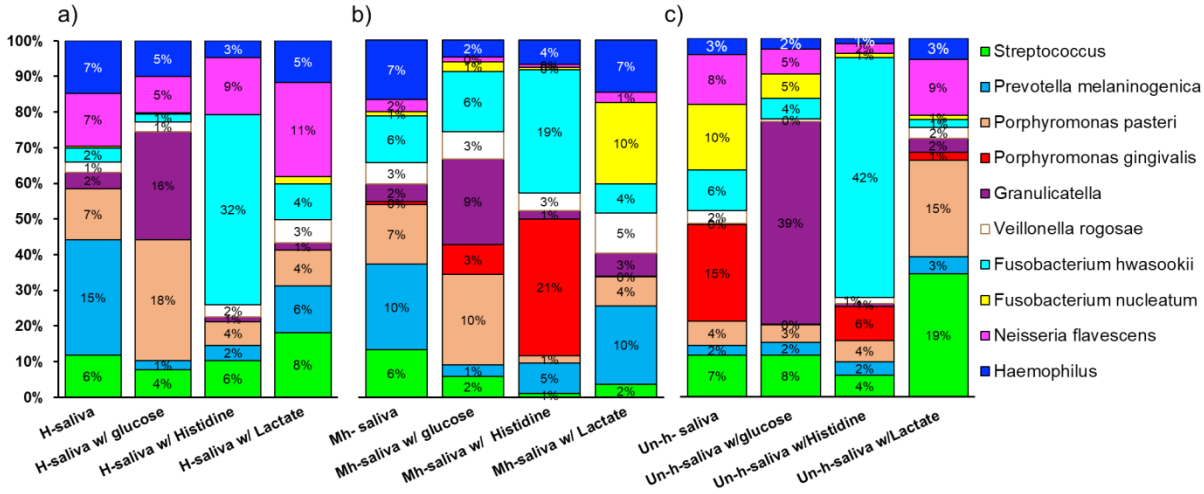

Figure 3.20 Bar chart showing the percentage enrichment of microbes from saliva of (a) healthy person saliva (H-saliva), (b) moderately healthy person saliva (Mh-saliva), (c) un-healthy persons saliva (Un-h saliva) on the electrode surface during current production tested with glucose, histidine and lactate respectively. A control saliva sample before enrichment was also added for comparison.

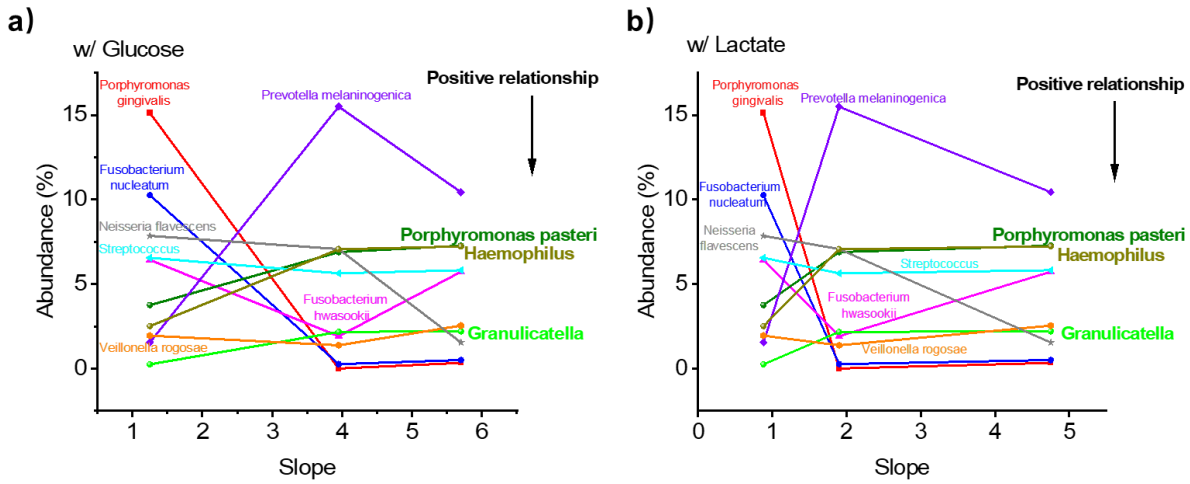

Figure 3.21 The potential correlation between the composition of abundant oral microbiota (>1%) determined by 16s rRNA sequencing and the maximum current slope of I*t*-t curves of H-saliva, Mh-saliva and Un-h-saliva with a) glucose or b) lactate, as an indicator of the bacterial species' association with current production by using glucose or lactate as the substrate.

3.4 Conclusion

This chapter investigated and compared the EET capabilities of the oral pathogen *P. gingivalis* using various amino substrates. With a coulombic efficiency (CE) of 2.8%, *P. gingivalis* considerably increased current with histidine metabolism compared to other substrates, which is around 1000 times higher than the CE that *P. gingivalis* was previously reported to have for glucose oxidation (0.003%). Pure strains of *A. actinomycetemcomitans* (Aa), *S. mutans* (Sm), *C. matruchotii* (Cm), and *C. ochracea* (Co) were examined, electrochemical investigations of human saliva samples, including amino acids and sugars were performed, and metabolic flux simulation was used to examine putative metabolic pathways. It is the first time that an amino acid associated EET capability has been reported. The electron transfer mechanism of *P. gingivalis* with histidine was also studied by using electrodes with different wettability, which proved the direct electron transfer by outer-membrane redox protein. Pure strain *P. gingivalis* was isolated from unhealthy saliva sample incubation trials, and its anodic currents were discovered in the presence of histidine.

Their magnitude was substantially higher than that generally reported for bacteria involved in glucose oxidation. Our findings demonstrate that amino acids, particularly histidine, which has an eight times greater current production rate than glucose, can serve as carbon sources for the asaccharolytic pathogen *P. gingivalis*. The finding of electrogenic activity in pathogens, in turn, sheds light on the potential benefits of using EET activity for biofilm monitoring. To reliably assess human oral hygiene for point-of-care (POC) and get real-time, lab-quality diagnostic results within minutes as opposed to hours, substrate-specific selective detection of EET-competent bacteria can be implemented as a real-time sensing device.

References

1. Oh, T.J., R. Eber, and H.L. Wang, *Periodontal diseases in the child and adolescent.* J Clin Periodontol, 2002. **29**(5): p. 400-10.
2. Preshaw, P.M., et al., *Periodontitis and diabetes: a two-way relationship.* Diabetologia, 2012. **55**(1): p. 21-31.
3. Cardoso, E.M., C. Reis, and M.C. Manzanares-Céspedes, *Chronic periodontitis, inflammatory cytokines, and interrelationship with other chronic diseases.* Postgrad Med, 2018. **130**(1): p. 98-104.
4. Cullinan, M.P. and G.J. Seymour, *Periodontal disease and systemic illness: will the evidence ever be enough?* Periodontology 2000, 2013. **62**(1): p. 271-286.
5. Ramenzoni, L.L., et al., *Oral Diagnostic Methods for the Detection of Periodontal Disease.* Diagnostics (Basel), 2021. **11**(3).
6. Li, T.J., et al., *Periodontal Pathogens: A Crucial Link Between Periodontal Diseases and Oral*

Cancer. Front Microbiol, 2022. **13**: p. 919633.

7. Popova, C., V. Dosseva-Panova, and V. Panov, *Microbiology of Periodontal Diseases. A Review.* Biotechnology & Biotechnological Equipment, 2014. **27**(3): p. 3754-3759.

8. Benso, B., *Virulence factors associated with Aggregatibacter actinomycetemcomitans and their role in promoting periodontal diseases.* Virulence, 2017. **8**(2): p. 111-114.

9. How, K.Y., K.P. Song, and K.G. Chan, *Porphyromonas gingivalis: An Overview of Periodontopathic Pathogen below the Gum Line.* Front Microbiol, 2016. **7**: p. 53.

10. Curtis, M.A., P.I. Diaz, and T.E. Van Dyke, *The role of the microbiota in periodontal disease.* Periodontol 2000, 2020. **83**(1): p. 14-25.

11. Nemoto, T., et al., *Discrimination of Bacterial Community Structures among Healthy, Gingivitis, and Periodontitis Statuses through Integrated Metatranscriptomic and Network Analyses.* mSystems, 2021. **6**(6): p. e0088621.

12. Malheiros Vde, J. and M.J. Avila-Campos, *Detection of pathogens from periodontal lesions.* Rev Saude Publica, 2004. **38**(5): p. 723-8.

13. Imamura, K., et al., *Evaluation of a novel immunochromatographic device for rapid and accurate clinical detection of Porphyromonas gingivalis in subgingival plaque.* J Microbiol Methods, 2015. **117**: p. 4-10.

14. Petit, M.D., et al., *Prevalence of periodontitis and suspected periodontal pathogens in families of adult periodontitis patients.* J Clin Periodontol, 1994. **21**(2): p. 76-85.

15. Mineoka, T., et al., *Site-specific development of periodontal disease is associated with increased levels of Porphyromonas gingivalis, Treponema denticola, and Tannerella forsythia in subgingival*

plaque. J Periodontol, 2008. **79**(4): p. 670-6.

16. Alhogail, S., et al., *On site visual detection of Porphyromonas gingivalis related periodontitis by using a magnetic-nanobead based assay for gingipains protease biomarkers.* Mikrochim Acta, 2018. **185**(2): p. 149.

17. Mättö, J., et al., *Detection of Porphyromonas gingivalis from saliva by PCR by using a simple sample-processing method.* J Clin Microbiol, 1998. **36**(1): p. 157-60.

18. Boutaga, K., et al., *Comparison of real-time PCR and culture for detection of Porphyromonas gingivalis in subgingival plaque samples.* J Clin Microbiol, 2003. **41**(11): p. 4950-4.

19. Galassi, F., et al., *Comparing culture, real-time PCR and fluorescence resonance energy transfer technology for detection of Porphyromonas gingivalis in patients with or without peri-implant infections.* J Periodontal Res, 2012. **47**(5): p. 616-25.

20. Tsuruda, K., A. Shimazu, and M. Sugai, *Detection of a single bacterial cell using a 16S ribosomal RNA-specific oligonucleotide probe designed to investigate periodontal pathogens.* Oral Microbiol Immunol, 2009. **24**(2): p. 133-40.

21. Su, C.Y., et al., *Detection of oral bacteria on the tongue dorsum using PCR amplification of 16S ribosomal RNA and its association with systemic disease in middle-aged and elderly patients.* Biomed Rep, 2019. **10**(1): p. 70-76.

22. Wu, X., et al., *16S rDNA analysis of periodontal plaque in chronic obstructive pulmonary disease and periodontitis patients.* J Oral Microbiol, 2017. **9**(1): p. 1324725.

23. Park, S., et al., *Washing- and Separation-Free Electrochemical Detection of Porphyromonas gingivalis in Saliva for Initial Diagnosis of Periodontitis.* Anal Chem, 2021. **93**(13): p. 5644-5650.

24. Svärd, A., et al., *Protein-Functionalized Gold Nanoparticles as Refractometric Nanoplasmonic Sensors for the Detection of Proteolytic Activity of Porphyromonas gingivalis.* ACS Applied Nano Materials, 2020. **3**(10): p. 9822-9830.

25. Naradasu, D., et al., *Microbial current production from Streptococcus mutans correlates with biofilm metabolic activity.* Biosens Bioelectron, 2020. **162**: p. 112236.

26. Naradasu, D., et al., *Electrochemical Characterization of Current-Producing Human Oral Pathogens by Whole-Cell Electrochemistry.* ChemElectroChem, 2020. **7**(9): p. 2012-2019.

27. Naradasu, D., W. Miran, and A. Okamoto, *Metabolic Current Production by an Oral Biofilm Pathogen Corynebacterium matruchotii.* Molecules, 2020. **25**(14): p. 3141.

28. Miran, W., et al., *Multivariate landscapes constructed by Bayesian estimation over five hundred microbial electrochemical time profiles.* Patterns, 2022: p. 100610.

29. Takahashi, N., T. Sato, and T. Yamada, *Metabolic pathways for cytotoxic end product formation from glutamate- and aspartate-containing peptides by Porphyromonas gingivalis.* J Bacteriol, 2000. **182**(17): p. 4704-10.

30. Roh, Y., et al., *Metal reduction and iron biomineralization by a psychrotolerant Fe(III)-reducing bacterium, Shewanella sp. strain PV-4.* Appl Environ Microbiol, 2006. **72**(5): p. 3236-44.

31. Okamoto, A., et al., *Rate enhancement of bacterial extracellular electron transport involves bound flavin semiquinones.* Proc Natl Acad Sci U S A, 2013. **110**(19): p. 7856-61.

32. Reffert, J.L. and W.J. Smith, *Fosfomycin for the treatment of resistant gram-negative bacterial infections. Insights from the Society of Infectious Diseases Pharmacists.* Pharmacotherapy, 2014. **34**(8): p. 845-57.

33. Norsigian, C.J., et al., *BiGG Models 2020: multi-strain genome-scale models and expansion across the phylogenetic tree.* Nucleic Acids Res, 2020. **48**(D1): p. D402-D406.

34. Yoshida, Y., et al., *Characterization of the phosphotransacetylase-acetate kinase pathway for ATP production in Porphyromonas gingivalis.* J Oral Microbiol, 2019. **11**(1): p. 1588086.

35. Curthoys, N.P. and J.C. Rabinowitz, *Formyltetrahydrofolate synthetase. Binding of folate substrates and kinetics of the reverse reaction.* J Biol Chem, 1972. **247**(7): p. 1965-71.

36. Ebrahim, A., et al., *COBRApy: COnstraints-Based Reconstruction and Analysis for Python.* BMC Syst Biol, 2013. **7**: p. 74.

37. Takahashi, N. and T. Sato, *Preferential utilization of dipeptides by Porphyromonas gingivalis.* J Dent Res, 2001. **80**(5): p. 1425-9.

38. Joshi, C.J., et al., *What are housekeeping genes?* PLoS Comput Biol, 2022. **18**(7): p. e1010295.

39. Silver, N., et al., *Selection of housekeeping genes for gene expression studies in human reticulocytes using real-time PCR.* BMC Mol Biol, 2006. **7**: p. 33.

40. Frandsen, E.V., et al., *Evidence of recombination in Porphyromonas gingivalis and random distribution of putative virulence markers.* Infect Immun, 2001. **69**(7): p. 4479-85.

41. Naradasu, D., et al., *Electrochemical Characterization of Current-Producing Human Oral Pathogens by Whole-Cell Electrochemistry.* ChemElectroChem, 2020. **7**(9): p. 2012-2019.

42. Washio, J., et al., *Amino acid composition and amino acid-metabolic network in supragingival plaque.* Biomed Res, 2016. **37**(4): p. 251-7.

43. Higham, S.M. and W.M. Edgar, *Human dental plaque pH, and the organic acid and free amino acid profiles in plaque fluid, after sucrose rinsing.* Arch Oral Biol, 1989. **34**(5): p. 329-34.

44. Li, F., et al., *Modular Engineering Intracellular NADH Regeneration Boosts Extracellular Electron Transfer of Shewanella oneidensis MR-1.* Acs Synthetic Biology, 2018. **7**(3): p. 885-+.

45. Li, F., et al., *Modular engineering to increase intracellular NAD(H/(+)) promotes rate of extracellular electron transfer of Shewanella oneidensis.* Nat Commun, 2018. **9**(1): p. 3637.

46. Han, S., et al., *NADH gene manipulation for advancing bioelectricity in Clostridium ljungdahlii microbial fuel cells.* Green Chemistry, 2016. **18**(8): p. 2473-2478.

47. Nemoto, T.K. and Y. Ohara-Nemoto, *Exopeptidases and gingipains in Porphyromonas gingivalis as prerequisites for its amino acid metabolism.* Jpn Dent Sci Rev, 2016. **52**(1): p. 22-29.

48. Masuda, K., et al., *Purification and characterization of arginine carboxypeptidase produced by Porphyromonas gingivalis.* Infect Immun, 2002. **70**(4): p. 1807-15.

49. Chopra, A., S.G. Bhat, and K. Sivaraman, *Porphyromonas gingivalis adopts intricate and unique molecular mechanisms to survive and persist within the host: a critical update.* J Oral Microbiol, 2020. **12**(1): p. 1801090.

50. Hirose, A., et al., *Electrochemically active bacteria sense electrode potentials for regulating catabolic pathways.* Nat Commun, 2018. **9**(1): p. 1083.

51. Grobbler, C., et al., *Use of SWATH mass spectrometry for quantitative proteomic investigation of Shewanella oneidensis MR-1 biofilms grown on graphite cloth electrodes.* Syst Appl Microbiol, 2015. **38**(2): p. 135-9.

52. Nakagawa, G., et al., *Metabolic Characteristics of a Glucose-Utilizing Shewanella oneidensis Strain Grown under Electrode-Respiring Conditions.* PLoS One, 2015. **10**(9): p. e0138813.

53. Matsuda, S., et al., *Electrochemical gating of tricarboxylic acid cycle in electricity-producing*

bacterial cells of Shewanella. PLoS One, 2013. **8**(8): p. e72901.

54. Miran, W., D. Naradasu, and A. Okamoto, *Pathogens electrogenicity as a tool for in-situ metabolic activity monitoring and drug assessment in biofilms.* iScience, 2021. **24**(2): p. 102068.

55. Deng, X., D. Luo, and A. Okamoto, *Electrode hydrophilicity enhanced the rate of extracellular electron uptake in Desulfovibrio ferrophilus IS5.* Electrochimica Acta, 2022. **421**: p. 140504.

56. Ding, C.M., et al., *Wettability-regulated extracellular electron transfer from the living organism of Shewanella loihica PV-4.* Angew Chem Int Ed Engl, 2015. **54**(5): p. 1446-51.

57. Moradali, M.F., et al., *Amino acids as wetting agents: surface translocation by Porphyromonas gingivalis.* The ISME Journal, 2019. **13**(6): p. 1560-1574.

58. Purcell, R.V., et al., *Distinct gut microbiome patterns associate with consensus molecular subtypes of colorectal cancer.* Sci Rep, 2017. **7**(1): p. 11590.

59. de Andrade, K.Q., C.L.C. Almeida-da-Silva, and R. Coutinho-Silva, *Immunological Pathways Triggered by Porphyromonas gingivalis and Fusobacterium nucleatum: Therapeutic Possibilities?* Mediators Inflamm, 2019. **2019**: p. 7241312.

60. Saito, A., et al., *Fusobacterium nucleatum enhances invasion of human gingival epithelial and aortic endothelial cells by Porphyromonas gingivalis.* FEMS Immunol Med Microbiol, 2008. **54**(3): p. 349-55.

61. Miles, D.O., J.K. Dyer, and J.C. Wong, *Influence of amino acids on the growth of Bacteroides melaninogenicus.* J Bacteriol, 1976. **127**(2): p. 899-903.

62. Lamont, R.J., H. Koo, and G. Hajishengallis, *The oral microbiota: dynamic communities and host interactions.* Nat Rev Microbiol, 2018. **16**(12): p. 745-759.

63. Takahashi, N., *Oral Microbiome Metabolism: From "Who Are They?" to "What Are They Doing?".* J Dent Res, 2015. **94**(12): p. 1628-37.

Chapter 4. Mediated EET-based Electrochemical Biosensor targeting *Porphyromonas gingivalis* from a Saliva Drop for Periodontitis Diagnosis

4.1 Introduction

Periodontal diseases are prevalent worldwide, especially in the elderly, which not only cause teeth pain and damage teeth, but lead to other systemic diseases [1-3]. Thus, point-of-care diagnosis for home care is critical to human health. Periodontitis is mainly caused by periodontal pathogens including *Aggregatibacter actinomycetemcomitans* (Aa), *Porphyromonas gingivalis* (*P. gingivalis*), *Tannerella forsythia* (Tf), *Treponema denticola* (Td) and *Fusobacterium nucleatum* (Fn) [4-8]. Detection of these pathogens can indicate illness of periodontitis for targeted therapy and predict oral condition for oral treatment. Therefore, quantity of researches for detecting these pathogens have been studied, among which *P. gingivalis* is the most often used as a marker of chronic and aggressive periodontitis causing tooth damage [9-13]. Traditional analysis methods of *P. gingivalis* provides culturing, polymerase chain reaction (PCR), DNA probe or enzyme-linked immunosorbent assay (ELISA), which are too laborious to achieve at home [14-16]. Electrochemical biosensor provides a potential way for point-of-care diagnosis of *P. gingivalis*. Multiple kinds of biosensors based on antibodies, DNA and PCR have been developed to detect *P. gingivalis* [17, 18]. However, these biosensors are other with low sensitivity and specificity, unstable, pretreatment-needed, or expensive, and activity is difficult to be detected by PCR-, DNA- or antibody-based sensors. Simple and sensitive biosensor of *P. gingivalis* is highly demanded for home diagnosis of periodontitis.

Recently, some well-known human pathogens, including *P. gingivalis* were shown to be electrogenic and correlations between the metabolic activities and electrochemical signals have been demonstrated [19-21], which could lead to the development of a real-time assay for drug assessment by directly measuring the current production associated with cellular metabolism [22]. Meanwhile, microbial current production is measurable using reusable, low-cost screen-printed electrode systems and single-potential amperometry (SA) techniques [23]. Electrochemical detection of *P. gingivalis* is possible on-site without any electrode modification. However, the current production generated from *P. gingivalis* is too less to be used for a sensitive biosensor

with glucose metabolism [20]. *P. gingivalis* utilizes amino acids to produce energy for survival [24], the specific current production with amino acids metabolism was studied. According to the results in chapter 3, *P. gingivalis* can generate extremely higher current with histidine compared with glucose. However, the current signal was still low on the screen-printed electrode, just few nanometers with prolonged response time (6-8 hrs). It is necessary to further increase the current production for sensitive electrochemical detection of *P. gingivalis*.

Soluble redox mediators such as flavins [25], quinones [26], and phenazines [27] mediate an indirect mechanism, which can highly enhance the EET efficiency [28]. These redox mediators diffuse across the lipid membranes of gram-negative bacteria or the thick cell wall matrices of gram-positive bacteria to shuttle electrons from/to redox proteins located in the cell interior [29, 30] or the cell wall [25], respectively. Therefore, it is possible that the current generation of *P. gingivalis* can be improved by redox mediators. It has been found that such menadione (Vitamin K3, VK3) and riboflavin (Vitamin B2, VB2) significantly increased current production of *Capnocytophaga ochracea* (*C. ochracea*, an oral pathogen) over 10-fold [31]. Li et al. studied quinone-mediated EET performance and found enhanced current generation by a fermenting bacterium Klebsiella pneumoniae L17 [26]. Besides, foodborne pathogen *Listeria monocytogenes* also utilizes a distinctive flavin-based EET mechanism [25]. It is well-known that many dyes can act as redox mediators [32-34]. However, the mediated-EET process haven't been studied in *P. gingivalis*.

In this chapter, the author studied the *P. gingivalis* current enhancement using various types of mediators for improving the sensitivity of EET-based electrochemical biosensor (EECB). A high-throughput system with 96-well SPCE, which can provide various advantages of one-pot screening and time saving, was used for screening various mediators to boost the current production of *P. gingivalis*. The 2-hydroxy-1,4-naphthoquinone (HNQ) shows the best current production, and therefore was chosen as the best candidate for developing and designing the *P. gingivalis* biosensor. Our developed *P. gingivalis* biosensor shows sensitive detection at low

number of cells (hundreds of times higher than without HNQ) and fast response with less than 30 min. Real monitoring of *P. gingivalis* has been carried out in real human saliva samples to confirm the on-site detection of *P. gingivalis*. The detection time was very short (less than 5 min) with high current production, leading to design fast response and sensitive *P. gingivalis* biosensor based on EECB in human saliva sample. The **Figure 4.1** depicts the scheme of our EET based biosensor of *P. gingivalis* form a saliva drop for real application. Our designed biosensor shows a significant progress in sensing and time response as compared to other conventional detection methods.

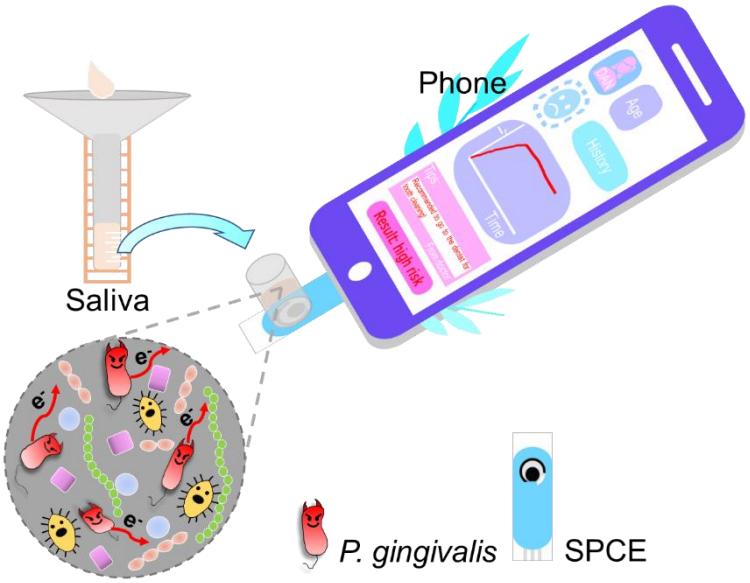

Figure 4.1 The scheme of extracellular electron transport (EET)-based biosensor of *P. gingivalis* for diagnosis of periodontitis with a saliva drop.

4.2 Experimental

4.2.1 Cell culture preparation

Porphyromonas gingivalis W83 strain was grown anaerobically in Gifu anaerobic medium at 37 °C till the growth reached the late exponential phase. Cells were then centrifuged at 7200 rpm and 37 °C for 10 min, and the resultant cell pellet was washed with defined medium (DM) twice to remove the cell secreted metabolites of the preculture medium. Cell cultures were

handled in COY anaerobic chamber filled with 100% N_2. DM contained (per liter) the following components: $NaHCO_3$, 2.5 g; $CaCl_2 \cdot 2H_2O$, 0.09 g; NH_4Cl, 1.0 g; $MgCl_2 \cdot 6H_2O$, 0.2 g; NaCl, 10 g; HEPES, 7.2 g.

4.2.2 Mediators screening using high-throughput screen printed electrode system

To find out the best mediator for higher current generation by *P. gingivalis*, 23 redox mediators (**Table 4.1**), including quinones, flavins and dyes, were tested in 96-well plate screen-printed carbon electrode system with carbon as working and counter electrode, and Ag/AgCl as reference electrodes (SPCE, purchased from Metrohm DropSens, surface area of each electrode in 96-well plate is 7.07 mm^2, **Figure 3.1a**) as well as 8-channel (8-ch) SPCE (working electrode: 4.9 mm^2, **Figure 4.2**). 10 Mm histidine was used as metabolic substrate for all experiments. The DM solution without any redox mediator was used as control and all mediators were dissolved in DM solution which purged N_2 for more than 30 minutes to remove oxygen. Firstly, 200 μM different mediators mix with 20 mM histidine were added to each well in 4 or 2 replicates (100 μL volume). 100 μL freshly prepared DM washed *P. gingivalis* cells (OD_{600} = 2.0) was then injected to each well to make total volume in each well up to 200 μL and reach the final OD_{600} = 1.0. The final concentration of each mediator was 100 μM. All solution in each well was mixed with pipette for several times to become homogeneous. Tin foil tape was used to cover the whole 96-well plate / 8-ch for preventing evaporation. 96-well plate / 8-ch was poised at +0.4 V vs standard hydrogen electrode (SHE) by high-throughput potentiostat to measure the single potential amperometry of each well. All procedures were handled in COY anaerobic chamber filled with 100% N_2 at 37 °C.

Table 4.1 Mediators' name used in this research and their abbreviation

Name	Abbreviation
Isatin	Isatin
7-Methoxy-1H-indole-2,3-dione	MID
1-Methylisatin	1-MI
5-Fluoroisatin	5-FI
5-Nitroisatin	5-NI
5-Methoxyisatin	5-MOI
6-Methoxyisatin	6-MOI
7-Fluoroisatin	7-FI
4-Fluoro-1H-indole-2,3-dione	FID
Basic Yellow 1	BY
riboflavin	RF
riboflavin sodium phosphate	FMN
Methyl viologen dichloride hydrate	MV
1-Acetylisatin	AI
Methyl 4-Hydroxybenzoate	MHB
Basic Blue 24	BB
Toluidine Blue O	TB
Methylene Blue	MB
Nile Blue Hydrogensulfate	NB
Safranin	SFO
2-hydroxy-1,4-naphthoquinone	HNQ
Anthroquinone-1-sulfonic acid sodium salt	AQS
Anthraquinone-1,5-disulfonic acid disodium salt	AQDS

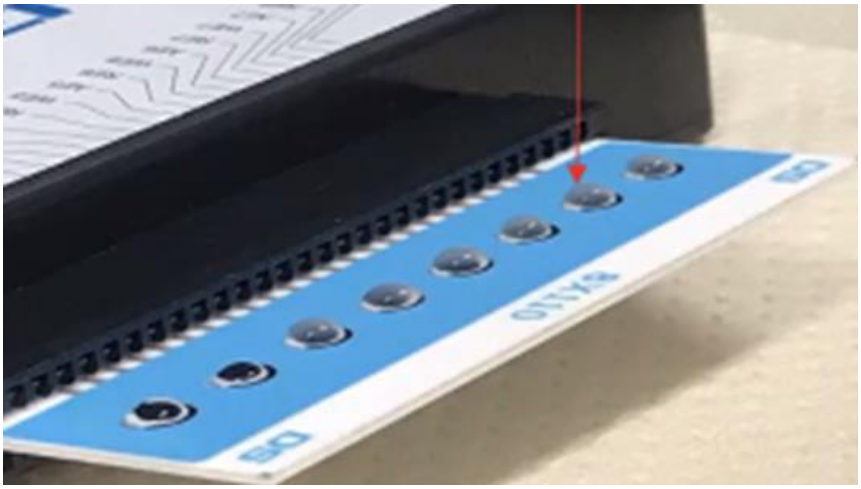

Figure 4.2 The 8-channel screen-printed carbon electrode (SPCE) system with carbon as working and counter electrode, and Ag/AgCl as reference electrodes.

4.2.3 Whole-cell electrochemical analysis of pure strains

Electrochemical measurements were conducted in single-chamber, three-electrode reactors (**Fig 3.1b**). Indium tin-doped oxide (ITO) grown on a glass substrate by spray pyrolysis deposition (SPD Laboratory, Inc., Japan) was used as the working electrode (resistance, 8 Ω/square; thickness, 1.1 mm; and surface area, 3.14 cm^2) and was placed at the bottom of the reactor. Platinum wire and Ag/AgCl (sat. KCl) were used as counter and reference electrodes, respectively. 4.5 mL DM was injected into the electrochemical cell as an electrolyte, and the solution was purged with N_2 gas for at least 15 min to remove the dissolved oxygen. Single-potential amperometry (SA) was started to detected the current under potentiostatic condition of +0.4 V vs a SHE. After the background current became stable, 0.5 mL of freshly prepared cell suspension of *P. gingivalis* pre-washed with DM having an optical density of 5.0 at 600 nm was injected into the electrochemical cell to reach a final OD_{600} of 0.5. After the current increased for several hours, histidine dissolved in DM was added to reactor to reach a final concentration of 10 mM. After that a certain concentration of 2-hydroxy-1,4-naphthoquinone (HNQ) solution was injected into the reactor to reach a final concentration of 100 μM. During the electrochemical measurements,

the reactor temperature was maintained at 37 °C, and the reactor was operated without agitation. Differential pulse voltammetry (DPV) was conducted before and after each step. Sterilized DM without any bacteria was used as control. Single-potential amperometry (SA) was measured with an automatic polarization system (VMP3, Bio Logic Company, France). DPV was conducted with an automatic polarization system (VMP3; Bio-Logic SAS Instruments, Paris, France) using the following parameters: from −0.6 to +0.6 V vs SHE; pulse increment, 5.0 mV; pulse amplitude, 50 mV; pulse width, 300 ms; and pulse period, 5.0 s. The potential was scanned from the negative to the positive direction. Baseline subtraction of the DPV curves was performed using Qsoas. The current production using different HNQ concentration was also measured using the similar procedure. Glucose as the substrate was also used for comparison.

4.2.4 Electrochemical incubation of pure strain and human saliva samples on screen-printed electrode

Current production of different cell number was detected by using an 8-ch SPCE system. Firstly, 100 μL DM with 10 mM histidine and 200 μM HNQ were added to each well. Single-potential amperometry (SA) was started to detected the current under potentiostatic condition of +0.4 V vs a SHE. After the background current became stable, 100 μL freshly prepared DM washed *P. gingivalis* cells with different OD was then injected to each well to make total volume in each well up to 200 μL and reach the final OD_{600} = 0.01～0.50. The final concentration of histidine and HNQ was 10 mM and100 μM, respectively. All solution in each well was mixed with pipette for several times to become homogeneous. Tin foil tape was used to cover 8-ch reactor for preventing evaporation. All procedures were handled in COY anaerobic chamber filled with 100% N_2 at 37 °C.

This human saliva study was approved by the Kyushu dental university Ethics Committee (ethical approval number: 19-61 and 21-23). Saliva samples were obtained from healthy volunteers having history of no tooth problems and unhealthy people having tooth problems. A 1 mL of saliva sample was collected in a 1.5 mL eppendorf and diluted up to 1.5 mL with anoxic

DM to stock for further use. All samples were centrifuged and pellets were resuspended in 200 μL anoxic DM. The procedure is totally the same with the measurement of different cell number by exchanging *P. gingivalis* cells to saliva samples. The medium without HNQ was used as control.

4.3 Results and Discussion

4.3.1 Mediator-screening for current enhancement of *P. gingivalis*

The effect of redox mediators on current production of *P. gingivalis* (Pg) was initially screened with different mediators by the high-throughput system (**Figure 3.2a**) using a 96-well channel (**Figure 3.1a**) and 8-channel (**Figure 4.2**) screen-printed electrode system (SPE) containing of carbon as working electrode (WE) at +0.4 V vs standard hydrogen electrode (SHE), platinum as counter electrode (CE) and Ag/AgCl as reference electrode (RE). 23 mediators were used in this study, which names and abbreviations were showed in **Table 4.1**. The current production without redox mediator was used as control. Histidine is used as the metabolic substrate for specific detection of *P. gingivalis*. There were four and two replicates in 96-well plate and 8-ch in each condition, respectively, which showed good repeatability (**Figure 4.4**). The I*t* versus time curves in 96-well SPCE system are showed in **Figure 4.4a**, and the corresponding average current production of four replicates was showed in **Figure 4.3a**. The current production of *P. gingivalis* with quinones (HNQ, AQS and AQDS) as mediators was detected in 8-ch system (**Figure 4.3c**, **Figure 4.4b**). The highest currents with these quinones were normalized by the current with HNQ in two independent experiments and the comparison of all the highest current production selected from all the average I*t*-t curves with error bar was showed in **Figure 4.3b**. *P. gingivalis* generated the highest current production (205.9 nA) with 2-hydroxy-1,4-naphthoquinone (HNQ) as redox mediator, which is more than 73 times compared with the control without any redox mediator (2.8 nA). Some blue dyes (eg. MB, TB, BB, NB), SFO, flavins (RF and FMN) and quinones (AQS and AQDS) also extremely increased the current production of *P.*

gingivalis. Due to the highest current production of *P. gingivalis*, HNQ was selected as the model mediator for studying mediated-EET of *P. gingivalis*.

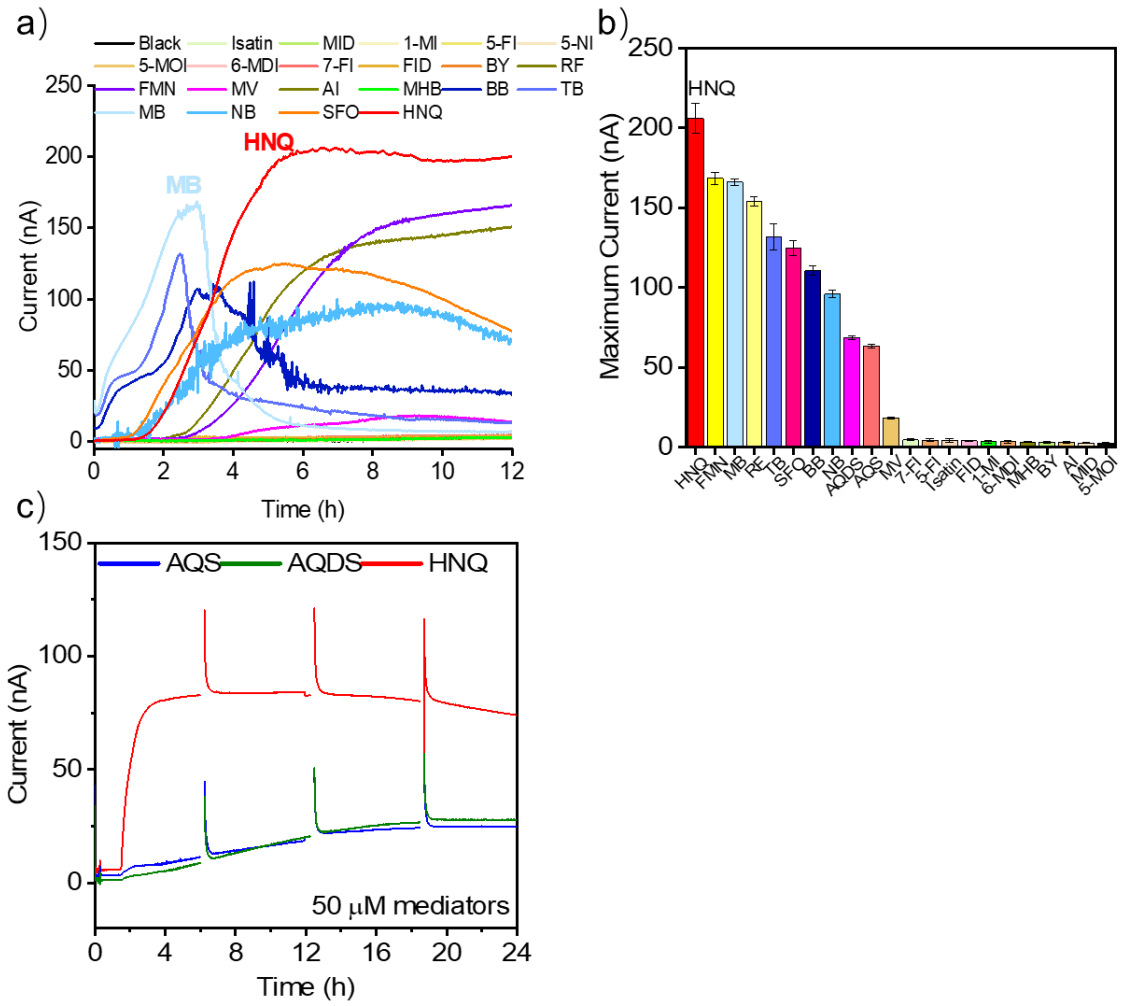

Figure 4.3 (a) The average current production with different mediators detected by 96-well SPCE system, the black control line is without any mediators; (b) Comparation of average peak current generated by *P. gingivalis* with all mediators in 96-well plate, data presented are taken from 4 replicates. (c) Average current production of *P. gingivalis* using quinones as mediators. Each mediator had a final concentration of 100 μM with 10 mM histidine as carbon and electron source.

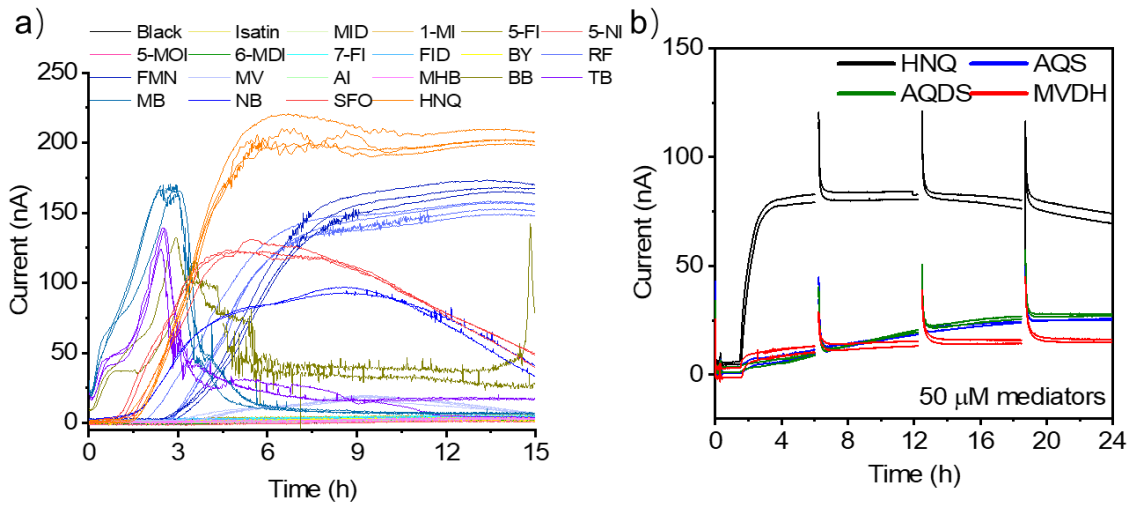

Figure 4.4 (a) Single-potential amperometry (SA) results of corresponding 4 replicates of all mediators in 96-well high-throughput screen-printed electrode system. (b) SA results of corresponding 2 replicates of 4 quinones mediators in 8-channel screen-printed electrode system.

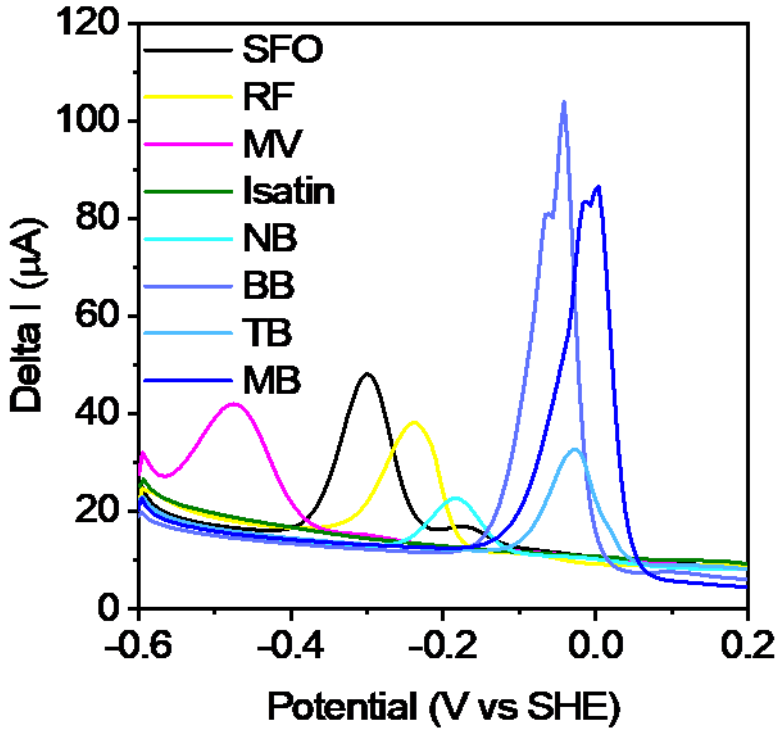

Mediator	MB	TB	BB	NB	HNQ	RF	SFO	MV
Redox potential	-0.011	-0.030	-0.052	-0.185	-0.230	-0.241	-0.301	-0.475

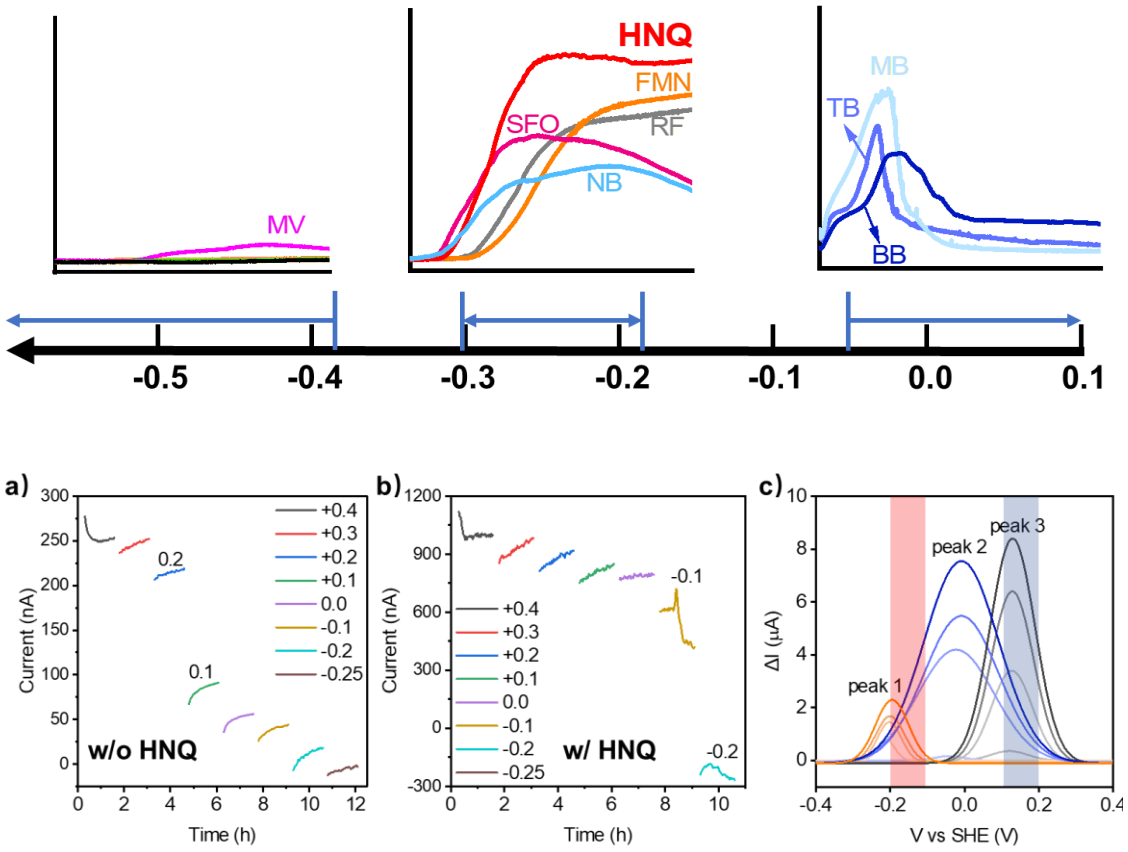

The whole-cell electrochemical measurement with HNQ was conducted in an indium tin-doped oxide (ITO) electrode system. The single-potential amperometry (SA) at +0.4 V vs SHE was measured along with the process as showed in **Figure 4.5a**, red line is with *P. gingivalis* cells, black line is negative control without bacteria. In this study, *P. gingivalis* cells, HNQ and histidine was separately added to the reactor with sterilized anoxic defined medium (DM). The DPV was measured before and after each adding step as arrows signals to reflect the redox reaction changes, and the baseline subtraction of the DPV was performed using Qsoas (**Figure 4.5b-d**, **Figure 4.6a**). As SA result showed in **Figure 4.5a**, the baseline current of DM was 0.13 μA. The current slightly increased after adding *P. gingivalis* cells (OD_{600}=0.5) and reached to 0.16 μA after 2 hrs. The

current increased 3.3 times after 10 mM histidine was injected for 2 hrs, which was consistent with the study of chapter 3. Surprisingly, the current production immediately and significantly increased and reached up to around 3.77 μA after adding 100 μM HNQ for 4 hrs, which is around 121 and 37 folds of that with only DM and with 10 mM histidine, respectively. However, there was no current observed in the negative control without *P. gingivalis* cells but histidine or/and HNQ. This indicates that histidine and HNQ cannot react with ITO electrode, and there was no redox reaction between histidine and HNQ at poised +0.4 V vs SHE. This result also proved the current production in positive reactor was generated by *P. gingivalis* cells.

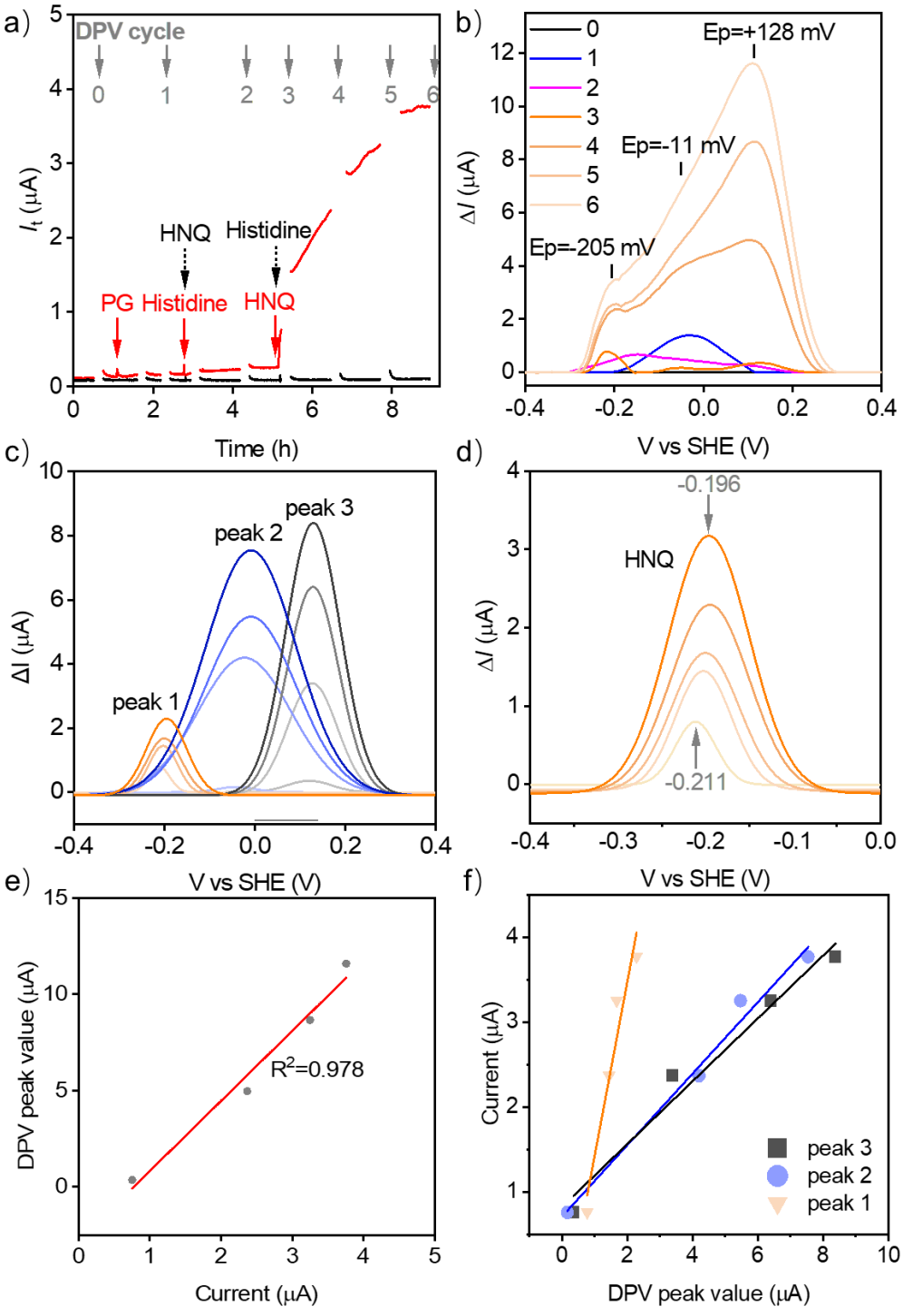

Figure 4.5 (a) Representative current production versus time measurements in the presence and absence of *P. gingivalis* (Pg) conducted in an anaerobic reactor equipped with indium tin-doped oxide (ITO) electrodes, with arrows representing the time for differential pulse voltammograms

analysis or injecting things. (b) The corresponding baseline-subtracted differential pulse voltammograms of positive condition before and after adding Pg, HNQ and histidine. (c) Separated three DPV peaks of differential pulse voltammograms in figure (b) after adding HNQ, orange curves presenting HNQ and other two presenting the redox proteins in outer-membrane; (d) Individual HNQ peaks of (c) increasing along with time increasing; (e) Plot of redox peak current at a potential of +0.11 V in figure (b) against the corresponding current in single-potential amperometry of (a); (f) Bacterial current production (I_t) plotted against baseline-subtracted three redox peaks.

To examine the potential mediated-EET pathways in *P. gingivalis*, a voltammetric approach, differential pulse voltammetry (DPV) at specific point was measured. All baselines of DPVs were subtracted by Qsoas. In the negative reactor, no DPV peak was detected with only DM (cycle 0 and 1 in **Figure 4.6a**). The DPV of histidine with DM was also measured and no peak was observed (**Figure 4.6b**). These results indicates both DM and histidine don't have any reaction with ITO electrode at potential from −600 to +600 mV vs SHE. While after HNQ injected, there was one redox peck at around −220 mV vs SHE was depicted as cycle 2 (orange line) in **Figure 4.6a**, which can be assigned to the redox cycling of HNQ. To prove this, the DPVs of different concentration of HNQ were measured as showed in **Figure 4.7b-c**, **Figure 4.7a** shows the corresponding current profile with glucose or histidine as the substrate, with arrows representing the time for DPV analysis. It is known that the DPV peak current was proportional to the concentration of analytes [35]. The redox peak current at −245 mV increased with higher HNQ concentration, and changed in current increase proportionally with the concentration of HNQ in a range of 10～200 μM (**Figure 4.7d**), which assigned as HNQ's redox peak. The current production of *P. gingivalis* with different HNQ concentration was measured, which shows current production increasing with higher HNQ concentration. However, after adding histidine to the reactor, the height of DPV peak current of HNQ dramatically decreased for around 5 times. The

similar result was also observed in the positive reactor, after adding histidine the DPV peak of redox protein of *P. gingivalis* also decreased (**Figure 4.5b**, cycle 1 and 2). To check whether HNQ can react with histidine, the absorbance spectra of HNQ, histidine and HNQ mixed with histidine (1:1 ratio) was measured by ultraviolet-visible (UV-vis) spectroscopy (**Figure 4.6c**). The HNQ's peak didn't change when adding histidine, indicating there was no reaction between histidine and HNQ. Therefore, the DPV peak decrease when adding histidine may be due to the fact that histidine can block ITO electrode surface. Because ITO surface is hydrophilic [36], which can be easily blocked by L-histidine with polar, positively charged, and hydrophilic characters.

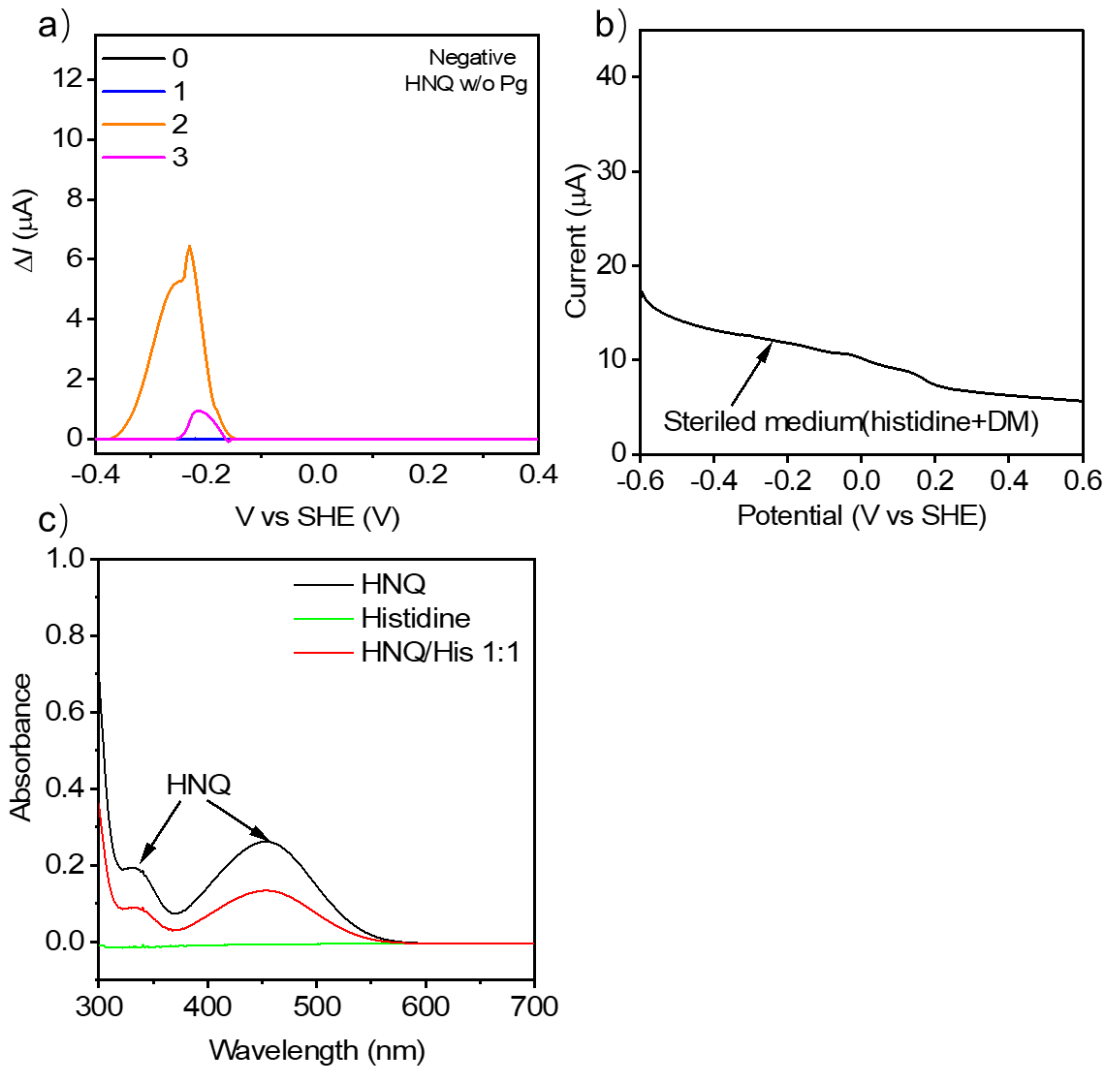

Figure 4.6 (a) The corresponding baseline-subtracted differential pulse voltammograms of

negative condition in the absence of *P. gingivalis* (Pg) before and after adding histidine and HNQ; (b) The differential pulse voltammograms of sterile medium with10 mM histidine and defined medium; (c) The ultraviolet-visible absorbance spectra of HNQ, histidine and HNQ mixed with histidine (1:1 ratio).

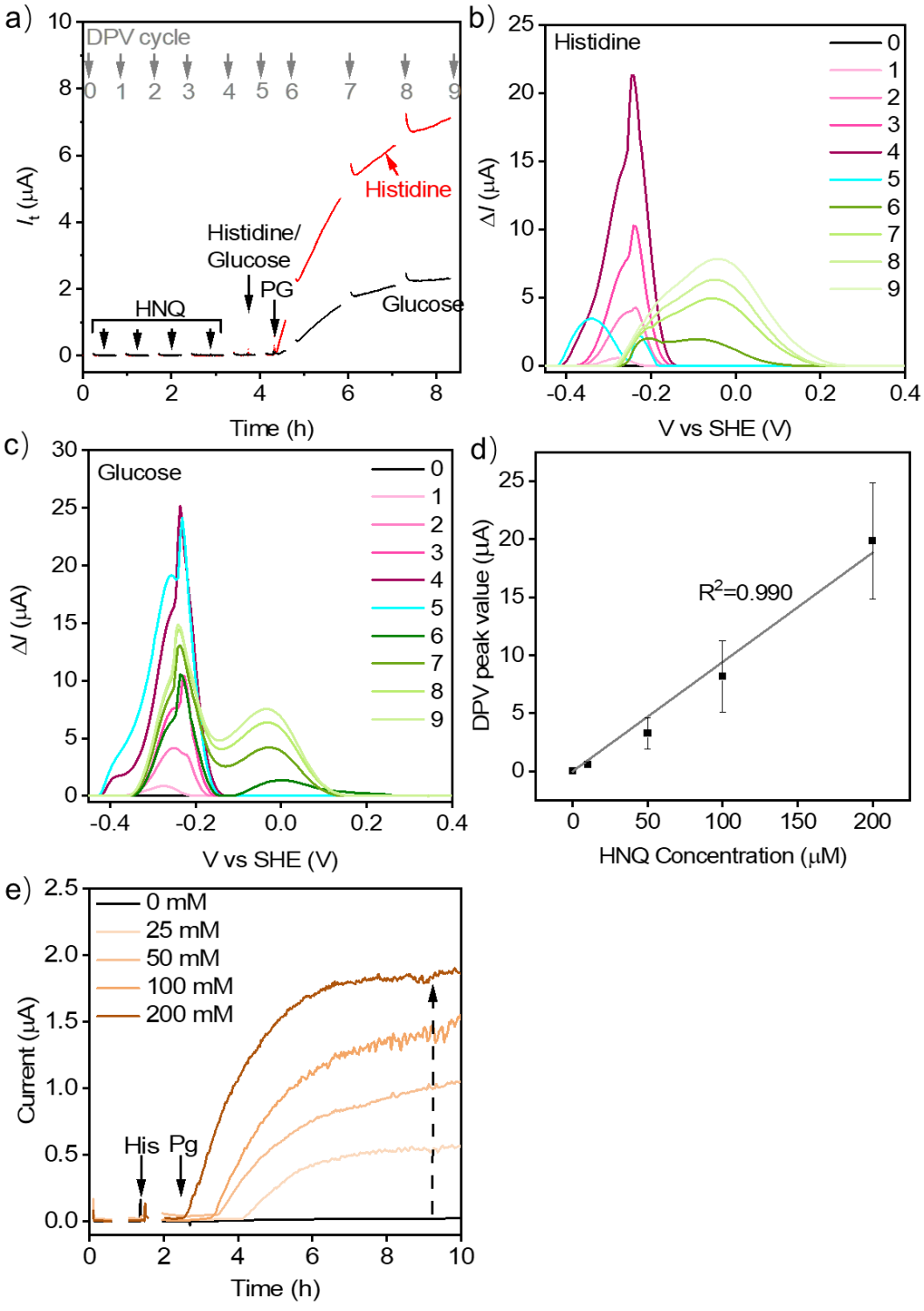

Figure 4.7 (a) Representative current production versus time measurements of *P. gingivalis* (Pg) with histidine or glucose as carbon source conducted in an anaerobic reactor equipped with indium tin-doped oxide (ITO) electrodes, with arrows representing the time for differential pulse

voltammograms analysis or injecting things, different concentration HNQ was sequentially injected before adding substrate and Pg cells; (b) The corresponding baseline-subtracted differential pulse voltammograms of Pg with glucose as the substrate before and after adding HNQ, glucose and Pg; (c) The corresponding baseline-subtracted differential pulse voltammograms of Pg with histidine as the substrate before and after adding HNQ, histidine and Pg; (d) Plot of redox peak current at the potential of about -0.24 V against the corresponding HNQ concentration; e) The single-potential amperometry of Pg with different concentration of HNQ conducted in an anaerobic reactor equipped with ITO electrodes.

The baseline-subtracted DPVs of positive control were reflected in **Figure 4.5b-d**. The highest redox peak current of DPV at around +110 mV increased with time (**Figure 4.5b**) and was positively correlated with the electricity produced (I*t*) by *P. gingivalis* (**Figure 4.5e**). The original DPV was divided into three individual peaks as showed in **Figure 4.5c**. The most negative peak at around +205 mV represents HNQ, which is similar with the peak of free HNQ in the absence of *P. gingivalis* (**Figure 4.6a**). Besides, baseline subtracted DPV revealed the redox peak current of *P. gingivalis* with two redox potentials (*Ep*) at approximately −11 mV and +128 mV (**Figure 4.5b**), which are consistent with reported literature [20]. In particular, all the three redox peaks increased with time and were positively correlated with the current production (**Figure 4.5f**). The DPV peaks currents were highly increased after HNQ was added, which was due to the mediated electron transfer by HNQ. These results indicates that the addition of HNQ can promote the delivery rate of electrons from *P. gingivalis* cells to the electrode. Importantly, the redox potential of the HNQ slightly shifted from −211 mV for ≤ 15 mV in the positive direction with increasing current (**Figure 4.5d**), which was closer to the redox peaks of *P. gingivalis* cells. This may be contributed to the binding of HNQ to redox protein of *P. gingivalis*, which was reported before in the bound riboflavin with OmcA of *Shewanalla* [37].

The number of electrons (n) involved in the redox reaction of HNQ with electrodes was

estimated from the half-width potential (Δ*Ep*/2) of the DPV signal. It was reported that HNQ can conduct 1-electron reductions without proton transfer or a 2-electron reduction accompanied by transfer of protons [38]. The small Δ*Ep*/2 of 50 mV of free HNQ in the absence of *P. gingivalis* (**Figure 4.6a**) and 56 mV at the beginning of *P. gingivalis* presence (**Figure 4.5c-d**) indicated that HNQ mediated the two-electron redox reaction. However, Δ*Ep*/2 of HNQ became 106 mV after *P. gingivalis* incubated with HNQ for several hours, which indicates the number of electron transfers changed from two electron (mediated) to one electron (bound electron transfer) together with the shift of *Ep*/2 from 56 mV to 106 mV [39, 40]. Furthermore, the Δ*Ep*/2 of middle redox peak (the left peak of *P. gingivalis*) was relatively constant with a value of 237±4 mV, while the Δ*Ep*/2 of right redox peak of *P. gingivalis* increased from 116 mV to 140 mV similar with HNQ's peak change. This indicates that it is possible for HNQ to bound with one of the outer-membrane redox proteins with a redox potential of +128 mV. Although the redox proteins for extracellular electron transfer of *P. gingivalis* haven't been defined, these results proved that HNQ acted as shuttle combined with cofactor of redox protein to promote current production in *P. gingivalis*.

4.3.2 Cell dependency of HNQ-mediated current production by *P. gingivalis*

For a biosensor application, it is important to study the detection limitation, which represent the cell number of *P. gingivalis* in this study. Therefore, the current production of different number of *P. gingivalis* cells (OD600 from 0～0.5) was measured with 100 μM and 1 mM HNQ (**Figure 4.8a-b**), respectively. The author used an 8-channel screen-printed carbon electrode system in this experiment to simulate practical application of our biosensor. Firstly, 100 μL of 20 mM histidine mixed with 200 μM / 2 mM HNQ dissolved in DM was added to each well. The single-potential amperometry (SA) at +0.4 V vs SHE was then measured along with the process. After the baseline of medium was stable, *P. gingivalis* cells with different OD600 = 2X were injected to each well to reach a gradient OD_{600} = X. As predicted, higher current was generated with more cells (**Figure 4.8a-b**). Electrogenic bacteria cells need to reach to or near the electrode surface to transfer

electron even with shuttles. The response time (the time that current started to increase after adding *P. gingivalis* cells) also increased with lower cell number, which is because settling velocity onto limited electron surface (working electrode: 4.9 mm2). With high OD_{600}=0.5/0.25 of *P. gingivalis* cells and 100 μM HNQ, the current started increasing after *P. gingivalis* was added for just 10/16 min and reached to a net current of 240/210 nA after 1.8/3.1 hrs (**Figure 4.8a**). However, with relatively low cell number, the current significant decreased and the response time was much longer. For instance, the response time increase to 87 min at OD_{600}=0.15 with a peak current of just 48 nA, and the highest current with *P. gingivalis* at OD_{600}=0.075 was even as low as 3 nA with a response time of 192 min. When the OD_{600} was low as 0.05, the current cannot be detected. This result indicates the detect limitation with 100 μM HNQ is OD600=0.075.

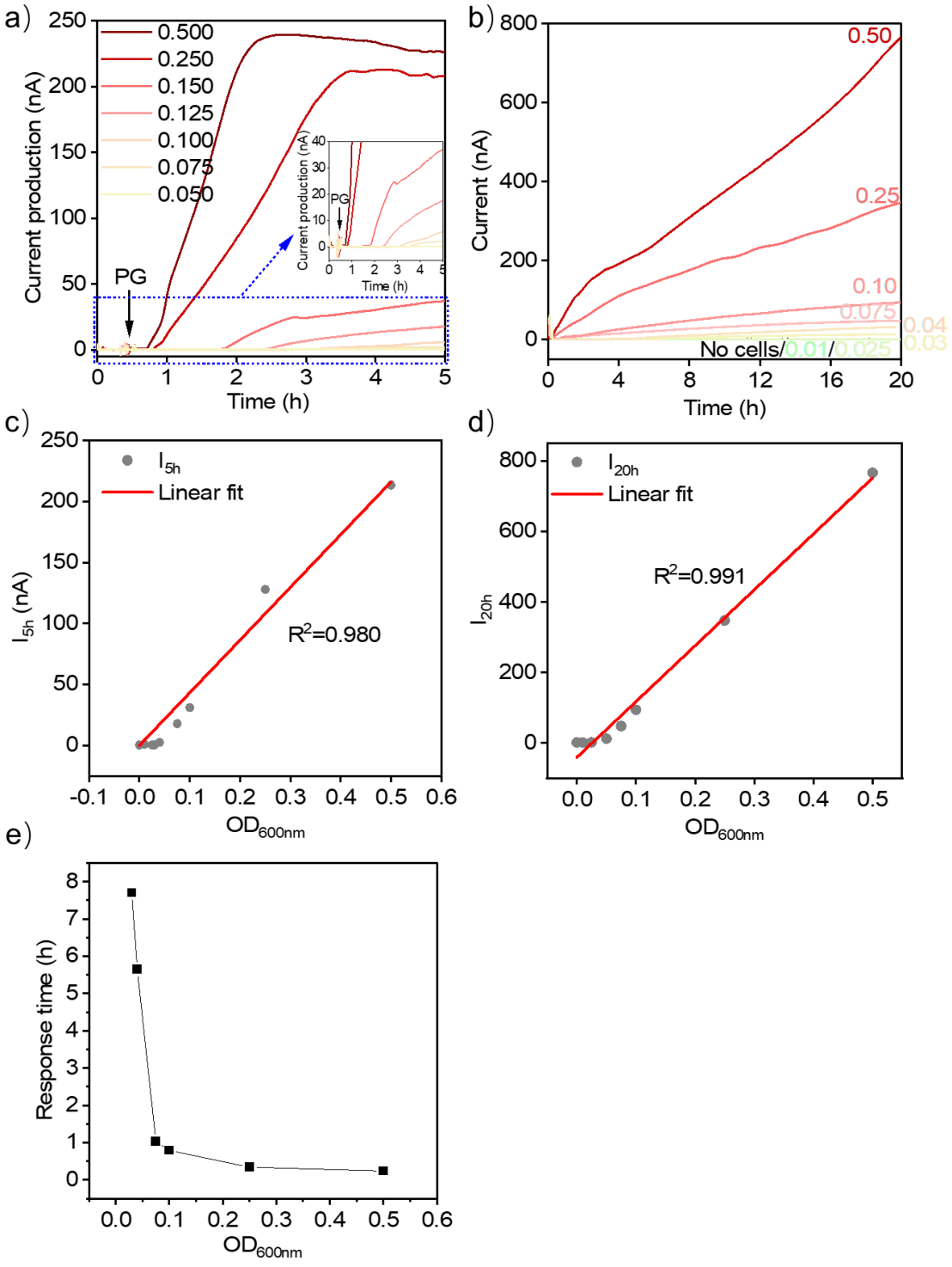

Figure 4.8 The cell number dependency of current production of *P. gingivalis* (Pg) conducted in an anaerobic 8-channel reactor equipped with screen-printed carbon electrodes poised at +0.4 V (versus SHE) in the presence of (a) 100 μM HNQ or (b) 1 mM HNQ; (c) The correlation between

cell number (OD_{600}) and corresponding current production of Pg with 1 mM HNQ at (c) 5 hrs (I_{5h}) and (d) 20 hrs (I_{20h}), respectively; (e) Plot of response time (the time that current started increasing after adding *P. gingivalis*) against the corresponding OD_{600}.

On another hand, with higher concentration of HNQ (1 mM), the current production kept increasing for more than 20 hrs with different number of *P. gingivalis* (**Figure 4.8b**). Not only the current production increased but response time decreased compared with low HNQ concentration (100 μM). This may be contributed to that more HNQ can always provide enough reduced-state of mediator for the long-distance electron transfer. With high OD_{600}=0.5, the peck current reached to around 750 nA with 1 mM HNQ, which was more than 3-fold compared to that with 100 μM HNQ. The corresponding response time was just 4 min, which was quicker 2.5 times than with low HNQ concentration. Furthermore, the detection limitation was enhanced by adding more HNQ mediator, which decreased to OD_{600}=0.03. But the response time was still long for several hours with low cell number (**Figure 4.8e**). The detection limitation needs to be further improved. Besides, it is also essential to find the relationship between analytes and signals for the development of biosensors. In this study, the current production at specific time was chosen as the analyzed signal. The relationships between cell number and current production at t=5 h and 20 h were plotted in **Figure 4.8c** and **d**, which showed good linear correlations with high R^2 value of 0.980 and 0.991, respectively. These results indicate that it is possible to calculate cell number by the current production of *P. gingivalis*.

Although the detection limitation of our biosensor was still lower compared with several other reported electrochemical biosensors for detection of *P. gingivalis.* The EET-based biosensor of *P. gingivalis* haven't been well-studied yet. To the best of our knowledge, this study is the first attempt to come true the EET-based electrochemical biosensor for practical applications in the detection of pathogenic bacteria. More and more researches are needed to focusing on this topic to further improve the performance by different ways. In our research, the author focused on

improving the sensitivity and specificity of our biosensor based on EET mechanism. For instance, the specific substrate, histidine, was found based on that EET is closely associated with metabolism. The sensitivity was improved by mediated EET process with HNQ. In fact, there are many other methods for this goal, such as electrode modification [41, 42], biofilm enrichment [43, 44], or other electrochemical detection methods [45], etc. There are many other types of electrochemical sensors can be used to detect EET capable bacteria with higher sensitivity, such as impendence-based or cyclic voltammetry-based electrochemical biosensors [45]. Electrode modification is also important, which can influence the biofilm formation and sensitivity of biosensor [46-50]. Some materials can be used to increase the electron transfer of biofilm, which would also increase the sensitivity of EET-based biosensor [51, 52]. It is believed that with the further deepening of research, the application of EET-based electrochemical biosensors will become a reality in the near future.

4.3.3 Electrochemical detection of saliva pathogens with HNQ

Human saliva samples were collected and used for practical application check. Based on the results described in chapter 3, unhealthy saliva with high amount of *P. gingivalis* showed the ability to generate much higher current with histidine fermentation as the substrate compared with that of healthy sample in indium tin-doped oxide (ITO) system (5 mL). It is unknown that whether HNQ mediated EET would change this trend. In this experiment, the author detected the current production of saliva samples from healthy and unhealthy people using histidine and HNQ as auxiliary in an 8-channel screen-printed electrode system. The current production of patient' saliva was measured with and without HNQ first. As showed in **Figure 4.9a**, without HNQ, the current generated by patient's saliva slowly raised up to just 27 nA after 24 hrs. While with HNQ as mediator, the current production immediately increased after adding patient's saliva and reached to the highest current (320 nA) within just 5 min, which was more than 150 times than without HNQ. The response time was significant short compared with other commercial methods, such as PCR (6 hrs), ELISA (4-12 hrs) and 16s rRNA (days to weeks) [53-55].

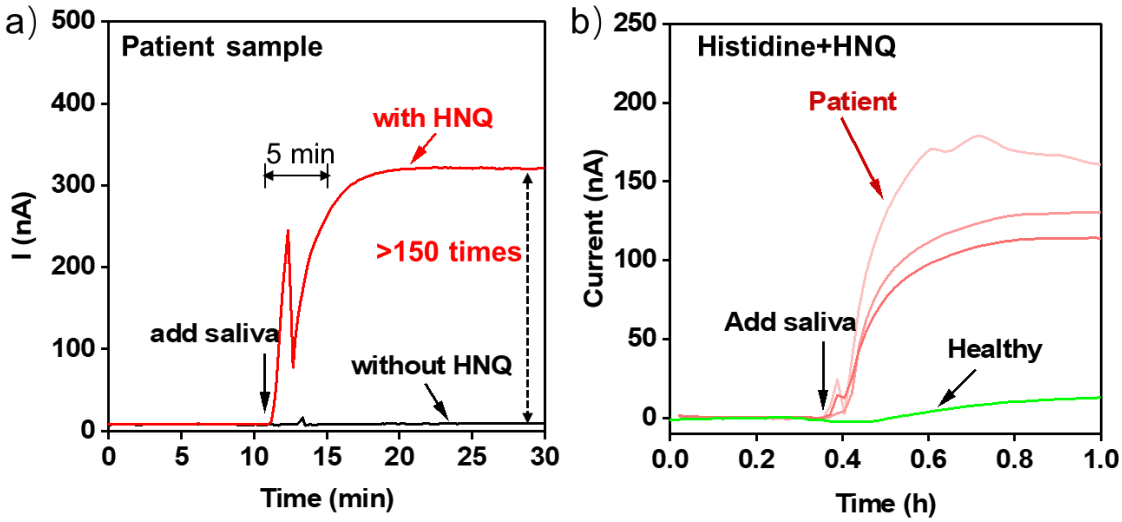

Figure 4.9 (a) Current production versus time measurements conducted in an anaerobic 8-channel reactor equipped with screen-printed carbon electrodes poised at +0.4 V (versus SHE) in the presence or absence of HNQ with periodontal patient's saliva sample; (b) Single-potential amperometry (SA) results of healthy (H-saliva), moderate-healthy (Mh-saliva) and patient (Un-h-saliva) samples with HNQ as the mediator and histidine as the substrate in an anaerobic 8-channel reactor equipped with screen-printed carbon electrodes poised at +0.4 V (versus SHE).

Due to HNQ is a common mediator in multiple electrochemically active microbes [26, 56, 57]. It is possible that HNQ also can enhance some other EET-capable bacteria in saliva samples. Therefore, healthy and unhealthy saliva samples were all measured for comparison (**Figure 4.9b**). It is surprising that all patient saliva samples exhibited significantly higher current levels compared to healthy saliva samples suggests the suitability of HNQ as a mediator for the EET-based electrochemical biosensor used in diagnosing salivary pathogens associated with periodontitis. It is also consistent with the results in the analysis of possible electrogenic bacteria and the electron transfer capability with different substrates. Specifically, the analysis indicates that only *P. gingivalis* and *F. nucleatum* exhibit a significant association with current production in the saliva microbiota when histidine is present, and the abundance of these two species

increases as periodontal disease progresses. Consequently, it is reasonable to expect that the current production in patient saliva primarily originates from these two species, even in the presence of a mediator such as HNQ. The use of HNQ enhances sensitivity proportionally, but it is essential to establish an appropriate range to effectively differentiate between healthy and unhealthy conditions. These findings provide further evidence supporting the feasibility of employing an electron transfer-based electrochemical biosensor for periodontitis diagnosis.

4.3.4 Methylene Blue (MB)-mediated current production by *P. gingivalis*

In the mediator-screening experiment, except for HNQ, methylene blue (MB) showed high sensitivity for the current production of *P. gingivalis*, especially the shortest response time. It is reported that MB can transfer electron from NADH to cytochrome C, which provide another EET pathway [58]. Therefore, the effect on MB as the mediator for the electron transfer of *P. gingivalis* was investigated. The whole-cell electrochemical measurement with HNQ was first conducted in an indium tin-doped oxide (ITO) electrode system. The single-potential amperometry (SA) at +0.4 V vs SHE was measured along with the process as showed in **Figure 4.10a**, red line is with histidine and MB, while blue and black lines are with only MB and histidine, respectively. The DPV was measured before and after adding *P. gingivalis* cells (**Figure 4.10b**). Before *P. gingivalis* was injected, the baseline current of each medium was measured. No current production was detected with only histidine in DM, while MB with and without histidine produced 0.4 and 0.2 μA current. This result indicates MB can react with ITO electrode at potential of +0.4 V vs SHE. The redox potential is around –6 mV (**Figure 4.10b**). After adding *P. gingivalis*, the current production with MB and histidine increased around 4-fold to a net current of 1.4 μA. The current also increased with only MB as a mediator, but due to the lack of carbon and electron source, the current was much lower than with histidine. MB reacted as a mediator with highly increased current though it is reactive with electrode. Therefore, MB can be used as an accelerator as long as the suitable scope of application is selected.

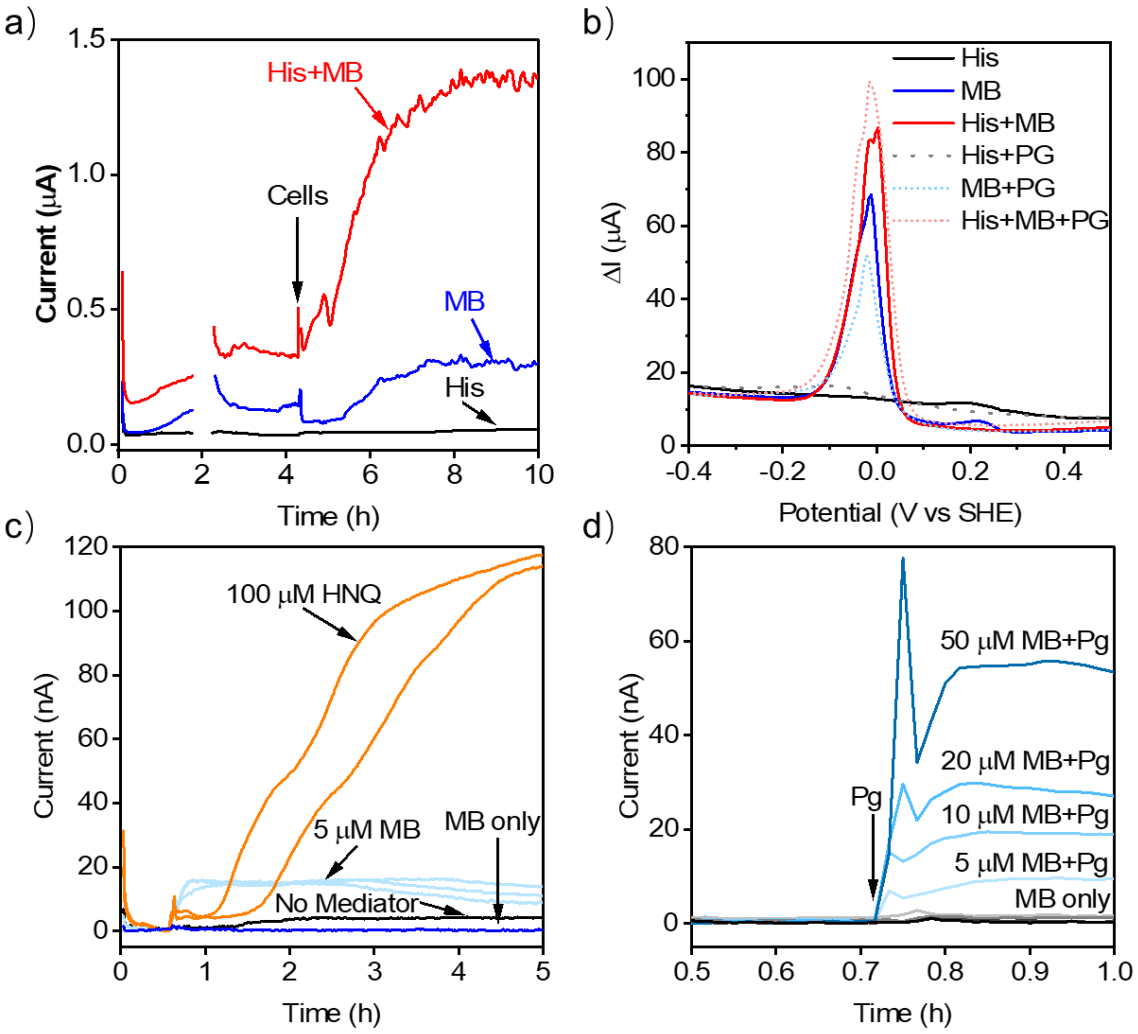

Figure 4.10 (a) Representative current production of *P. gingivalis* in the presence of sole histidine, methylene blue (MB) or histidine mixed with MB conducted in an anaerobic reactor equipped with indium tin-doped oxide (ITO) electrodes; (b) The corresponding differential pulse voltammograms in the presence of sole histidine, MB or histidine mixed with MB before and after adding *P. gingivalis*. (c) Current production of *P. gingivalis* conducted in an anaerobic 8-channel reactor equipped with screen-printed carbon electrodes poised at +0.4 V (versus SHE) with and without 100 μM HNQ or 10 μM MB; (d) Current production versus time measurements in the presence and absence of *P. gingivalis* conducted in an anaerobic 8-channel reactor equipped with screen-printed carbon electrodes poised at +0.4 V (versus SHE) with different concentration of MB.

To compare the performance of MB with HNQ as the mediator for the electrochemical detection of *P. gingivalis*. Current production of *P. gingivalis* was measured in an anaerobic 8-channel reactor equipped with screen-printed carbon electrodes (SPCE) poised at +0.4 V (versus SHE) with and without 100 μM HNQ or 10 μM MB (**Figure 4.10c**). The smaller amount of MB was used to control the baseline causing by reactive MB itself. Surprising, no current production was detected with only MB in the SPCE system (**Figure 4.10c**, dark blue), which was probably because of the carbon electrode. The SPEC system was different from ITO system, the working electrode, counter electrode as well as reference electrode, which could strongly influence the reaction. However, after *P. gingivalis* cells were added, the current immediately increased and reached to the highest within just few minutes (**Figure 4.10c**, light blue), which was significantly shorter than with HNQ as the mediator (**Figure 4.10c**, orange). The highest current produced by *P. gingivalis* with 10 μM MB was 3.8-fold higher than without any mediators, while was 14% of current with 100 μM HNQ due to the lower concentration of MB (10 μM). This result demonstrates the strong applicability of MB as a promoter on EET-based biosensors of *P. gingivalis*. The author further increased the concentration of MB to enhance the current production and check whether higher MB concentration would generate baseline current in SPCE system. The result was showed as **Figure 4.10d**. With higher MB concentration the current increased and reached the highest current almost at the same time (≤ 5 min). Besides, there were no observed baseline current even with 50 μM MB, which indicates MB is suitable for the electrochemical biosensor development with SPCE. These results suggest that MB is a potential and suitable mediator for the development of EET-based biosensor of *P. gingivalis* as well as periodontitis with high sensitivity and quick response.

4.4 Conclusion

For the development of an extracellular electron transfer (EET)-based biosensor of *P.*

gingivalis, one of the key biomarkers of periodontitis, to diagnose and predict periodontal and systemic disease, the effect of various types of mediators for improving the current production from *P. gingivalis* toward a highly sensitive and fast response EET-based electrochemical biosensor (EECB) was studied. Among 23 mediators tested, HNQ showed the highest current production, which was 50 times higher than the absence of redox mediator. Electrochemical assay with saliva samples from periodontitis patient demonstrated that current production was much higher than that from healthy sample, and the detection time was less than 5 min. Because conventional periodontal pathogen detection using 16S rRNA sequencing costs and takes time (**Table 4.2**), our identification of appropriate redox mediator may enable fast response and high sensitivity for hygiene biosensor at home with significantly low cost.

Table 4.2 The performance and cost comparison of different biosensor types

Method	Time	Cost
PCR	6 hrs	$149/1 Kit
ELISA	6 hrs	$420/1 Kit
16s RNA	weeks	$3-10 collection kit+$50 sequencing
Our work	5 min	$3 electrode (reusable)

References

1. Oh, T.J., R. Eber, and H.L. Wang, *Periodontal diseases in the child and adolescent.* J Clin Periodontol, 2002. **29**(5): p. 400-10.
2. Preshaw, P.M., et al., *Periodontitis and diabetes: a two-way relationship.* Diabetologia, 2012. **55**(1): p. 21-31.
3. Cardoso, E.M., C. Reis, and M.C. Manzanares-Céspedes, *Chronic periodontitis, inflammatory*

cytokines, and interrelationship with other chronic diseases. Postgrad Med, 2018. **130**(1): p. 98-104.

4. Li, T.J., et al., *Periodontal Pathogens: A Crucial Link Between Periodontal Diseases and Oral Cancer.* Front Microbiol, 2022. **13**: p. 919633.

5. Popova, C., V. Dosseva-Panova, and V. Panov, *Microbiology of Periodontal Diseases. A Review.* Biotechnology & Biotechnological Equipment, 2014. **27**(3): p. 3754-3759.

6. Benso, B., *Virulence factors associated with Aggregatibacter actinomycetemcomitans and their role in promoting periodontal diseases.* Virulence, 2017. **8**(2): p. 111-114.

7. How, K.Y., K.P. Song, and K.G. Chan, *Porphyromonas gingivalis: An Overview of Periodontopathic Pathogen below the Gum Line.* Front Microbiol, 2016. **7**: p. 53.

8. Curtis, M.A., P.I. Diaz, and T.E. Van Dyke, *The role of the microbiota in periodontal disease.* Periodontol 2000, 2020. **83**(1): p. 14-25.

9. Malheiros Vde, J. and M.J. Avila-Campos, *Detection of pathogens from periodontal lesions.* Rev Saude Publica, 2004. **38**(5): p. 723-8.

10. Imamura, K., et al., *Evaluation of a novel immunochromatographic device for rapid and accurate clinical detection of Porphyromonas gingivalis in subgingival plaque.* J Microbiol Methods, 2015. **117**: p. 4-10.

11. Petit, M.D., et al., *Prevalence of periodontitis and suspected periodontal pathogens in families of adult periodontitis patients.* J Clin Periodontol, 1994. **21**(2): p. 76-85.

12. Mineoka, T., et al., *Site-specific development of periodontal disease is associated with increased levels of Porphyromonas gingivalis, Treponema denticola, and Tannerella forsythia in subgingival*

plaque. J Periodontol, 2008. **79**(4): p. 670-6.

13. Alhogail, S., et al., *On site visual detection of Porphyromonas gingivalis related periodontitis by using a magnetic-nanobead based assay for gingipains protease biomarkers.* Mikrochim Acta, 2018. **185**(2): p. 149.

14. Mättö, J., et al., *Detection of Porphyromonas gingivalis from saliva by PCR by using a simple sample-processing method.* J Clin Microbiol, 1998. **36**(1): p. 157-60.

15. Boutaga, K., et al., *Comparison of real-time PCR and culture for detection of Porphyromonas gingivalis in subgingival plaque samples.* J Clin Microbiol, 2003. **41**(11): p. 4950-4.

16. Galassi, F., et al., *Comparing culture, real-time PCR and fluorescence resonance energy transfer technology for detection of Porphyromonas gingivalis in patients with or without peri-implant infections.* J Periodontal Res, 2012. **47**(5): p. 616-25.

17. Park, S., et al., *Washing- and Separation-Free Electrochemical Detection of Porphyromonas gingivalis in Saliva for Initial Diagnosis of Periodontitis.* Anal Chem, 2021. **93**(13): p. 5644-5650.

18. Svärd, A., et al., *Protein-Functionalized Gold Nanoparticles as Refractometric Nanoplasmonic Sensors for the Detection of Proteolytic Activity of Porphyromonas gingivalis.* ACS Applied Nano Materials, 2020. **3**(10): p. 9822-9830.

19. Naradasu, D., et al., *Microbial current production from Streptococcus mutans correlates with biofilm metabolic activity.* Biosens Bioelectron, 2020. **162**: p. 112236.

20. Naradasu, D., et al., *Electrochemical Characterization of Current-Producing Human Oral Pathogens by Whole-Cell Electrochemistry.* ChemElectroChem, 2020. **7**(9): p. 2012-2019.

21. Naradasu, D., W. Miran, and A. Okamoto, *Metabolic Current Production by an Oral Biofilm*

Pathogen Corynebacterium matruchotii. Molecules, 2020. **25**(14): p. 3141.

22. Miran, W., D. Naradasu, and A. Okamoto, *Pathogens electrogenicity as a tool for in-situ metabolic activity monitoring and drug assessment in biofilms.* iScience, 2021. **24**(2): p. 102068.

23. Miran, W., et al., *Multivariate landscapes constructed by Bayesian estimation over five hundred microbial electrochemical time profiles.* Patterns, 2022: p. 100610.

24. Takahashi, N., T. Sato, and T. Yamada, *Metabolic pathways for cytotoxic end product formation from glutamate- and aspartate-containing peptides by Porphyromonas gingivalis.* J Bacteriol, 2000. **182**(17): p. 4704-10.

25. Light, S.H., et al., *A flavin-based extracellular electron transfer mechanism in diverse Gram-positive bacteria.* Nature, 2018. **562**(7725): p. 140-144.

26. Li, X., et al., *Electron transfer capacity dependence of quinone-mediated Fe(III) reduction and current generation by Klebsiella pneumoniae L17.* Chemosphere, 2013. **92**(2): p. 218-24.

27. Rhodes, Z., et al., *Using structure-function relationships to understand the mechanism of phenazine-mediated extracellular electron transfer in Escherichia coli.* iScience, 2021. **24**(9): p. 103033.

28. Deng, X., D. Luo, and A. Okamoto, *Defined and unknown roles of conductive nanoparticles for the enhancement of microbial current generation: A review.* Bioresour Technol, 2022. **350**: p. 126844.

29. Hu, M., et al., *Nano-Fe(3)C@PGC as a novel low-cost anode electrocatalyst for superior performance microbial fuel cells.* Biosens Bioelectron, 2019. **142**: p. 111594.

30. Rawson, F.J., A.J. Downard, and K.H. Baronian, *Electrochemical detection of intracellular and*

cell membrane redox systems in Saccharomyces cerevisiae. Scientific Reports, 2014. **4**.

31. Zhang, S., et al., *A Human Pathogen Capnocytophaga Ochracea Exhibits Current Producing Capability.* Electrochemistry, 2020. **88**(3): p. 224-229.

32. Chen, R.-p., et al., *Enhancement on the microbial extracellular electron transfers by modified lignin materials: Application on decolorization of azo dye.* Journal of Materials Research and Technology, 2021. **15**: p. 5265-5276.

33. Qin, J., et al., *Accelerated anaerobic biodecolorization of sulfonated azo dyes by magnetite nanoparticles as potential electron transfer mediators.* Chemosphere, 2021. **263**: p. 128048.

34. Liu, Y., et al., *Extracellular electron transfer in electroactive anaerobic granular sludge mediated by the phenothiazine derivative.* Journal of Power Sources, 2022. **527**: p. 231212.

35. N.Z.N, A., et al., *Embedded 32-bit Differential Pulse Voltammetry (DPV) Technique for 3-electrode Cell Sensing.* IOP Conference Series: Materials Science and Engineering, 2018. **340**: p. 012016.

36. Deng, X., D. Luo, and A. Okamoto, *Electrode hydrophilicity enhanced the rate of extracellular electron uptake in Desulfovibrio ferrophilus IS5.* Electrochimica Acta, 2022. **421**: p. 140504.

37. Hong, G. and R. Pachter, *Bound Flavin-Cytochrome Model of Extracellular Electron Transfer in Shewanella oneidensis: Analysis by Free Energy Molecular Dynamics Simulations.* J Phys Chem B, 2016. **120**(25): p. 5617-24.

38. Hijji, Y.M., B. Barare, and Y. Zhang, *Lawsone (2-hydroxy-1,4-naphthoquinone) as a sensitive cyanide and acetate sensor.* Sensors and Actuators B: Chemical, 2012. **169**: p. 106-112.

39. Okamoto, A., et al., *Rate enhancement of bacterial extracellular electron transport involves bound*

flavin semiquinones. Proc Natl Acad Sci U S A, 2013. **110**(19): p. 7856-61.

40. *<ac50008a031.pdf>*.

41. Shi J, M.D., *Surface Modification Approaches for Electrochemical Biosensors. Biosensors - Emerging Materials and Applications.* . InTech, 2011.

42. Cho, I.H., D.H. Kim, and S. Park, *Electrochemical biosensors: perspective on functional nanomaterials for on-site analysis.* Biomater Res, 2020. **24**: p. 6.

43. Conners, E.M., K. Rengasamy, and A. Bose, *Electroactive biofilms: how microbial electron transfer enables bioelectrochemical applications.* J Ind Microbiol Biotechnol, 2022. **49**(4).

44. Katuri, K.P., et al., *Electroactive biofilms on surface functionalized anodes: The anode respiring behavior of a novel electroactive bacterium, Desulfuromonas acetexigens.* Water Res, 2020. **185**: p. 116284.

45. Grieshaber, D., et al., *Electrochemical Biosensors - Sensor Principles and Architectures.* Sensors (Basel), 2008. **8**(3): p. 1400-1458.

46. Adarakatti, P.S. and S.K. Kempahanumakkagari, *Modified electrodes for sensing.* 2018. **15**: p. 58-95.

47. Wang, J., *Modified electrodes for electrochemical sensors.* Electroanalysis, 1991. **3**(4-5): p. 255-259.

48. Alexandru Ciucu, A., *Chemically Modified Electrodes in Biosensing.* Journal of Biosensors & Bioelectronics, 2014. **05**(03).

49. Erkmen, C., et al., *Layer-by-layer modification strategies for electrochemical detection of biomarkers.* Biosensors and Bioelectronics: X, 2022. **12**: p. 100270.

50. Theyagarajan, K. and Y.J. Kim, *Recent Developments in the Design and Fabrication of Electrochemical Biosensors Using Functional Materials and Molecules.* Biosensors (Basel), 2023. **13**(4).

51. Mukhi, M. and A.S. Vishwanathan, *Beneficial Biofilms: a Minireview of Strategies To Enhance Biofilm Formation for Biotechnological Applications.* Appl Environ Microbiol, 2022. **88**(3): p. e0199421.

52. Jose A. Cornejo, C.L., Sofia Babanova, Carlo Santoro, Kateryna Artyushkova, Linnea Ista, Andrew J. Schuler and Plamen Atanassov, *Surface Modification for Enhanced Biofilm Formation and Electron Transport in Shewanella Anodes.* Journal of The Electrochemical Society, 2015. **162**(9): p. H597.

53. Ahmed, W., et al., *Real-time PCR detection of pathogenic microorganisms in roof-harvested rainwater in Southeast Queensland, Australia.* Appl Environ Microbiol, 2008. **74**(17): p. 5490-6.

54. Tabatabaei, M.S. and M. Ahmed, *Enzyme-Linked Immunosorbent Assay (ELISA).* Methods Mol Biol, 2022. **2508**: p. 115-134.

55. Worthington, T., et al., *A rapid ELISA for the diagnosis of intravascular catheter related sepsis caused by coagulase negative staphylococci.* J Clin Pathol, 2002. **55**(1): p. 41-3.

56. Su, J.F., et al., *The mixotrophic denitrification characteristics of Zoogloea sp. L2 accelerated by the redox mediator of 2-hydroxy-1,4-naphthoquinone.* Bioresour Technol, 2020. **311**: p. 123533.

57. Yagishita, T., T. Horigome, and K. Tanaka, *Effects of light, CO2 and inhibitors on the current output of biofuel cells containing the photosynthetic organism Synechococcus sp.* Journal of Chemical Technology & Biotechnology, 2007. **56**(4): p. 393-399.

58. Yang, S.H., et al., *Alternative mitochondrial electron transfer for the treatment of neurodegenerative diseases and cancers: Methylene blue connects the dots.* Prog Neurobiol, 2017. **157**: p. 273-291.

Chapter 5. Conclusion and Future prospects

5.1 Conclusion

In this study, the author focused on the extracellular electron transfer (EET and EEU)-based electrochemical biosensors of bio-corrosive bacteria for diagnosis of biocorrosion in different environment. To develop a biosensor, the high sensitivity and quick response were the two most important performance parameters. Therefore, the author was committed to improving the sensor's specificity and sensitivity based on the electrical interaction between electrode and electrogenic bio-corrosive bacteria. In detail, the effect of electrode surface property, metabolic pathway, and shuttles on electron transfer rate was studied. The author even investigated human saliva samples for periodontitis biosensor development. Firstly, the EEU process *Desulfovibrio ferrophilus* IS5 (IS5), an important sulfate-reducing bacteria (SRB) that is crucial for understanding the mechanism underlying anaerobic iron corrosion, for the prediction and detection of iron corrosion was studied in **Chapter 2**. The author examined the impact of electrode wettability on the sensitivity of EEU-based electrochemical biosensor of IS5 and the electron transport mechanism at the interfaces between cells and electrodes. With increasing electrode hydrophilicity, current generation coupled with sulfate reduction increased by as much as nine-fold and displayed a positive linear correlation with the number of cells attached to the electrodes, which indicates IS5-mediated EEU most likely requires direct cell attachment to the electrode surfaces. These results indicates that in an IS5-enriched environment, it may be necessary to modify the surface by hydrophobic materials to prevent biocorrosion of metal pipe. Besides, an EET-based electrochemical biosensor of *P. gingivalis*, an important biomarker of periodontitis and causing dental corrosion, in human saliva for the early diagnosis of periodontal diseases was developed. The weak electrogenic capability of *P. gingivalis* with glucose oxidation was reported recently. For the development of biosensor with high sensitivity by using human sample that have numbers of communities, the specific and high current generated by *P. gingivalis* should be achieved. Based on the special amino acid metabolic pathway, the current generation of *P. gingivalis* was studied by using different types of metabolic substrates, including single, dipeptide

and peptides of several amino acids and sugars in **Chapter 3**. Among these substrates, with histidine *P. gingivalis* generated significantly high current compared with other EET-capable oral pathogens. Notably, the current production of patient saliva sample with higher abundant of *P. gingivalis* was much more than healthy saliva without *P. gingivalis*, which indicated histidine can be used as the specific substrate of the EET-based electrochemical biosensor of *P. gingivalis* in human saliva. In the real application of EET-based electrochemical biosensor for home care, it is suitable to utilize the screen-printed electrode (SPE) which have very small electrode area. However, *P. gingivalis* generated low current on SPE even with histidine. Different types of mediators were screened by a high-throughput system with SPE to increase electron transfer of *P. gingivalis* in **Chapter 4**. Among these mediators HNQ significantly increased current production of *P. gingivalis*, which was 73 times more than without HNQ. By using HNQ, current signal of *P. gingivalis* cells of small number can be detected. Furthermore, with HNQ patient saliva produced much higher current within just 5 min than without HNQ, also higher than healthy saliva with HNQ, which proved the specificity of our EET-based biosensor. Based on the analysis of bacteria community with the current production of human saliva, there were other potential saliva pathogens that were also contributed to the current production of saliva samples.

5.2 Future prospects

Based on these studies, the utilization of extracellular electron transfer capability of electrochemically active microorganism for the development of biosensors for early diagnosis and prediction of environmental poisoning is applicable with high sensitivity and low cost. Although our biosensor exhibited a lower detection limit compared to several other reported electrochemical biosensors for pathogen detection, the exploration of EET-based biosensors remains relatively limited. To the best of our knowledge, this study represents the first endeavor to realize the practical application of an EET-based electrochemical biosensor for the detection of

pathogenic bacteria. However, further extensive research efforts are required to enhance the performance of such biosensors using diverse methodologies. In our research, our primary focus was on improving the sensitivity and specificity of the biosensor by leveraging the EET mechanism. For instance, the author identified a specific substrate due to its close association with EET and bacterial metabolism. Moreover, the sensitivity was enhanced through the mediated EET process. The author also investigated the electrode wettability's effect on electron uptake rate to suggest the further electrode modification. It is worth noting that numerous alternative approaches exist to achieve similar objectives, such as electrode modification [1, 2] and biofilm enrichment [3, 4]. The modification of electrodes is crucial, as it influences biofilm formation and biosensor sensitivity [5-9]. The incorporation of specific materials can augment electron transfer within the biofilm, subsequently enhancing the sensitivity of EET- and EEU-based biosensors [10, 11]. Combined mediator-materials composites also enhance redox reactions. For instance, 2-hydroxy-1,4-naphthoquinone-graphene oxide (HNQ-GO) composite had been applied as an recyclable catalyst to enhance Cr(VI) reduction by *Shewanella xiamenensis* [12]. Additionally, other types of electrochemical sensors, such as those based on impendence or cyclic voltammetry [13, 14], can be employed for the detection of EET-capable bacteria with heightened sensitivity. Considering the continuous advancement of research in this field, it is anticipated that the practical implementation of EET- and EEU-based electrochemical biosensors will be realized in the near future.

EET- and EEU-based biosensors are expected to play an important role in the field of environmental detection, prediction, and prevention or remediation strategies. These biosensors have great potential to address challenges related to monitoring and understanding environmental processes, facilitating timely interventions and guiding mitigation measures. The integration of these biosensors into environmental monitoring frameworks promises to enhance the ability to detect, assess, and predict the presence and behavior of various pollutants, pathogens, and other environmentally relevant entities. By utilizing EET- and EEU-based biosensors, real-time and

accurate data on key environmental parameters can be collected, enabling proactive decision-making and intervention strategies. Timely detection and monitoring of pollutants, pathogens, and other ecological stressors enables rapid response measures, such as containment, remediation, or prevention, thereby minimizing adverse environmental impacts. Furthermore, the predictive capabilities provided by these specific biosensors can help predict potential environmental threats or changes. By continuously monitoring and analyzing the EET process, these biosensors can provide valuable insights into the dynamics of microbial communities and their interactions with the environment. This knowledge can inform predictive models and help identify potential risks, allowing preventive measures or targeted interventions to mitigate adverse outcomes. Overall, the integration of EET- and EEU-based biosensors into environmental monitoring systems holds great promise for improved detection, prediction, and prevention or remediation strategies. Continued research and development in this field will undoubtedly contribute to the advancement of environmental monitoring technologies, fostering a more sustainable and resilient approach to environmental management and protection.

References

1. Shi J, M.D., *Surface Modification Approaches for Electrochemical Biosensors. Biosensors - Emerging Materials and Applications.* . InTech, 2011.
2. Cho, I.H., D.H. Kim, and S. Park, *Electrochemical biosensors: perspective on functional nanomaterials for on-site analysis.* Biomater Res, 2020. **24**: p. 6.
3. Conners, E.M., K. Rengasamy, and A. Bose, *Electroactive biofilms: how microbial electron transfer enables bioelectrochemical applications.* J Ind Microbiol Biotechnol, 2022. **49**(4).
4. Katuri, K.P., et al., *Electroactive biofilms on surface functionalized anodes: The anode respiring*

behavior of a novel electroactive bacterium, Desulfuromonas acetexigens. Water Res, 2020. **185**: p. 116284.

5. Adarakatti, P.S. and S.K. Kempahanumakkagari, *Modified electrodes for sensing.* 2018. **15**: p. 58-95.

6. Wang, J., *Modified electrodes for electrochemical sensors.* Electroanalysis, 1991. **3**(4-5): p. 255-259.

7. Alexandru Ciucu, A., *Chemically Modified Electrodes in Biosensing.* Journal of Biosensors & Bioelectronics, 2014. **05**(03).

8. Erkmen, C., et al., *Layer-by-layer modification strategies for electrochemical detection of biomarkers.* Biosensors and Bioelectronics: X, 2022. **12**: p. 100270.

9. Theyagarajan, K. and Y.J. Kim, *Recent Developments in the Design and Fabrication of Electrochemical Biosensors Using Functional Materials and Molecules.* Biosensors (Basel), 2023. **13**(4).

10. Mukhi, M. and A.S. Vishwanathan, *Beneficial Biofilms: a Minireview of Strategies To Enhance Biofilm Formation for Biotechnological Applications.* Appl Environ Microbiol, 2022. **88**(3): p. e0199421.

11. Jose A. Cornejo, C.L., Sofia Babanova, Carlo Santoro, Kateryna Artyushkova, Linnea Ista, Andrew J. Schuler and Plamen Atanassov, *Surface Modification for Enhanced Biofilm Formation and Electron Transport in Shewanella Anodes.* Journal of The Electrochemical Society, 2015. **162**(9): p. H597.

12. Li, Y., et al., *Application of 2-hydroxy-1,4-naphthoquinone- graphene oxide (HNQ-GO) composite*

as recyclable catalyst to enhance Cr(VI) reduction by Shewanella xiamenensis. Journal of Chemical Technology & Biotechnology, 2019. **94**(2): p. 446-454.

13. Grieshaber, D., et al., *Electrochemical Biosensors - Sensor Principles and Architectures.* Sensors (Basel), 2008. **8**(3): p. 1400-1458.

14. Dăscălescu, D. and C. Apetrei, *Development of a Novel Electrochemical Biosensor Based on Organized Mesoporous Carbon and Laccase for the Detection of Serotonin in Food Supplements.* Chemosensors, 2022. **10**(9): p. 365.

List of Publication

[1] Xiao Deng, **Dan Luo**, Akihiro Okamoto, *Electrode hydrophilicity enhanced the rate of extracellular electron uptake in Desulfovibrio ferrophilus IS5*, Electrochimica Acta, 2022, 421, 140504.

[2] Xiao Deng, **Dan Luo**, Akihiro Okamoto, *Defined and unknown roles of conductive nanoparticles for the enhancement of microbial current generation: A review*, Bioresource technology, 2022, 350, 126844.

Acknowledgment

As I approach the end of my Ph.D journey in Japan, time seems to have flown by, leaving me with a multitude of emotions and a deep sense of gratitude. Reflecting on my research experience, there are numerous individuals to whom I owe immense thanks.

First and foremost, I express my heartfelt gratitude to my mentor, Prof. Okamoto. When I initially joined the group, transitioning from a different field of study, I faced many challenges and uncertainties. However, Pro. Okamoto patiently guided me and provided invaluable suggestions. Despite his busy schedule, he always showed genuine interest in the progress of my experiments and readily answered my questions. His willingness to assist in modifying presentations greatly enhanced my skills. Despite being the group leader, he fostered a friendly and approachable atmosphere, creating a harmonious and supportive environment. I am profoundly grateful to Prof. Okamoto for his unwavering support throughout my doctoral journey. I will forever cherish his guidance and strive harder in my future scientific endeavors. With his expectations as my motivation, I aim to pass on his patient teaching to future generations and students.

I would also like to extend my gratitude to Senior Sister Xiao Deng for her help. She generously offered me guidance and suggestions in my work, always ready to help me analyze problems encountered during experiments. Together, we successfully completed part of my graduation thesis and collaborated on various tasks. Beyond work, Senior Sister Deng showed genuine care for me, and I sincerely thank her for her support. Additionally, I extend my heartfelt wishes for the health and happiness of her little baby.

Furthermore, I am deeply grateful to the members of other laboratories who aided me in my research. As a newcomer to the field of biological experiments, their advice proved indispensable, especially that of Dr. Divya Naradasu and Dr. Wenyuan Huang. Their guidance has greatly benefited my scientific endeavors. I also extend my thanks to Ms. Uematsu Miwa, Ms. Yamguchi

Chiharu, the former secretary ITOH Yoshie, as well as the caring support I received from Sister Chialun Ho, Xinxin Wen and Ms. Kangmin Yan in both work and personal matters. I will always hold in my heart their kindness and assistance. My gratitude also extends to other team members (Dr. Miran Waheed, Dr. Fujikawa Takashi, Dr. Takano Sotaro, Dr. Emran Mohammed, Dr. Pham Duyen Minh, Mr. Ihara Souta), technicians, and colleagues for their help.

In addition, I am profoundly thankful to my family and my boyfriend, who reside in China, for their constant love, encouragement, and support. It is their unwavering support that has allowed me to pursue my studies in Japan with peace of mind. I am also grateful to the friends I have made in Japan, whose companionship has enriched my life, brought me happiness, and left a lasting impact.

Lastly, I would like to express my appreciation to myself for the dedication and hard work I have put into this journey. I vow to continue striving for excellence, pushing myself to achieve greater heights in the future.

Overall, I am filled with gratitude towards all the individuals who have played a role in shaping my doctoral experience. Their support and guidance have been instrumental in my growth, both as a researcher and as an individual.